TECHNISCHE UNIVERSITÄT MÜNCHEN

Helmholtz Zentrum München

Deutsches Forschungszentrum für Gesundheit und Umwelt

Institut für Entwicklungsgenetik

Aldehyde dehydrogenase 1 A1 is expressed by cancer stem cells and mediates chemoresistance in human glioblastoma

Andrea Schäfer

Vollständiger Abdruck der von der Fakultät Wissenschaftszentrum Weihenstephan für Ernährung, Landnutzung und Umwelt der Technischen Universität München zur Erlangung des akademischen Grades eines

Doktors der Naturwissenschaften

genehmigten Dissertation.

Vorsitzender:	Univ.-Prof. Dr. S. Scherer
Prüfer der Dissertation:	1. Univ.-Prof. Dr. W. Wurst
	2. Univ.-Prof. Dr. J. Schlegel

Die Dissertation wurde am 06.08.2012 bei der Technischen Universität München eingereicht und durch die Fakultät Wissenschaftszentrum Weihenstephan für Ernährung, Landnutzung und Umwelt am 20.11.2012 angenommen.

Table of contents

A. Summary

The “cancer stem cell” (CSC) theory explains tumor heterogeneity by the existence of a cellular subset with stem-like characteristics. CSCs seem to be capable of self-renewal, of escaping therapy and inducing tumor re-growth. Recurrence also accounts for the devastating prognosis of glioblastoma (GBM, WHO grade IV), the most common and most aggressive primary brain tumor. Despite extensive therapy, including surgical resection and combined radio-chemotherapy, the prognosis for GBM patients remains poor. Hence, there is a need to characterize resistant tumor cell populations in order to identify appropriate biomarkers and therapeutic targets in human GBM. Aldehyde dehydrogenase 1 A1 (ALDH1A1), a member of the human aldehyde dehydrogenase superfamily, constitutes a novel candidate CSC marker in various solid tumors. This cytoplasmic enzyme acts upon oxidative stress response, differentiation and drug resistance. Recently, we described the functional role of ALDH1A1 in the maintenance and expansion of stem-like GBM cells. ALDH1A1 expression was associated with the generation of neurospheres while inhibition or knockdown of ALDH1A1 attenuated sphere formation and induced neural differentiation.

The aim of the present investigation was i) to characterize the interaction of ALDH1A1 with signaling pathways apparently involved in the maintenance of a stem-like phenotype and ii) to analyze the role of ALDH1A1 in mediating chemoresistance in human GBM.

The present work indicates that the generation of neurospheres depends on both ALDH1A1 expression and PTEN/PI3K/Akt signaling. Activation of PTEN/PI3K/Akt pathway and overexpression of ALDH1A1 increased neurosphere formation, while blocking the pathway, as well as inhibition or depletion of ALDH1A1 reduced sphere formation. Strikingly, inhibition of PTEN/PI3K/Akt signaling decreased ALDH1A1 expression *in vitro*, indicating a crucial role of this pathway in the maintenance of a self-renewing ALDH1A1 positive cell pool.

Since drug resistance and tumor recurrence are associated with the existence of CSCs, we analyzed whether ALDH1A1 mediates chemoresistance in human GBM. The current standard chemotherapeutic in the treatment of GBM is temozolomide (TMZ), an orally administered alkylating agent. The DNA-repair protein O^6-methylguanine DNA methyltransferase (MGMT) antagonizes the cytotoxic effect of TMZ and is the most important predictive factor for response to therapy in human GBM.

We found that ALDH1A1 overexpression predicted resistance to TMZ *in vitro*, independently of the MGMT status. Notably, chemical inhibition or knockdown of ALDH1A1 re-sensitized ALDH1A1/MGMT positive cells to TMZ, as indicated by increased cytotoxicity, reduced clonogenicity and cell cycle arrest. Moreover, analysis of ALDH1A1 expression in tissue sections of GBM patients revealed a significant correlation between expression of this enzyme and an unfavorable outcome, independently of the patients' MGMT status. Strikingly, the percentage of ALDH1A1 positive cells in recurrent GBMs was significantly higher compared to the respective primary tumors. This suggests that these cells are able to escape therapy and to induce tumor re-growth.

Finally, the mechanism of ALDH1A1 mediated resistance to TMZ was analyzed. The present data demonstrate a pivotal role of ALDH1A1 in handling oxidative stress. We found TMZ to induce oxidative stress by the development of superoxide radicals within the cells. The superoxide radicals peroxidize membrane lipids and culminate in the formation of highly reactive aldehydes such as 4-hydroxynonenal (4-HNE). These aldehydes rapidly bind to cellular proteins and DNA, giving rise to toxic aggregates. ALDH1A1 is able to bind and detoxify these reactive aldehydes. In line with these findings, only ALDH1A1 negative cell lines were found to undergo cell cycle arrest and displayed DNA damage following exposure to 4-HNE or TMZ.

The data of the present study demonstrate that ALDH1A1 is not only a marker for therapy resistant GBM cells with stem cell characteristics, but also a direct mediator of chemoresistance. Therefore ALDH1A1 serves as a feasible predictor of clinical outcome and a potential therapeutic target in the future treatment of human malignancies.

B. Introduction

1. Malignant gliomas

Gliomas are intrinsic tumors of the brain. According to their histopathology they are classified into astrocytoma (related to astrocytes), oligodendroglioma (related to oligodendrocytes), oligoastrocytoma and ependymoma (related to ependymal cells), respectively. Astrocytomas account for more than 70% of gliomas (Preusser et al., 2011; www.cbtrus.org, 2012). Based on the growth pattern, including infiltrative and proliferative potential, the overall prognosis as well as the tumors tendency to recur, astrocytomas are graded into four categories according to the World Health Organization (WHO) classification of tumors of the central nervous system. Low-grade astrocytomas (WHO grade I and II) are declared to as low malignant. WHO grade I pilocytic astrocytomas are slow-growing, benign tumors with a 10-year survival rate of more than 90% following total resection. WHO grade II astrocytomas show low-level proliferation, diffuse infiltrative growth and tend to progress to malignant high-grade astrocytomas (grade III or IV). Beside infiltrative potential, WHO grade III anaplastic astrocytomas show anaplasia and mitotic activity. Astrocytic tumors with additional microvascular proliferation and necrosis are classified as grade IV neoplasm with a devastating prognosis. Grade IV astrocytic tumors include glioblastoma, giant cell glioblastoma and gliosarcoma (Louis et al., 2007).

2. Glioblastoma

2.1 Epidemiology and etiology

Glioblastoma (GBM) is the most common malignant primary brain tumor, accounting for approximately 50% of all gliomas (Louis et al., 2007; www.cbtrus.org, 2012). This fatal disease occurs more frequently in elderly, with a median age at diagnosis of 64 years (Schwartzbaum et al., 2006). In Europe and North America the yearly incidence rate for GBM is 3-4 newly diagnosed cases per 100,000 people (Brown et al., 2009; Ohgaki and Kleihues, 2005; Wohrer et al., 2009; www.cbtrus.org, 2012). The rate of GBM cases among men is 1.6 fold higher than among women. Further, GBM is twice as common in Caucasian as it is in African or Asian descendants (Ohgaki and Kleihues, 2005; Schwartzbaum et al., 2006).

The reason for this gender-specific and ethnological preponderance remains unclear. Extensive epidemiological studies are performed to identify genetic or environmental contributors to glioma incidence. To date, the only relevant environmental factor associated with increased glioma risk, is therapeutic radiation. X-irradiation, in particular in childhood, correlates with an elevated risk for gliomas and meningeomas (Neglia et al., 2006). Exposure to endo- or exogenous chemicals such as N-nitroso compounds or polycyclic aromatic hydrocarbons induced brain tumors in animal trials, but was not applicable to human epidemiological studies (Gurney et al., 2002; Ohgaki and Kleihues, 2005; Ruder et al., 2004). Other examined factors such as cell phone use, head trauma or medication showed no significant correlation with a higher glioma risk (Inskip et al., 2001; Lahkola et al., 2007). Various inherited syndromes such as neurofibromatosis 1 and 2, retinoblastoma, or Li-Fraumeni syndrome have been associated with an increased risk for gliomas. Despite these rare inherited diseases, no familiar aggregation for malignant gliomas could be found (Li et al., 1995; Schwartzbaum et al., 2006).

2.2 Histology and molecular pathology

2.2.1 Primary and secondary GBM

Histopathologically, GBMs are heterogeneous, infiltrative and proliferative neoplasms showing neovascularization and necrosis within the tumor mass (Figure 1).

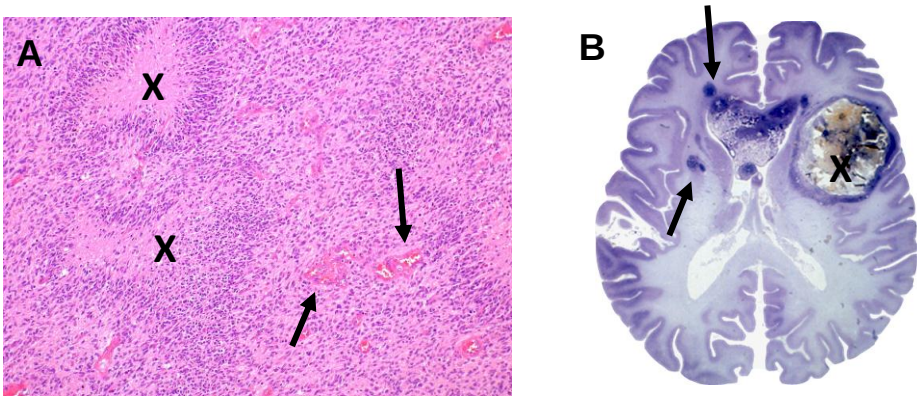

Figure 1: Neuropathology of glioblastoma

A, Hematoxylin-eosin staining: cellular glial tumor showing necrosis (X) and microvascular proliferates (arrows). B, Nissl stained axial brain-section: large necrotic area in the right cerebral hemisphere (X) with an edge of vital nissl-positive tumor cells infiltrating the surrounding brain tissue, resulting in secondary tumors in the left hemisphere (arrows).

Approximately 95% of all GBMs develop *de novo* (primary glioblastomas), while 5% emerge from WHO grade II or III astrocytomas (secondary glioblastomas) (Ohgaki and Kleihues, 2011). Regarding histology, primary and secondary GBMs can hardly be distinguished. In the past, diagnosis was performed based on previous clinical data. Present studies indicate that both forms develop through different genetic alterations (Figure 2). Mutation of isocitrate dehydrogenase 1 and 2 (IDH1/2) is found frequently in secondary GBMs (> 80%), while it is rare in primary GBMs (< 5%). Genetic alterations that are prevalent in primary glioblastomas are loss of heterozygosity (LOH) 10p, epidermal growth factor receptor (EGFR) gene amplification and phosphatase and tensin homolog (PTEN) mutations. TP53 mutations, LOH 19q and LOH 22q are prevalent in secondary GBMs, while LOH 10q and $p16^{INK4a}$ occur equally in primary and secondary neoplasms (Nobusawa et al., 2009; Ohgaki et al., 2004; Ohgaki and Kleihues, 2011; Yan et al., 2009b). TP53 encodes the protein p53, which is involved in cell cycle regulation, DNA damage repair, apoptosis, differentiation and neovascularization. Data on TP53, LOH 10p and $p16^{INK4a}$ as predictive factors are contradictory (Ohgaki et al., 2004; Schmidt et al., 2002). LOH 10q is the most frequent genetic alteration in the development of primary and secondary GBMs. Studies have demonstrated that LOH 10q is the only genetic alteration being significantly associated with a poor clinical prognosis (Ohgaki et al., 2004; Terada et al., 2002).

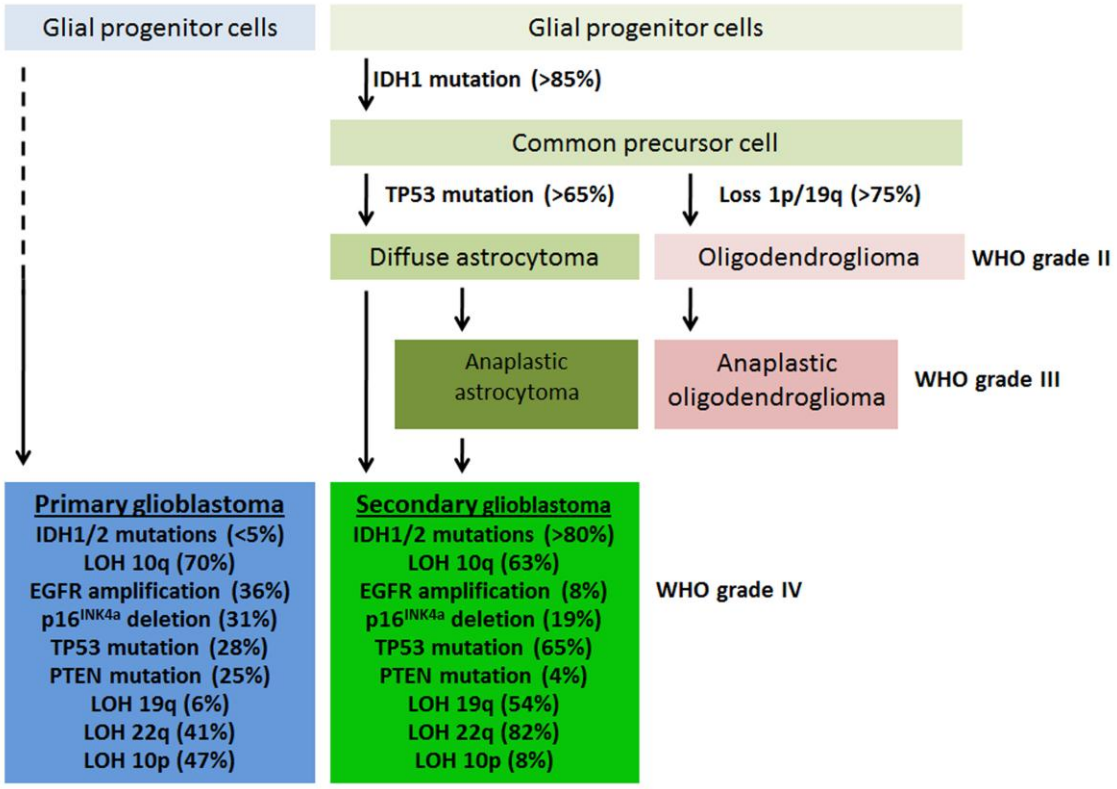

Figure 2: Genetic pathways to astrocytic and oligodendroglial diffuse gliomas

Model of glial tumor progression modified after Ohgaki *et al.* (Ohgaki et al., 2004; Ohgaki and Kleihues, 2005; Ohgaki and Kleihues, 2011).

2.2.2 IDH1/2 mutations

The enzyme IDH1 is localized in the cytoplasm and in peroxisomes while IDH2 is part of the citric acid cycle within the mitochondria. Both enzymes catalyze the oxidative decarboxylation of isocitrate to α-ketoglutarate and thereby regenerate NADPH. In 2009, Yan *et al.* found IDH1/2 mutations in more than 70% of all grade II and III astrocytomas, oligodendrogliomas and secondary glioblastomas. In addition, glioblastomas with IDH1 mutations often have TP53 mutations (80%) but rarely feature common alterations such as EGFR amplification or PTEN mutation (Ohgaki and Kleihues, 2011; Yan et al., 2009a; Yan et al., 2009b). IDH1 mutations are preferentially present in younger patients and they correlate with a favorable outcome (Nobusawa et al., 2009). As IDH1/2 alterations are found frequently in low grade astrocytomas and oligodendrogliomas, mutation seems to occur at an early stage of glioma progression. This argues for common precursor cells of astrocytomas, secondary glioblastomas and oligodendrogliomas.

A single amino acid within the isocitrate binding site is affected by the mutations: R132 of IDH1 and analogously R172 of IDH2 (Yan et al., 2009a; Yan et al., 2009b). Nevertheless, the functional role of IDH1/2 mutation is not yet fully understood. Mutated IDH1 was shown to have a lowered substrate affinity and to build heterodimers with its wild-type counterpart. These enzyme-complexes feature only 4% of the wild-type IDH1 activity, resulting in reduced α-ketoglutarate and NADPH levels (Zhao et al., 2009). Therefore, one possible contribution of mutant IDH1 to gliomagenesis is the stabilization of hypoxia inducible factor 1 (HIF1A) by the decrease of α-ketoglutarate levels. HIF1A is a transcription factor that is stabilized under low-oxygen conditions; it plays a crucial role in the regulation of genes involved in glucose metabolism, angiogenesis and other tumor growth promoting pathways. Prolylhydroxylases use α-ketoglutarate as a cofactor for the degradation of HIF1A in the presence of oxygen. Furthermore, attenuated IDH1/2 activity results in lower NADPH levels within the cell. These reduction equivalents are required for glutathione production, which is essential for the protection against oxidative stress. IDH1 mutations also result in a gain of function of the enzyme which is then able to catalyze the NADPH-dependent reduction of alpha-ketoglutarate to R(-)-2-hydroxyglutarate (2HG). This potentially oncogenic product might be involved in gliomagenesis (Dang et al., 2010). In addition, IDH1/2 mutations might contribute to the Warburg effect by changing metabolites and thereby promoting glycolysis (Vander Heiden et al., 2009; Yan et al., 2009a).

2.2.3 EGFR alterations

The EGFR is a 170-kDa transmembrane receptor that belongs to the ErbB family, a group of four receptor tyrosine kinases (EGFR, Her2, Her3 and Her4). The EGFR glycoprotein is composed of three regions: a 622 aa N-terminal extracellular domain containing two cysteine rich parts involved in ligand binding and receptor dimerization, a single hydrophobic alpha-helical transmembrane domain and a 542 aa intracellular part with tyrosine kinase activity. Upon ligand binding to the N-terminus (e.g. EGF, TGFα, amphiregulin, epiregulin) EGFR forms homo- or heterodimers (e.g. EGFR/Her2). Dimerization induces autophosphorylation of the intrinsic, intracellular tyrosine-residues at the C-terminal part. Subsequently different effector-molecules are recruited to the phosphorylation site, binding by their own phosphotyrosine-binding SH2 (Src-homology 2*)* or PTB (phospho-tyrosine binding) domains.

Binding induces downstream activation of various pathways including Akt, MAPK or JAK/Stat signaling. These pathways are involved in the regulation of many biological processes including cell migration, adhesion, proliferation and apoptosis (Figure 3) (Jorissen et al., 2003).

Identification of EGFR alterations has been a hallmark in cancer research. In more than one-third of GBM cases, EGFR is amplified, over-expressed, or mutated (Ohgaki et al., 2004). The most common mutation is deletion of the exons 2-7 from the extracellular domain resulting in a constitutively active receptor. This truncated EGFRvIII variant is exclusively present in tumors with EGFR overexpression or gene amplification, but is only expressed in a subpopulation of cells within the tumor mass (Aldape et al., 2004; Nishikawa et al., 2004). Despite various animal and cell culture studies showing enhanced tumorigenicity of EGFR alterations, data on the predictive value of EGFR mutations remain ambiguous. It was shown that GBMs with overexpression of the secreted glycoprotein YKL-40, which mediates tumor invasion and angiogenesis, and EGFRvIII are more malignant (Nutt et al., 2005; Pelloski et al., 2007). Nevertheless, most studies argue against a prognostic importance of EGFR aberrations (Nagane et al., 1996; Ohgaki et al., 2004; Schmidt et al., 2002; Smith et al., 2001).

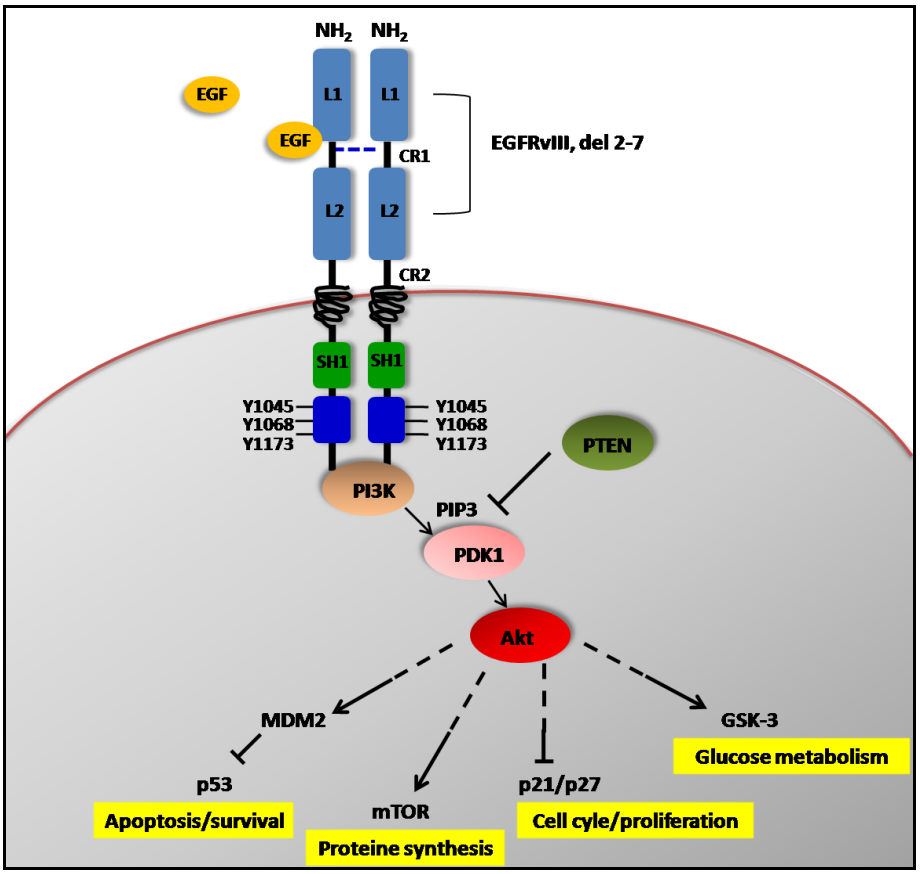

Figure 3: Model of EGFR dependent PI3K/Akt activation with respective downstream targets

L1, L2 (ligand binding domains); CR1, CR2 (cysteine rich domains); SH2 (tyrosine kinase domain) catalyzing phosphorylation of tyrosine residues (Y)

2.2.4 PTEN mutations

The tumor suppressor gene PTEN is located on chromosome 10q23 and encodes the phosphatase PTEN. PTEN dephosphorylates phosphatidylinositol (3,4,5)-trisphosphate (PIP3) and thereby negatively regulates Akt (protein kinase B) pathway (Figure 3). PTEN acts as an important regulator of proliferation, apoptosis and tumor invasion (Simpson and Parsons, 2001). Mutations of this phosphatase occur in approximately 30% of GBM cases, predominately in primary GBMs. To date, data on the predictive value of PTEN remain contradictory (Carico et al., 2012; Ohgaki et al., 2004; Ohgaki and Kleihues, 2011). Strikingly PTEN/PI3K/Akt pathway has been shown to regulate brain tumor stem cell characteristics such as side population and neurosphere formation (Bleau et al., 2009; Chen et al., 2010; Phillips et al., 2006).

2.3 Molecular subclasses of glioblastoma

Despite LOH 10q and IDH1/2 mutations, none of the frequent alterations in glioblastomas clearly demonstrate a prognostic value. Furthermore, GBMs are highly heterogeneous tumors harboring subpopulations of cells that differ regarding their expression profile, genetic alterations, growth rates and drug response. Therefore *The Cancer Genome Atlas* (TCGA) network identified four subtypes of glioblastoma with prognostic relevance: proneural, neural, classical and mesenchymal (Phillips et al., 2006; Verhaak et al., 2010).

The classical subclass includes tumors that show high levels of EGFR gene amplification, EGFRvIII expression and deletion of $p16^{INK4a}$, but lack mutations of the tumor suppressor genes TP53, NF1 (neurofibromatosis type I) or IDH1. Other nomenclatures describe a proliferative subtype due to high levels of Ki-67 in immunohistochemistry (Phillips et al., 2006). Regarding molecular markers and signaling pathways, this subtype shows characteristics of neural stem cells or transit amplifying cells. Glioblastomas of the mesenchymal subclass represent the most malignant neoplasms. They show rare NF1 expression, but feature mesenchymal and angiogenesis markers including YKL-40 or VEGF (vascular endothelial growth factor). Necrosis and inflammatory infiltration are frequently found in mesenchymal GBMs. The classical and the mesenchymal subclass share some characteristics: amplification of chromosome 7 paired with loss of chromosome 10, frequent PTEN mutations and they express markers characteristic for neural stem cells. In addition, these patients are older when diagnosed and have a poor prognosis compared to those with tumors of the proneural group, even though patients with classical or mesenchymal GBMS benefit from aggressive therapy.

Proneural glioblastomas frequently show mutations in the IDH1 gene, while PTEN mutations are rare. Tumors within this subclass often express genes associated with the process of neurogenesis such as the transcription factors SOX (Sry-related HMG box) or Olig2 (oligodendrocyte transcription factor 2). Patients with proneural GBMs are younger when diagnosed and have a better prognosis, while the median survival is not improved by aggressive treatment. Glioblastomas of the neural subclass have mutations in many of the same genes as the other groups without any predominant alterations.

They are characterized by a rather differentiated phenotype showing markers similar to those of neurons, astrocytes or oligodendrocytes in normal brain tissue. All subclasses either retain their specific signature upon relapse or recur with a mesenchymal phenotype.

3. The cell of origin: Clonal evolution versus cancer stem cell theory

Glioblastomas comprise heterogeneous cell populations and despite resection, irradiation and chemotherapy, relapse occurs regularly. These findings give reason to alternative theories of the origin of this heterogeneity (Figure 4). As initially described by Vogelstein *et al.* for colorectal cancer and later adapted to glioma by Ohgaki *et al.*, tumor progression is thought to be an evolutionary process (Ohgaki et al., 2004; Vogelstein et al., 1988). A glial progenitor represents a monoclonal origin of a neoplasm that gains heterogeneity by expansion and acquisition of mutations. In the clonal evolution theory, the fittest cells persist under therapy and are capable to induce tumor re-growth.

A second theory explains tumor heterogeneity with the cancer stem cell (CSC) paradigm. A therapy-resistant subpopulation with stem cell characteristics is reputed to be capable of self-renewal and to give rise to progenitor cells with limited properties comparable to transit amplifying cells that further differentiate (Bonavia et al., 2011). This hypothesis of hierarchically ordered cells within the tumor is based on the finding that a subpopulation of cancer cells showed similarity to normal stem cells, regarding self-renewal, phenotype and surrounding niches (Calabrese et al., 2007; Gilbertson and Rich, 2007; Reya et al., 2001).

Both theories: clonal evolution and the CSC theory are not mutually exclusive, but rather complementary. Notwithstanding the tumor bulk arises from a glial progenitor or a stem cell, similar mechanisms must maintain cellular heterogeneity. Surrounding glial cells, neurons, endothelial cells and extracellular matrix establish a microenvironment in which GBMs progress. Furthermore, irradiation and chemotherapy as well as oxygen levels within the neoplasm may play a major role in tumor expansion (Bonavia et al., 2011).

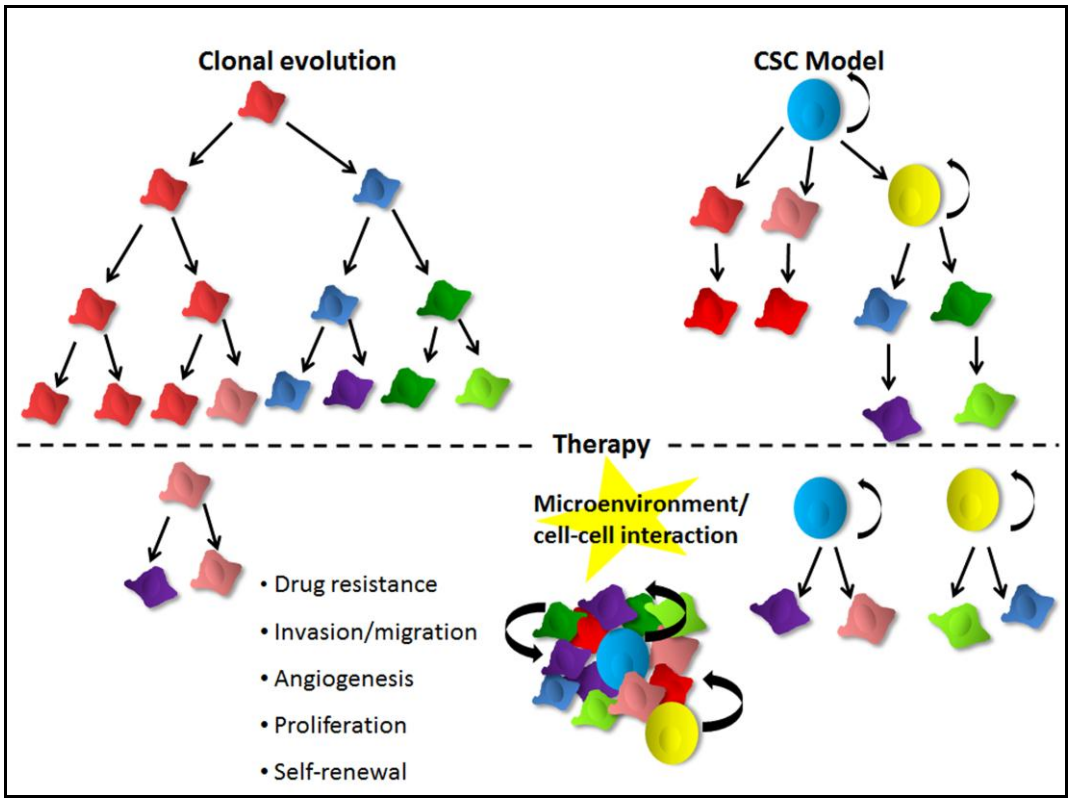

Figure 4: Models for heterogeneity origin of glioblastomas

Clonal evolution versus CSC theory modified after Bonavia *et al.* (Bonavia et al., 2011). In both models, heterogeneity is maintained by interaction of tumor cells with the microenvironment and with cells within the tumor.

4. Brain tumor stem cells or brain tumor cells with stem cell characteristics

Since first discovered in leukemia, cells featuring the potential to self-renew and to drive tumor formation and re-growth were also described in various solid tumors (Al-Hajj et al., 2003; Bonnet and Dick, 1997; Ricci-Vitiani et al., 2007). Singh *et al.* were the first to identify and purify a population with stem cell properties in solid brain tumors (Singh et al., 2003). These cells shared the ability to form spheroids (neurospheres) when grown in neurobasal medium and they expressed CD133 and nestin. The transmembrane glycoprotein CD133, also known as prominin-1 serves as a stem cell marker of hematopoietic (Yin et al., 1997) and neural cells (Uchida et al., 2000). CD133 and nestin, an intermediate filament protein expressed by undifferentiated neuroepithelial cells (Tohyama et al., 1992) and tumors of the CNS (Dahlstrand et al., 1992), used to be considered as robust markers of stemness in malignant glioma.

Recent studies challenged the prominent role of these markers with reports on CD133 negative (CD133-) cells showing stem-cell characteristics (Beier et al., 2007; Chen et al., 2010).

Besides analysis of various neural or embryonic stem cell markers such as musashi or Sox-2, functional assays have been explored to characterize stemness of brain tumor cells (Fotovati et al., 2011). The side population assay is based on the fact, that stem-like brain tumor cells possess ABC transporters that enable them to pump out chemotherapeutics (Bleau et al., 2009). ABC transporter positive cells can be analyzed by flow cytometry as they are able to exclude Hoechst dye. The neurosphere assay is another method to investigate functional properties of brain tumor stem-like cells. Single neural stem cells or brain tumor cells grow to spheroids under serum-free conditions in the presence of mitogens such as epidermal growth factor and fibroblast growth factor (Reynolds and Weiss, 1992). Tumorigenicity after serial transplantation in mouse models is another tool to describe stem-like tumor cells. Furthermore brain tumor cells with stem cell characteristics can differentiate into all three neural lineages: oligodendroglial, astrocytic and neuronal, as described by expression of galactocerebroside (GalC), glial fibrillary acidic protein (GFAP) or beta-III-tubulin (Tuj1) (Beier et al., 2007; Singh et al., 2004).

To date, it is unknown whether stem-like brain tumor cells are derived from neural stem cells that degenerate or from de-differentiation of a glial progenitor. Nevertheless, the microenvironment plays a crucial role in the maintenance of stemness. Glioblastomas are characterized by distinct hypoxic areas. While acute hypoxia leads to apoptosis or necrosis in the majority of normal and malignant cells, some subpopulations within the tumor adapt to stepwise or chronic deoxygenation. In these cells, hypoxia induces metabolic changes and genetic alterations that allow survival and proliferation under low-oxygen conditions. Hypoxia-driven cellular changes are partially caused by stabilization of the transcription factors HIF1A and HIF2A that are involved in the regulation of brain tumor stem cell characteristics (Seidel et al., 2010).

5. Treatment of glioblastoma

Following diagnosis by stereotactic biopsy or surgical resection and histopathology, complete resection is performed when feasible. Gross total resection, as recently determined by the fluorescent marker 5-aminoevulinic acid, improved the progression-free survival by 6-months (Stummer et al., 2006). Patients with a good performance status are treated with radiotherapy and concomitant and adjuvant temozolomide (TMZ) as described by Stupp *et al.* (Stupp et al., 2005). Combined radio-chemotherapy increased the median survival of patients with newly diagnosed GBM from 12.1 to 14.6 months (Figure 5) (Avgeropoulos and Batchelor, 1999; Stupp et al., 2005).

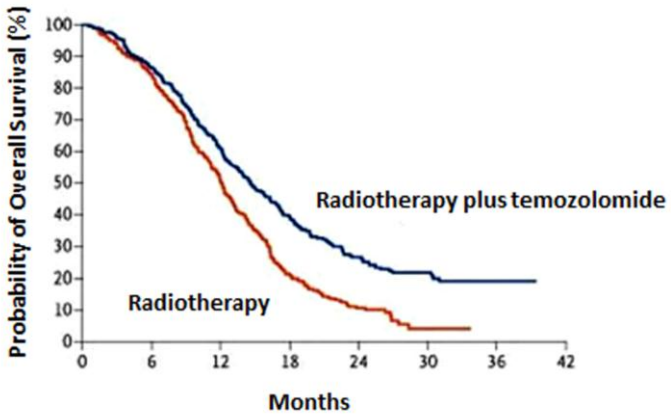

Figure 5: Kaplan-Meier plot of patient overall survival according to treatment group

The median survival benefit was 2.5 months: median survival was 14.6 months with radiotherapy plus temozolomide and 12.1 months with radiotherapy alone (Stupp et al., 2005).

Despite aggressive therapy, glioblastomas recur regularly. Magnetic resonance imaging (MRI) is the primary tool for pre- and postoperative monitoring of GBM patients. In addition, positron emission tomography (PET) is used to explore the extension of malignant lesions and to specify malignant foci prior to resection or radiotherapy (Figure 6). When coupled with the labeled amino acid ^{18}F-ethyltyrosine, the PET tracer is selectively internalized by high-grade glioma cells (FET-PET).

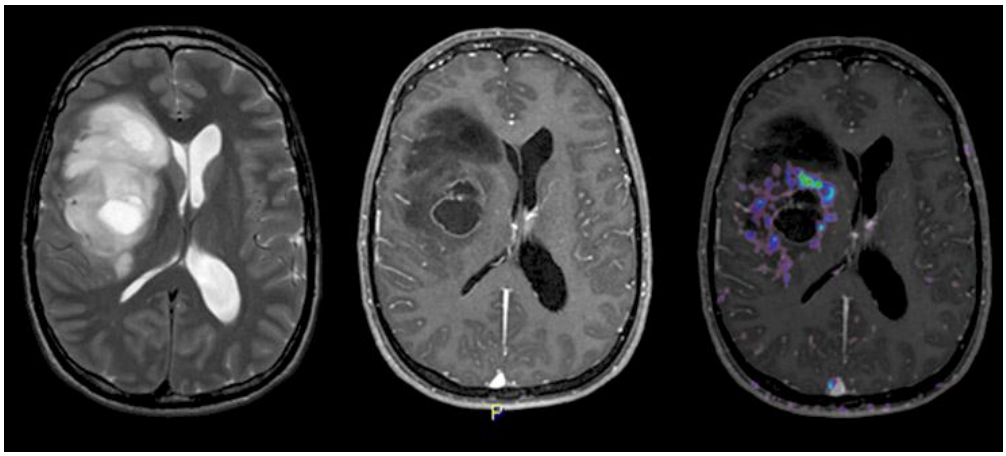

Figure 6: Magnetic resonance imaging (MRI) of right fronto-temporal glioblastoma

T2-weighted displaying edema and mass effects (left), T1-weighted showing necrotic tumor core (middle), ^{18}F-ethyltyrosine positron emission tomography (FET-PET) overlay reflecting hyper- metabolic areas around the necrotic lesion (right) (Weller, 2011).

Despite advances in the therapy of malignant glioma, glioblastoma is still a fatal diagnosis; efforts are made to find alternative treatment options. There are current trials on two inhibitors of angiogenesis: bevacizumab (Lai et al., 2011), a monoclonal antibody selectively binding to VEGF and cilengitide (Stupp et al., 2010), a pentapeptide that blocks αvβ3 and αvβ5 integrin activation. Bevacizumab is approved for the treatment of glioblastomas in the USA and Switzerland, but not in the European Union. Furthermore, a trial on immunotherapy of glioblastoma patients with an EGFRvIII-targeted peptide vaccine is ongoing (Sampson et al., 2010). Whether these new treatment approaches are feasible remains unclear.

6. Mechanisms of therapy resistance

The orally administered alkylating agent TMZ is spontaneously hydrolyzed to its active form 3-methyl-(triazen-1-yl) imidazole-4-carboxamide (MTIC). MTIC transfers methyl groups to the DNA, including the N^7 and O^6 position of guanine and the O^3 position of adenine. The O^6-methylguanine (O^6-MG) adduct mispairs with thymine during replication, resulting in futile cycles of mismatch repair (MMR) and double-strand breaks (DSBs) (Karran and Bignami, 1994; Karran et al., 1993). Possible results of O^6-MG lesions are prolonged G2/M arrest, cellular senescence, mitotic catastrophe and induction of apoptosis (Friedman et al., 2000; Sarkaria et al., 2008).

The DNA-repair protein O^6-methylguanine DNA methyltransferase (MGMT) removes O^6-MG adducts and thus antagonizes the cytotoxic effect of TMZ. In 2005, Hegi *et al*. demonstrated that patients with an epigenetically silenced MGMT promoter (MGMT-) have an improved clinical outcome (Hegi et al., 2005). Besides MGMT expression, other known mechanisms of TMZ resistance include deficiencies in the MMR pathway, which render cells tolerant to O^6-MG lesions and the base excision repair pathway (BER). Following TMZ treatment, various human glioblastoma cell lines exhibit an increased activity of poly (ADP-ribose) polymerase 1 (PARP1), an enzyme involved in BER. Activated PARP1 recruits DNA repair proteins to DNA lesions including factors of the BER system, DNA ligase III and DNA polymerase (Friedman et al., 1997; Tang et al., 2011).

Regardless of the fact that MGMT represents a major mechanism in TMZ resistance, there are patients profiting from TMZ treatment despite expression of MGMT as well as patients with an epigenetically silenced MGMT promoter showing no response (Gaspar et al.; Hegi et al., 2008). Thus, there must be subpopulations of cells within the tumor that feature additional mechanisms of TMZ resistance and that are capable to induce tumor re-growth (Bao et al., 2006).

7. Aldehyde dehydrogenase 1 A1

Aldehyde dehydrogenase 1 A1 (ALDH1A1) is a member of the human aldehyde dehydrogenase superfamily, a group of $NAD(P)^+$ dependent oxidoreductases that catalyze the oxidation of various aldehydes to their corresponding carboxylic acids. ALDH isoforms are expressed in the cytoplasm, nucleus, mitochondria or peroxisomes of the majority of human tissues including testis, brain, lens, liver, lung and retina (Marchitti et al., 2008; Sladek, 2003). The cytoplasmic isoenzyme ALDH1A1, located on chromosome 9 at 9q21.13, is involved in multiple biological processes such as oxidative stress response (Marchitti et al., 2008), cell differentiation (Chute et al., 2006) and drug resistance (Hilton, 1984; Muramoto et al., 2010). One of its main substrates is retinal, which is irreversibly oxidized to retinoic acid by ALDH1A1, ALDH1A3 and ALDH8A1. Retinoic acid is involved in many biological processes including transcriptional regulation and development.

It acts on nuclear retinoic acid receptor (RAR) and retinoid X receptor (RXR), which bind to DNA as heterodimers and induce expression of genes involved in cell cycle regulation or differentiation (Appel and Eisen, 2003; Zhao et al., 1996) (Figure 7).

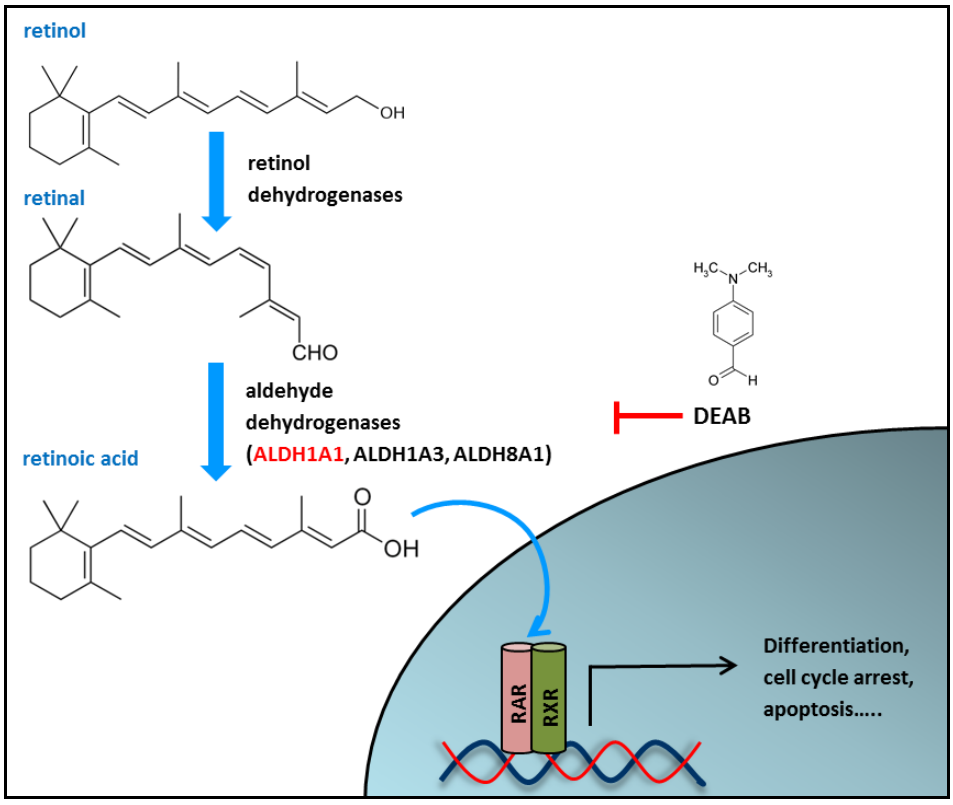

Figure 7: Role of ALDH1A1 in retinoid signaling pathway

Retinol (vitamin A) is oxidized by the retinol dehydrogenase to retinal, the substrate of ALDH1A1. Aldehyde dehydrogenases catalyze the conversion of retinal to retinoic acid, which acts on RAR and RXR. The heterodimer RAR/RXR regulates the expression of genes involved in differentiation and cell cycle control.

Furthermore, ALDH1A1 binds and detoxifies cellular aldehydes derived from peroxidation of membrane lipids. These aldehydes such as malondialdehyde (MDA) and 4-hydroxynonenal (4-HNE) are highly reactive and bind to cellular proteins and DNA, giving rise to etheno-DNA adducts and other toxic aggregates (Brooks and Theruvathu, 2005; Gago-Dominguez et al., 2005). ALDHs were also shown to play a pivotal role in the protection against other DNA-damaging agents such as cyclophosphamide, mitomycin c, or Vp-16 (Colvin et al., 1988; Hilton, 1984; Magni et al., 1996; Pappa et al., 2005).

In particular the ALDH isoenzymes ALDH1A1, ALDH1A3 and ALDH3A1 are described to have a functional role in the expansion and differentiation of normal neural or hematopoietic stem cells (Corti et al., 2006; Muramoto et al., 2010). In 2007, Ginestier *et al.* described ALDH1 as a marker of normal and malignant mammary stem cells. ALDH1 positive breast cancer cells were capable of self-renewal, differentiation and they generated tumors recapitulating the heterogeneity of the parental tumor when xenotransplanted into mice (Ginestier et al., 2007). Since then, the isoenzyme ALDH1A1 was found to characterize tumor stem cells and to correlate with poor clinical prognosis in various solid tumors, including colon carcinoma and prostate cancer (Ginestier et al., 2007; Huang et al., 2009; Li et al., 2010). Recently, we introduced ALDH1A1 as a novel marker for glioblastoma cells with stem cell characteristics (Rasper et al., 2010). Cells expressing high protein levels of this enzyme generated neurospheres, while inhibition of ALDH1A1 led to a significant decrease in sphere formation and clonogenic capacity. In addition, cellular differentiation was observed after treatment of glioblastoma cells with the ALDH1A1 inhibitor 4-diethylaminobenzaldehyde (DEAB).

8. Objective

Despite aggressive therapy, including surgical gross resection and combined radio-chemotherapy with temozolomide, the prognosis of patients with glioblastoma remains poor. Tumor relapse occurs regularly and might be due to therapy-resistant subpopulations of cells that are able to induce tumor re-growth. Data on the predictive value of common genetic alterations found in glioblastomas remain ambiguous. Thus, additional predictive biomarkers and targets for GBM therapy are of highest clinical interest.

To date, alterations in the EGFR/PTEN/PI3K/Akt signaling represent a hallmark in glioblastoma progression; a strong correlation between mutations in this pathway and the expression of stem cell characteristics was found before. Recently, we demonstrated the functional role of ALDH1A1 in the maintenance and expansion of a stem-like phenotype in glioblastoma. One aim of the present investigation was to further characterize the interaction of this cytoplasmic enzyme with pathways involved in the acquisition of stem cell characteristics.

Furthermore, ALDH1A1 is involved in oxidative stress response, differentiation and drug resistance. Strikingly, ALDH1A1 was shown to mediate resistance to treatment with DNA damaging agents in other tumor entities than glioblastoma. Therefore, the second aim of the present project was to analyze the role of ALDH1A1 in mediating chemoresistance and its value as a predictor of clinical outcome in glioblastoma patients.

C. Materials and methods

1. Technical devices

Device	Model	Producer
Cell counter	Casy 1®	SchärfeSytem, Reutlingen Germany
Centrifuges	5471R	Eppendorf AG, Hamburg, Germany
	4K15	Sigma, Deisenhofen, Germany
CO_2 incubator	HERAcell®	Thermo Fisher Scientific Inc, Waltham, MA, USA
DNA Sequencer	Genetic Analyzer 3130	Applied Biosystems GmbH, Weiterstadt, Germany
Electrophoresis cell	Mini-Protean® tetra cell	Bio-Rad Laboratories, Inc., Munich, Germany
Flow cytometer	FACS Calibur™	Becton Dickinson GmbH, Heidelberg, Germany
Gel Imaging System	Eagle Eye™ II	Stratagene, Heidelberg, Germany
Irradiation device	RS225A	Gulmay Medical Ltd., Chertsey , UK
Laboratory scales	Basic	Sartorius, Göttingen, Germany
Magnetic stirrer	RCT basic	IKA®-Werke GmbH & Co. KG, Staufen, Germany
Microplate reader	Asys Expert plus	Biochrom AG, Berlin, Germany
	Infinite F200 PRO	Tecan Group Ltd., Männedorf, Switzerland
Microscopes	Axiovert 25	Carl Zeiss AG, Jena, Germany
	ApoTome	Carl Zeiss AG, Jena, Germany
	Eclipse TS100	Nikon, Düsseldorf, Germany
Microtome	Microm HM 355	Thermo Fisher Scientific Inc, Waltham, MA, USA
pH-meter	EL-30	Mettler-Toledo GmbH, Giessen, Germany
Power Supplies	PowerPac 300	Bio-Rad Laboratories, Inc., Munich, Germany
	PowerPAC HC	Bio-Rad Laboratories, Inc., Munich, Germany
Real-time PCR system	Lightcycler® 480 II	Roche Diagnostics GmbH, Mannheim, Germany
Semi-dry transfer cell	Trans-Blot® SD	Bio-Rad Laboratories, Inc., Munich, Germany
Shaker	Minishaker MS1	IKA®-Werke GmbH & Co. KG, Staufen, Germany
	Orbital Shaker IKA-VIBRAX-VXR	IKA®-Werke GmbH & Co. KG, Staufen, Germany
Spectrophotometers	NanoDrop 2000c	Thermo Fisher Scientific Inc, Waltham, MA, USA

	DU®530	Beckmann, Munich, Germany
Thermal cycler	GeneAmp® PCR System 9700	Applied Biosystems GmbH, Weiterstadt, Germany
	Mastercycler® gradient	Eppendorf AG, Hamburg, Germany
X-ray film processor	Konica SRX-101A	Konica Minolta GmbH, Langenhagen, Germany

2. Chemicals, reagents and cytostatics

Substances	**Abbr.**	**Producer**
4-Diethylaminobenzaldehyde	DEAB	Sigma-Aldrich, Munich, Germany
4-Hydroxynonenal	HNE	Merck KGaA, Darmstadt, Germany
Acetic acid		Carl Roth GmbH + Co. KG, Karlsruhe, Germany
Agarose		Biozym Scientific GmbH, Hessisch Oldendorf, Germany
Amino-n-caprioic-acid		Sigma-Aldrich, Munich, Germany
Ammonium chloride	NH_4Cl	Carl Roth GmbH + Co. KG, Karlsruhe, Germany
Ammoniumperoxosulphate	APS	Carl Roth GmbH + Co. KG, Karlsruhe, Germany
BDBacto™ Peptone	Peptone	Becton Dickinson GmbH, Heidelberg, Germany
BDBacto™ Tryptone	Tryptone	Becton Dickinson GmbH, Heidelberg, Germany
Bovineserumalbumin	BSA	Bio-Rad Laboratories, Munich, Germany
Bromphenol-blue		Sigma-Aldrich, Munich, Germany
Citric acid monohydrate		Carl Roth GmbH + Co. KG, Karlsruhe, Germany
Deferoxamine	DFX	Sigma-Aldrich, Munich, Germany
Diamidino-phenylindole	DAPI	Roche Diagnostics, Mannheim, Germany
Diaminofluoresceindiacetatesolution	DAF2/DA	Enzo Life Sciences GmbH, Lörrach, Germany
DiethylamineNONOate	NONOate	Sigma-Aldrich, Munich, Germany
Dihydroethidium	DHE	Life Technologies, Darmstadt, Germany
Dimethylsulfoxide	DMSO	Carl Roth GmbH + Co. KG, Karlsruhe, Germany
Dimethylformamide	DMF	Carl Roth GmbH + Co. KG, Karlsruhe, Germany
Dithiothreitol	DTT	Sigma-Aldrich, Munich, Germany
Ethanol		Carl Roth GmbH + Co. KG, Karlsruhe, Germany

Ethidium bromide		Sigma-Aldrich, Munich, Germany
Ethylenediaminetetraacetic acid	EDTA	Carl Roth GmbH + Co. KG, Karlsruhe, Germany
Formaldehyde		Carl Roth GmbH + Co. KG, Karlsruhe, Germany
Gelatin Type A		Sigma-Aldrich, Munich, Germany
Glycerol		Carl Roth GmbH + Co. KG, Karlsruhe, Germany
Glycine		Carl Roth GmbH + Co. KG, Karlsruhe, Germany
Hämatoxylin-Eosin	HE	Carl Roth GmbH + Co. KG, Karlsruhe, Germany
Hydrochloricacid	HCl	Carl Roth GmbH + Co. KG, Karlsruhe, Germany
Hydrogen peroxide	H_2O_2	Carl Roth GmbH + Co. KG, Karlsruhe, Germany
Isopropanol		Carl Roth GmbH + Co. KG, Karlsruhe, Germany
Magnesium chloride	$MgCl_2$	Carl Roth GmbH + Co. KG, Karlsruhe, Germany
Magnesium sulfate	$MgSO_4$	Carl Roth GmbH + Co. KG, Karlsruhe, Germany
Methanol		Carl Roth GmbH + Co. KG, Karlsruhe, Germany
Meyer'shemalaun		Carl Roth GmbH + Co. KG, Karlsruhe, Germany
N-Acetyl-L-cysteine	NAC	Sigma-Aldrich, Munich, Germany
Nocodazole		Sigma-Aldrich, Munich, Germany
Nonidet P-40		Sigma-Aldrich, Munich, Germany
Phenylmethylsulfonylfluoride	PMSF	Sigma-Aldrich, Munich, Germany
Phosphate buffered saline	PBS	PAA, Pasching, Austria
Potassium chloride	KCl	Carl Roth GmbH + Co. KG, Karlsruhe, Germany
Propidiumiodid	PI	Sigma-Aldrich, Munich, Germany
Rotiphorese® NF-acrylamide/ bis-acrylamide solution		Carl Roth GmbH + Co. KG, Karlsruhe, Germany
Skimmed milk powder		Merck KGaA, Darmstadt, Germany
Sodium chloride	NaCl	Carl Roth GmbH + Co. KG, Karlsruhe, Germany
Sodium dodecyl sulfate	SDS	Carl Roth GmbH + Co. KG, Karlsruhe, Germany

Sodium hydroxide	NaOH	Carl Roth GmbH + Co. KG, Karlsruhe, Germany
Staurosporin		Sigma-Aldrich, Munich, Germany
Tango™-Buffer		Fermentas GmbH, St. Leon-Rot, Germany
Temozolomide	TMZ	Sigma-Aldrich, Munich, Germany
Tetramethylethylendiamine	TEMED	Carl Roth GmbH + Co. KG, Karlsruhe, Germany
Tris		Carl Roth GmbH + Co. KG, Karlsruhe, Germany
Triton-X-100		Sigma-Aldrich, Munich, Germany
Trypan blue solution		Carl Roth GmbH + Co. KG, Karlsruhe, Germany
Tween-20		Carl Roth GmbH + Co. KG, Karlsruhe, Germany
Xylol		Carl Roth GmbH + Co. KG, Karlsruhe, Germany
Yeast extract		Sigma-Aldrich, Munich, Germany

3. Software

Software	Software producer
Adobe® Photoshop® CS5, *Adobe® Acrobat® X Suite*	Adobe Systems incorporated, San Jose, CA, USA
Axiovision Rel. 4.8.	Carl Zeiss Microscopy, LLC, Thornwood, NY, USA
FlowJo analysis software	Tree Star, Inc., Ashland, OR, USA
GraphPad Prism®	GraphPad Software, La Jolla, CA, USA
NIS Elements F 3.2	Nikon Instruments Inc., Melville, NY, USA
Primer3 program	http://frodo.wi.mit.edu/
SPSS Statistics	IBM Deutschland GmbH, Ehningen, Germany

4. Cell culture

4.1 Consumables and additives

Substances/Materials	Abbreviation	Producer
Accutase		PAA, Pasching, Austria
Akt 1/2 kinase inhibitor	Akti	Sigma-Aldrich, Munich, Germany
B-27® Supplement	B27	Life Technologies, Darmstadt, Germany

Basic Fibroblast Growth Factor, human recombinant	bFGF	Life Technologies, Darmstadt, Germany
Collagenase Type I	CLS I	Biochrom AG, Berlin, Germany
Dulbecco's Modified Eagle Medium GlutaMAX-I, high Glucose	DMEM	Life Technologies, Darmstadt, Germany
Epidermal growth factor	EGF	Millipore, Billerica, MA, USA
Fetal bovine serum	FBS	Biochrom AG, Berlin, Germany
Geneticin	G418	Biochrom AG, Berlin, Germany
Ham's F-12 NutrientMixture	Ham's F-12	Life Technologies, Darmstadt, Germany
KnockOut™ D-MEM		Life Technologies, Darmstadt, Germany
Knockout™ Serum Replacement		Life Technologies, Darmstadt, Germany
Leukemia inhibitory factor, human recombinant	LIF	Millipore, Billerica, MA, USA
L-Glutamine	L-Gln	PAA, Pasching, Austria
MEM Non-Essential Amino Acids	MEM NEAA	Life Technologies, Darmstadt, Germany
Minimum Essential Medium	MEM	Life Technologies, Darmstadt, Germany
Minimum Essential Medium, no phenol red	MEM	Life Technologies, Darmstadt, Germany
N-2 Supplement	N2	Life Technologies, Darmstadt, Germany
Nerve growth factor, recombinant human	NGF	Life Technologies, Darmstadt, Germany
Neubauerhemocytometer		VWR International GmbH, Darmstadt, Germany
Penicillin/Streptomycin	P/S	Biochrom AG, Berlin, Germany
Phosphate buffered saline	PBS	PAA, Pasching, Austria
Puromycindihydrochloride	Puromycin	Sigma-Aldrich, Munich, Germany
Serological pipettes, cell scraper, centrifuge tubes		SARSTEDT AG & Co., Nümbrecht, Germany
Tissue culture dishes/flasks/test plates		TPP Techno Plastic Products AG, Trasadingen, Switzerland

4.2 Buffers and Media

Cell freezing medium	90% FBS, 10% DMSO
DMEM + FBS	DMEM supplemented with 10% (v/v) FBS, 2mM glutamine, 100U/ml penicillin and 100µg/ml streptomycin
Erythrocytes lysis buffer	1.55 M NH_4Cl, 100mM $KHCO_3$, 10mM EDTA, ad 500 ml H_2O

MEM + FBS	MEM supplemented with 15% (v/v) FBS, 2mM glutamine, 100 U/ml penicillin and 100µg/ml streptomycin
Neurobasal medium	Knockout-DMEM and Ham's F12 (1:1) supplemented with 1% penicillin/streptomycin, 2mM glutamine, 10% knockout serum replacement, 1% N2-supplement, 1µg/ml natural mouse laminin, 1% non-essential amino acids, 10ng/ml basic FGF and 50ng/ml EGF
Neurobasal medium + B27	Serumfree DMEM supplemented with 2% (v/v) B27, 2mM L-glutamine, 100U/ml penicillin, 100µg/ml streptomycin, 20ng/ml basic FGF, 50ng/ml EGF, 20ng/ml LIF
Differentiation medium	Knockout-DMEM and Ham's F12 (1:1) supplemented with 1% penicillin/streptomycin, 2mM glutamine, 10% FBS, 2% B27-supplement, 1% non-essential amino acids, 50ng/ml NGF

4.3 Cultivation and cryopreservation of GBM cell lines

The human glioblastoma cell lines LN18 (Ishii et al., 1999) (mutated p53 (mtp53)), G139 (Kraus et al., 1999) (mtp53), LN229 (Ishii et al., 1999) (mtp53) and U87MG (Ponten and Macintyre, 1968) were maintained in Dulbecco's modified Eagle's medium (DMEM) with 10% (v/v) FBS, glutamine and antibiotics under standard cell culture conditions at 37°C and 5% CO_2. T98G (Stein, 1979) (mtp53) glioblastoma cells were provided by Dr. Inge Tinhofer (Charité University Hospital, Berlin, Germany) and were maintained in Minimum essential medium (MEM) supplemented with 15% (v/v) FBS, glutamine and antibiotics. Adherent GBM cells were passaged twice weekly. Therefore, 1.5ml accutase was applied per 10 cm-diameter culture dish for cell detachment.

The human glioblastoma cell line R28 (Beier et al., 2008) was obtained from Dr. Christoph Beier (University Hospital Aachen, Germany) and was cultured in serumfree DMEM supplemented with B27, LIF, FGF and EGF (neurobasal medium + B27). Cultivation under these serumfree conditions preserves the tumors original molecular characteristics and prevents differentiation. R28 cells were passaged 1:2 every 7-10 days. Neurospheres were collected by centrifugation at 150 g for 5 minutes, washed with PBS and dissociated by incubation with accutase for 20 minutes at 37°C. Half of the cell culture medium was changed every 2-3 days.

For cryopreservation, cells were harvested at 70% confluence and dissolved in freezing medium. After gradual freezing in an isopropanol container for 2 days at -80°C, cells were stored at -180°C in liquid nitrogen.

4.4 Primary cell culture

For primary cell culture, freshly resected glioblastoma specimens were obtained with patients' consent according to the TUM medical faculty's guidelines for tissue preservation. Following resection, tumor tissue was stored in sterile serum free cell culture medium at 4°C and was processed within 24 hours. Tumor samples were mechanically dissociated with sterile scalpel blades and consequently enzymatically digested with 2mg/ml collagenase I for 1 - 3 hours. Following dissociation, cells were collected by centrifugation at 200g for 5 minutes and washed once with PBS. If necessary, erythrocytes were lysed with ammonium chloride buffer (erythrocytes lysis buffer). Single cell suspensions were cultured in both supplemented DMEM and neurobasal medium under standard cell culture conditions at 37°C and 5% CO_2.

4.5 Cell authentication and Mycoplasma-test

Authentication of the human cell lines LN18, LN229 and T98G was performed prior to the experiments by analyzing microsatellites with Cell ID™ Systems (Promega Corporation, Madison, USA). Therefore genomic DNA was isolated with QIAamp® DNA Mini Kit (Qiagen, Hilden, Germany). Following purification, 2ng DNA was used as template with Cell ID™ SystemPCR Master Mix. After DNA amplification, nine human loci, including D21S11, TH01, TPOX, vWA, Amelogenin, CSF1PO, D16S539, D7S820, D13S317 and D5S818 were analyzed as described by the manufacturer with capillary electrophoresis. STR (short tandem repeat) genotype was evaluated with GeneMapper® ID software and compared to data available on the ATCC-LGC Standards homepage (LGC Standards, Wesel, Germany).

Prior to the experiments and then every 2-3 months, all cell lines were tested by a nested PCR for mycoplasma infections. Therefore 100µl of the cell culture supernatant was boiled for 5 minutes at 95°C. Following brief centrifugation, 5µl of the supernatant served as template for the first PCR.

The primers, which detect 11 species of mycoplasma (M. fermentans, M. hyorhinis, M. arginini, M. orale, M. salivarium, M. hominis, M. pulmonis, M. arthritidis, M. neurolyticum, M. hyopneumoniae, M. capricolum) and one species ureaplasma (U. urealyticum) were from PCR mycoplasma detection set (TAKARA, Otsu, Japan). The product of the first PCR served as template for the second PCR. Amplification sizes of both PCRs are itemized on the manufacturer's homepage.

Table 1: Nested PCR to test for mycoplasma infections

	1st PCR	2nd PCR
Aqua dest.	12.25µl	16.25µl
10x buffer (15mM Mg^{2+})	2.5µl	2.5µl
dNTPS (1.25mM each)	4.0µl	4.0µl
Primer-Supermix	1.0µl	1.0µl
Taq Polymerase (5.000U/ml)	0.25µl	0.25µl
Template	5µl	1µl
Annealing Temp.	55°C	55°C

4.6 Neurosphere formation and differentiation

To investigate neurosphere formation, cells were grown in serum-free neurobasal medium. R28 cells were maintained in neurobasal medium with B27 as described above (4.2). For non-adherent growth conditions the culture dishes were covered with 0.1% gelatin. Medium was changed every 3 days and neurospheres were split every 7-10 days after dissociation with accutase.

Neurospheres were counted and sized using a Zeiss Axiovert 25 microscope. Spheres derived from R28 cells were analyzed using an Eclipse TS100 microscope. Either spheres per 10 seeded cells or the number of spheres per microscopic field (n=15) were analyzed.

Neural differentiation of GBM neurospheres was performed by growth in differentiation medium supplemented with NGF (4.2). Medium was changed every 3 days and expression of specific markers was analyzed after 10-14 days of cultivation.

4.7 Immunofluorescence

To visualize differentiation, neurospheres were grown adherent on poly-D-lysine/laminin coated glass coverslips (Becton Dickinson, Heidelberg, Germany) for 10 days in differentiation medium. Prior to fixation with 4% formaldehyde/PBS for 30 minutes at room temperature, cells were washed with PBS. Membranes of fixed cells were then permeabilized by incubation with 0.25% Triton X-100/PBS for 10 minutes. Following another washing step with PBS, blocking of unspecific binding sites was performed for 30 minutes with 5% goat serum (Dako Deutschland, Hamburg, Germany) diluted in Dako REAL^{TM} Antibody solution (Dako). Incubation with primary antibodies (anti-GFAP, 1:500; anti-Tuj1, 1:200; anti-GalC, 1:100) was performed overnight at 4°C. Cells were washed stringently with PBS prior to exposure to secondary FITC-labeled antibody (1:100) for 1 hour at room temperature. Following another washing step, nuclei were stained with DAPI (2 mg/ml). After mounting cells with VectaShield mounting medium (Vector Laboratories, Burlingame, CA, USA) coverslips were applied to microscope slides and analyzed with Nikon Eclipse TS100 microscope.

4.8 ALDH1A1 knockdown with shRNA

Knockdown of ALDH1A1 (NM_000689) in LN18, T98G and R28 cells was obtained by transduction with MISSION® shRNA Lentiviral Transduction Particles (Sigma-Aldrich, Munich, Germany). Five different clones were tested (Clone ID: TRCN0000026415, TRCN0000026417, TRCN0000026482, TRCN0000026498, TRCN0000026502). As mock control, MISSION® pLKO.1-puro control transduction particles (Sigma-Aldrich, Munich, Germany) were applied.

First a puromycin killing curve was established to evaluate minimum toxic doses. Therefore $1x10^4$ cells per well were seeded on a 96-well plate and incubated overnight. Then cells were treated in duplicates with increasing concentrations of puromycin (500, 1000, 2000, 4000, 6000, 8000, 10,000ng/ml). Viability of treated cells was checked after three and five days with Cell Proliferation Kit I (MTT assay) (Roche Diagnostics, Mannheim, Germany). Lowest concentration of puromycin, leading to a complete cell killing after 3-5 days was applied for selection of transduced cells.

For transduction, $8x10^3$ cells per well were plated to a 96-well plate and incubated overnight. At a sub-confluent level, fresh medium was added prior to transfection. Lentiviral particles were added drop-wise in duplicates at different multiplicities of infection (MOIs) (MOI 1, 2, 5, 10). Fresh medium without puromycin was added 12-16 hours after transfection and cells were cultured for 24 hours. Then selection with 4µg/ml puromycin started until all non-transfected control cells were dead. Following selection, single cell colonies were analyzed for ALDH1A1 knockdown on mRNA level by relative quantitative real-time PCR and on protein level by Western blot analysis. Positive knockdown clones were maintained in medium supplemented with 4µg/ml puromycin.

4.9 Cellular viability assays

Cytotoxicity of various treatments was estimated with colorimetric Cell Proliferation Kit I (MTT) according to manufacturer's instructions (Roche). MTT, a yellow tetrazole, is reduced to purple formazan crystals by cellular reductases of metabolic active cells. After addition of a DMSO-containing solubilization solution the formazan dye was quantified using a microplate reader. The absorbance at 595nm correlates to the number of viable cells. Untreated control cells served as control for 100% viability.

Prior to plating cells for colony formation assay, viability was analyzed with trypan blue staining. Therefore 20µl cell suspension was mixed with 80µl 0.4% trypan blue solution and counted in a Neubauer-hemocytometer. Trypan blue is a vital stain that does not permeate intact membranes and thus only stains dead cells with a distinctive blue color.

4.10 Colony formation assay

Colony formation assay was performed to evaluate the clonogenic capacity of treated cells. Following treatment with mere TMZ (200, 500µM) and DEAB (300µM) or with TMZ + DEAB, LN18 cells were plated in duplicates on a 6-well plate with a total of 150 or 300 viable cells per well. Following 14 days incubation, colonies were stained applying diff-quick set (Medion Diagnostics, Duedingen, Switzerland) and counted.

4.11 ß-galactosidase staining to analyze senescence of GBM cells

Senescence was analyzed by detection of β-galactosidase activity at pH 6.0. An enlarged cell size and expression of pH-dependent β-galactosidase are symptomatic for senescent cells. The senescence assay was performed with β-galactosidase staining kit according to the manufacturer's instructions (New England Biolabs, Frankfurt, Germany). In brief, cells were fixed and incubated with a staining solution at pH 6.0 containing X-gal. After overnight incubation, development of a blue color indicates hydrolysis of the substrate X-gal by the enzyme β-galactosidase.

5. Western blot analysis

5.1 Buffers and solutions

5x SDS protein sample buffer	312.5mM Tris-Cl pH 6.8, 10% (w/v) SDS, 50% (v/v) glycerol, 250mM DTT, 0.05% (w/v) bromphenol-blue, ad 10ml H_2O
10x SDS running buffer	250mM Tris, 1.92M glycine, 1% (w/v) SDS, ad 500ml H_2O
10x TBS buffer	24.2g Tris, 80.0g NaCl, pH 7.6 with acetic acid, ad 1000ml H_2O
Blocking buffer	1xTTBS + 5% (w/v) skimmed milk powder
Membrane stripping solution	100ml methanol, 100ml acetic acid, ad 1000ml H_2O
Primary antibody solution	1xTTBS
Secondary antibody solution	1xTTBS + 5% (w/v) skimmed milk powder
Transfer buffers	anode I: 300mM Tris, 20% (v/v) methanol, ad 500ml H_2O
	anode II: 25mM Tris, 20% (v/v) methanol, ad 500ml H_2O
	cathode: 25mM Tris, 20% (v/v) methanol, 40mM amino-n-caprioric-acid ad 500ml H_2O
Washing buffer (TTBS)	1xTBS, 0.1% (v/v) Tween-20

5.2 Antibodies

Antibody	Dilution	Producer
Akt rabbit pAb	1:5000	New England Biolabs, Frankfurt, Germany
ALDH1 mouse mAb	1:500	Becton Dickinson GmbH, Heidelberg, Germany
Anti-Human IDH1^{R132H} (clone H09)	1:20 (IHC)	Dianova GmbH, Hamburg, Germany
Anti-mouse HRP-linked pAb	1:10,000	New England Biolabs, Frankfurt, Germany
Anti-rabbit HRP-linked pAb	1:10,000	New England Biolabs, Frankfurt, Germany
Beta III-tubulin (TU-20) mouse mAb	1:1000	New England Biolabs, Frankfurt, Germany
Cleaved PARP (Asp214) rabbit pAb (Human Specific)	1:1000	New England Biolabs, Frankfurt, Germany
EGFR Ab-12 (Cocktail R19/48)	1:2000	Thermo Fisher Scientific Inc, Waltham, MA, USA
EGFR rabbit pAb	1:5000	New England Biolabs, Frankfurt, Germany
GAPDH (clone GAPDH-71.1) mouse mAb	1:50,000	Sigma-Aldrich, Munich, Germany
HIF1A rabbit pAb	1:1000	New England Biolabs, Frankfurt, Germany
MGMT rabbit pAb	1:2500	New England Biolabs, Frankfurt, Germany
PARP rabbit pAB	1:1000	New England Biolabs, Frankfurt, Germany
phospho-Akt (Ser473) rabbit pAb	1:10,000	New England Biolabs, Frankfurt, Germany
phospho-EGFR (Tyr1068)(1H12) mouse mAb	1:2500	New England Biolabs, Frankfurt, Germany
Phospho-GSK-3alpha/beta (Ser21/9) rabbit pAb	1:2000	New England Biolabs, Frankfurt, Germany
phospho-Histone H2A.X (Ser139) rabbit pAb	1:1000	New England Biolabs, Frankfurt, Germany
phospho-mTOR (Ser2448) rabbit pAb	1:1000	New England Biolabs, Frankfurt, Germany
phospho-PTEN (Ser380/Thr382/383) rabbit pAb	1:2500	New England Biolabs, Frankfurt, Germany
PTEN rabbit pAb	1:2500	New England Biolabs, Frankfurt, Germany
Tubulin, beta III isoform, clone TU-20 mAB	1:1000	Millipore, Billerica, MA, USA
α-Tubulin (clone DM1A) mouse mAb	1:20,000	Sigma-Aldrich, Munich, Germany

5.3 Protein isolation

For cell lysis, 10x lysis buffer (New England Biolabs) was diluted in H_2O and supplemented with 1mM PMSF and 1x PhosSTOP Phosphatase Inhibitor Cocktail (Roche). Adherent cells were harvested with a cell scraper after rinsing with PBS; suspension cells were collected by centrifugation and washed. Following 5 minutes incubation with lysis buffer on ice, cell debris was pelleted by centrifugation at 13,000rpm for 10 minutes. The supernatant was transferred to a fresh tube and protein amount was determined by bradford assay containing coomassie® brilliant blue G-250 dye (Bio-Rad Laboratories, Munich, Germany). The coomassie blue dye shifts from 465nm to 595nm when bound to basic and aromatic amino acid residues, especially arginine. Each cuvette was filled with 198µl PBS, 200µl Triton-X-100 (0.01% in PBS), 2µl protein sample and 600µl bradford reagent (1:4 in PBS). Absorption was measured at 595nm with a UV/Vis spectrophotometer. For quantification, a calibration-curve with BSA was established (0, 2, 4, 6, 8µg).

5.4 SDS-PAGE and Western blotting

Following isolation, equal amounts of protein (10µg) were separated by SDS-PAGE. The anionic detergent SDS denatures secondary and tertiary structures based on hydrogen bonds and leads to an equally distributed negative charge of each protein. Disulfide bonds are reduced by dithiothreitol (DTT). Heating the samples for 5 minutes at 96°C with SDS sample buffer further promotes protein denaturation and facilitates SDS binding. The protein mixtures were then separated according to their molecular weight in a discontinuous "Laemmli" system. The stacking gel (5%) contains tris-glycine at pH 6.8 and the running gel (7.5%, 10%, or 12.5%) resolves at a pH 8.8. PageRuler™ plus prestained protein ladder (Fermentas, St. Leon-Rot, Germany) was used as molecular weight marker. Gels for PAGE were either purchased (Mini-PROTEAN TGX Precast Gels; Bio-Rad Laboratories) or prepared as described in Table 2.

Table 2: Preparation of gels for SDS-PAGE

	stacking gel		running gel	
Gel density	5%	7.5%	10%	12.5%
Acrylamide [µl]	836	2540	2660	4200
1M Tris-Cl [µl]	626	3740	2000	3740
aqua dest [µl]	3500	2860	3320	2000
20% SDS [µl]	25	50	50	50
10% APS [µl]	25	50	50	50
TEMED [µl]	10	25	25	25

Separation was done at 200V for 45 minutes with precast gels and at 110V for 1-2 hours with freshly prepared gels. Afterwards, proteins were transferred to a methanol-activated PVDF membrane (Immobilon-P membrane; Millipore, Billerica, MA, USA) in a semi-dry blot system at 225mA for 40 – 90 minutes, depending on the molecular weight of the protein of interest. Blotting paper (Sartorius blotting paper; VWR International, Darmstadt, Germany) was soaked with transfer buffers as stated above. Unspecific binding sites were blocked with 5% skimmed milk powder in TTBS for 1 hour. Incubation with primary antibodies was carried out ON at 4°C in the respective dilution. After a washing step (3x7 minutes, TTBS), the membrane was incubated for 1 hour at room temperature with HRP-conjugated secondary immunoglobulins. Immunoreactivity was visualised by addition of HRP substrate (Immobilon Western Chemiluminescent HRP substrate; Millipore) and exposure to chemiluminescence detection film (Amersham Hyperfilm™ ECL™; GE Healthcare, Munich, Germany). Anti-alpha-tubulin or anti-GAPDH antibodies served as loading controls. Prior to the re-incubation with another primary antibody, membranes were either washed stringently wit 1xTTBS or bound antibodies were removed by incubation in membrane stripping solution. Following 30-60 minutes incubation with stripping solution, unspecific binding sites were again blocked with 5% skimmed milk powder in TTBS.

6. Analysis on mRNA level: RT-PCR and qPCR

6.1 Buffers and solutions

TE-Puffer (1x)	1ml TrisHCl (pH 8.0), 200µl 0.5 M EDTA, ad 1000ml H_2O
RLN buffer	50mMTris-Cl (pH 8.0), 140mM NaCl, 1.5mM $MgCl_2$, 0.5 % (v/v) Nonidet P-40 (1.06g/ml)
10x PCR buffer	200µl Tris-HCl (1M, pH 8.3), 1ml KCl (1M), 2mg Gelatine, ad 2ml H_2O

6.2 RNA isolation and reverse transcription

Total RNA extraction and purification was carried out using RNeasy® Mini Kit (Qiagen). $1x10^6$ cells were harvested, washed with ice-cold PBS and centrifuged at 13,000rpm and 4°C for 1 minute. The pellet was resolved in 175µl RLN buffer, containing the nonionic detergent Nonidet P-40 for lysis of the cell membrane. After 5 minutes incubation, nuclei and cell debris were removed by centrifugation (13,000rpm, 4°C, 2 minutes). The supernatant was quickly mixed with 600µl RLT, a guanidine-thiocyanate–containing lysis buffer which inactivates RNases and 430µl 96% ethanol to ensure binding of RNA to the silica membrane. Purification of the RNA was then performed as described by the manufacturer. Following elution with RNase free water, concentration was measured with the spectrophotometer NanoDrop™ 2000c and RNA was stored at -80°C. An absorbance of 1 unit at 260nm corresponds to 40µg of RNA per ml (A260 = 1 = 40µg/ml).

Following total RNA isolation, reverse transcription of 500ng – 1000ng mRNA into cDNA was performed using SuperScript® II Reverse Transcriptase kit (Life Technologies) and random hexanucleotides (Roche) according to the protocol provided by the producer. Transcribed cDNA was either used for reverse transcriptase PCR (RT-PCR) or real-time quantitative PCR (qPCR).

6.3 Oligonucleotides for RT-PCR and qPCR

Table 3: Oligonucleotide sequences for RT-PCR and qPCR

All primers were designed using Primer3 program;

Gene	Accession-number		Sequence (5' -3')	T_m [°C]	Product-size [bp]	Applic.
ALDH1A1	NM_000689	forw rev	tgttgagcgggctaagaagt gtttggccccttctttcttc	62	134	RT-PCR, qPCR
ALDH1A3	NM_000693	forw rev	tctcgacaaagccctgaagt gtccgatgtttgaggaagga	55	233	RT-PCR
ALDH3A1	NM_000691	forw rev	gcagacctgcacaagaatga gctccgagtggatgtagagc	55	163	RT-PCR
ALDH7A1	NM_001182	forw rev	cgagccaatagcaagagtcc cttcacccacaccttccact	55	218	RT-PCR
ALDH8A1	NM_001193480	forw rev	tggtgagcataggtgctctg caccgtgggaagcataaagt	57	164	RT-PCR
ALDH2	NM_000690	forw rev	acaatggcaagccctatgtc catcacaaccacgtttccag	55	248	RT-PCR
GAPDH	NM_002046	forw rev	tgttccaatatgattccaccca tactcagcgccagcatc	62	145	qPCR
EGFR	NM_005228	forw rev	ggctctggaggaaaagaaag gggcacagatgattttggtc	56	581	RT-PCR
EGFRvIII		forw rev	ggctctggaggaaaagaaag tgatggaggtgcagtttttg	56	1028(wt); 227(vIII)	RT-PCR
MGMT	NM_002412.3	forw rev	cccggatatgctgggacag cccagacactcaccaagtcg	60		Methy-QESD

Table 4: Oligonucleotides for RT-PCR and sequencing of PTEN

Gene	Exon		Sequence (5' -3')
PTEN	5	forw. rev	accgccaaatttaattgcag tagggcctcttgtgccttta
PTEN	6	forw rev	taaaggcacaagaggcccta tcacctttagctggcagacc
PTEN	7	forw rev	cggaacttgcaatcctcagt gcatcttgttctgtttgtggaa
PTEN	8.1	forw rev	ttccacaaacagaacaagatgc tctgcacgctctatactgcaa
PTEN	8.2	forw rev	gcgtgcagataatgacaagg gctagcctctggatttgacg

PTEN	8.3	forw	caggaccgagaggaaacctca
		rev	gctagcctctggatttgacg

6.4 Analysis of various ALDH isoforms on mRNA level

Expression of various ALDH isoforms on mRNA level was analyzed with reverse transcription PCR (RT-PCR) with AmpliTaq Gold® DNA polymerase (Applied Biosystems, Darmstadt, Germany). Annealing temperatures for respective primer pairs are described in Table 3. Following PCR, 10µl product were mixed with 2µl 6x DNA loading buffer and separated on a 1% agarose gel.

Table 5: PCR-mix for RT-PCR of ALDH isoforms

	PCR-mix
H_2O	15.25µl
10x buffer (15mM Mg^{2+})	2.5µl
dNTPS (each 1.25mM)	4.0µl
Forward primer (20µM)	0.5µl
Reverse Primer (20µM)	0.5µl
Taq Polymerase (5/µl)	0.25µl
cDNA (from 500ng RNA)	2.0µl

Table 6: PCR program for RT-PCR of ALDH isoforms

	Temp. [°C]	Duration	
Denaturation:	95	5 min.	single
Denaturation:	95	30 sec.	35 cycles
Primer annealing:	55-62	30 sec.	
Elongation:	72	30 sec.	
Elongation:	72	7 min.	single
Cooling:	4	∞	single

6.5 Optimization of annealing temperatures by gradient PCR

Prior to relative quantitative real-time PCR, a gradient PCR was performed to detect optimum annealing temperatures and to avoid non-specific secondary bands by application of most stringent parameters. LN18 cDNA (from 1µg RNA), diluted 1:50, served as template.

A master-mix containing 10µl SYBR Green I Master® (Roche), 3µl H_2O, 2µl primer mix (each 5µM) and 5µl cDNA per PCR tube was prepared to ensure equal template loading. Finally, gradient PCR was run with gradually increasing temperatures on each position of the thermal cycler. Following PCR, 10µl product were mixed with 2µl 6x DNA loading buffer and separated on a 1% agarose gel. For optimum annealing, the temperature was chosen at which no unspecific bands occurred and a maximum of product was obtained.

Table 7: PCR program for gradient PCR (*Gradient 8)

	Temp. [°C]	Duration	
Denaturation:	94	4 min.	single
Denaturation:	94	30 sec.	34 cycles
Primer annealing:	G=8*	30 sec.	
Elongation:	72	30 sec.	
Elongation:	72	7 min.	single
Cooling:	4	∞	single

6.6 Quantification of ALDH1A1 knockdown by qPCR

SYBR green real time PCR was used for relative quantification of ALDH1A1 expression on mRNA level compared to the housekeeping gene GAPDH. SYBR green is an asymmetrical cyanine dye that intercalates into double-stranded DNA. Fluorescence of the dye is greatly enhanced when bound to DNA. During amplification, increasing amounts of SYBR green molecules bind to newly synthesized DNA. At the end of the elongation step of each cycle, fluorescence is measured to monitor the newly amplified DNA amount. A standard curve for GAPDH and ALDH1A1 was prepared using the LightCycler 480 to calculate PCR efficiencies. Under optimum conditions, the target sequence is doubled in each cycle during the exponential amplification phase, giving an efficiency of 2.0. However, the efficiency of amplification is often variable among primers and templates. In a PCR systems with 90% doubling, efficiency would be 1.9. Therefore a serial dilution of the cDNA was performed to create a standard curve (1:4 in six steps). The slope of the linear regression determines the efficiency of amplification. The efficiency for ALDH1A1 and GAPDH amplification was 1.6.

Relative quantification was carried out using the LightCycler 480. A master-mix with 6µl H_2O, 1µl primer-mix (each 20µM) and 10µl SYBR green mix per sample was prepared. Each sample was measured in duplicates with 3µl cDNA (from 1µg RNA; 1:2 dilution) as template. An initial denaturation for 5 minutes at 95°C was followed by 46 cycles of 95°C for 15 s, 62°C for 20 s and 72°C for 10 s (single; fluorescence detection). Melting point analysis was performed by heating the PCR products from 50 to 95°C with an increase of 0.2°C/s while fluorescence was monitored continuously.

The quality of ALDH1A1 knockdown was calculated from the differences of the ct-values from wild-type cells and knockdown (or mock) cells normalized to GAPDH according to the formula:

$$Knockdown\ (\%) = 100 - \left(\frac{E(ALDH1A1)^{ct_{wt} - ct_{knockdown}}}{E(GAPDH)^{ct_{wt} - ct_{knockdown}}} \times 100 \right)$$

$$= 100 - \left(\frac{E^{\Delta ct_{ALDH_1A_1}}}{E^{\Delta ct_{GAPDH}}} \times 100 \right)$$

ct: cycle threshold; E: PCR efficiency

7. Quantification of MGMT promoter methylation

Quantification of MGMT promoter methylation was assessed by a specific relative quantitative real-time PCR technique named MethyQESD, as described by Bettstetter *et al.* (Bettstetter et al., 2008). In principle, the MGMT promoter DNA was digested with the methylation-sensitive endonuclease Hin6I, which exclusively cuts unmethylated CGCG recognition sites (methylation-quantification digestion, MQD) and the methylation independent endonucleases *Xba*I and *Dra*I (methylation independent calibrator digestion, CalD). Following digestion, the MGMT promoter methylation status was determined by relative quantitative real-time PCR.

Genomic DNA from cell culture or FFPE tissue samples was isolated with QIAamp® DNA Mini Kit (Qiagen). For each sample, 7µl DNA (1–300ng/µl) were digested overnight at 37°C in a total volume of 20µl 1xTango™-Buffer with 30U Hin6I and XbaI/DraI (Fermentas; each 15U), respectively.

Table 8: Digestion mix for quantification of MGMT promoter methylation

	MQD	CalD
DNA	7.0µl	7.0µl
10x Tango-buffer	2.0µl	2.0µl
Hin6I; XbaI/DraI (10U/µl)	3.0µl	3.0µl
H_2O	8.0µl	8.0µl

Prior to methylation specific real-time PCR, the restriction enzymes were inactivated by incubation at 75°C for 15 minutes. Digested DNA was stored at 4°C. Both, the methylation quantification batch and the calibrator DNA were used for PCR in duplicates. The applied primers flank the Hin6I sites of interest, so that only indigested hypermethylated DNA is amplified. XbaI and DraI have no restriction sites within the amplicon, so that 100% of the DNA is amplified. Digested DNA of methylation-positive U87MG cells served as control for positive methylation; digested DNA of non-methylated blood DNA was used as a control for 0% methylation. Real-time PCR was carried out using the LightCycler 480 with 3µl digested DNA in a total volume of 20µl, containing 1µM of each primer and 10µl SYBR Green master mix.

The master-mix was distributed to a Lightcyler 480 multiwell plate 96 (Roche). Prior to covering plates with adhesive foil, 3µl of each digestion (MQD/CAlD) was added in duplicates. An initial denaturation for 5 minutes at 95°C was followed by 46 cycles of 95°C for 10 s, 60°C for 17 s, 72°C for 10 s and 84°C for 1 s. Melting point analysis was performed by heating the PCR products from 50 to 95°C with an increase of 0.2°C/s while fluorescence was monitored continuously.

The proportion of methylated template was calculated from the differences of the ct-values from the CalD and MQD (=ΔC_t) according to the formula: methylation (%) =$E^{\Delta C}{}_t \times 100$ (E: PCR efficiency). The cut-off for MGMT positive and MGMT negative tumors was determined by analysis of martingale residuals (Therneau TM, 1990). Tumor tissues with ≤ 20% MGMT promoter methylation were considered to be MGMT positive; specimens with > 20% MGMT promoter methylation were referred to as MGMT negative.

8. Immunohistochemical analysis of ALDH1A1 and IDH1^{R132H} expression

8.1 Buffers and solutions

Citrate buffer pH 6.0	2.1g citric acid monohydrate, pH 6.0 with NaOH, ad 1000ml H_2O
10x Tris buffer	60.5g Tris, 90g NaCl, pH 7.6 with HCl, ad 1000ml H_2O

8.2 Immunohistochemistry and patient characteristics

Immunohistochemical (IHC) analysis of ALDH1A1 expression on primary surgical specimens of seventy patients diagnosed as primary glioblastoma (WHO IV (Louis et al., 2007)) was performed on FFPE (formalin fixed paraffin embedded) tissue. The specimens were collected with patients' consent (according to the TUM medical faculty's guidelines for tissue preservation) at the Klinikum rechts der Isar, Technische Universität München (RDI, TUM) (n=55) and the Berufsgenossenschaftliche Klinik Murnau (n=15). Only GBM patients surviving at least two months after surgical resection and receiving adjuvant therapy were included (median survival was 16.6 months). Fifty of these patients received radiotherapy plus concomitant and adjuvant temozolomide as described by Stupp *et al*. (Table 9) (Stupp et al., 2005).

The tissue was sectioned 2-mm thick and deparaffinized. A citric acid based buffer (pH 6.0) was used for epitope unmasking. Following a washing step with Tris buffer (pH 7.6) for 5 minutes, endogenous peroxidase was quenched with 3% H_2O_2 for 15 minutes at room temperature. Blocking with Avidin/Biotin blocking kit (Vector Laboratories, Inc., Burlingame, CA, USA) for 15 minutes was performed to minimize non-specific staining resulting from endogenous avidin-biotin activity. Non-specific binding sites were blocked with 5% normal goat serum, diluted in Dako REAL^{TM} antibody solution. Each tissue section was incubated with 200µl primary ALDH1A1 antibody, diluted in Dako antibody solution (1:500) ON at 4°C. Detection was performed with Dako REAL^{TM} Detection System, Peroxidase/DAB+, Rabbit/Mouse (Dako). First, biotinylated secondary antibody was applied for 15 minutes in a humidified chamber at room temperature, followed by 15 minutes incubation with streptavidin peroxidase antibody. Finally, tissue slides were incubated with DAB chromogen working solution for 4 minutes and counterstained with Meyer's hemalaun.

Liver tissue served as positive control for ALDH1A1 expression. Four squares per FFPE sections were counted and averaged by Julian Teufel. ALDH1A1 positive cells were presented as percentage of total cell number. IHC staining of ALDH1A1 was performed by Julian Teufel and Ingrid Hoepner (Institute of Pathology, Technische Universität München). IHC staining of isocitrate dehydrogenase 1 (IDH1) with R132H point mutation (clone H09) was performed with an automated staining system to verify diagnosis as primary GBM (Nobusawa et al., 2009). The cut-off for ALDH1A1 high and ALDH1A1 low tumors was determined by analysis of martingale residuals (Therneau TM, 1990). Tumor tissues with ≤ 10% positive cells were considered to be ALDH1A1 low, specimens with > 10% ALDH1A1 positive cells were referred to as ALDH1A1 high.

Table 9: Characteristics of seventy primary surgical specimens of glioblastoma patients

*Patients receiving therapeutic regimen as described by Stupp *et al.* (Stupp et al., 2005); **Resection plus radiotherapy, radiotherapy and concomitant TMZ or adjuvant TMZ; ***Age of the patients when diagnosed;

	Total	**MGMT**				**ALDH1A1**			
		Methylation		**No methylation**		**≤ 10 %**		**> 10 %**	
	no.	**no.**	**%**	**no.**	**%**	**no.**	**%**	**no.**	**%**
Patients	70	17	24.3	53	75.7	42	60	28	40
Treatment									
standard*	50	13	18.6	37	52.9	33	47.1	17	24.3
others**	20	4	5.7	16	22.9	9	12.9	11	15.7
Sex									
male	50	13	18.6	37	52.9	31	44.3	19	27.1
female	20	4	5.7	16	22.9	11	15.7	9	12.9
Age*(years)**									
≤ 60	28	7	10	21	30	21	30	7	10
61-70	27	6	8.6	21	30	14	20	13	18.6
> 70	15	4	5.7	11	15.7	7	10	8	11.4

9. Analysis of cell cycle distribution

In order to explore the impact of TMZ on ALDH1A1 negative or knockdown cells, cellular DNA content was analyzed flow cytometrically. Determination of DNA content by staining with propidiumiodid (PI) provides information about their stage of proliferation. Cell nuclei contain different amounts of DNA in the cell cycle phases G0, G1, S, G2 and M. During G1 phase, cells feature two complete sets of chromosomes (2N). During S Phase, DNA is synthesized and DNA amount is intermediate between G1 and G2. In G2 phase, doubled DNA content defines a tetraploid stage (4N). Following RNA and protein synthesis, G2 phase culminates in mitosis (M phase). Regarding DNA amount, G2 and M phase are indistinguishable. Finally 2N daughter cells either continue cell cycle or enter a resting G0 stage. Cells in G0 are either quiescent or senescent and DNA content corresponds to cells in G1 phase. Thus cell cycle stages G0/G1, S and G2/M may be defined by PI staining and flow cytometric analysis. Apoptotic cells with fragmented DNA appear as subG1 population.

DNA quality control particles (Becton Dickinson) were applied to verify doublet discrimination function. CEN particles are made of chicken blood and contain single nuclei, doublets triplets and some larger aggregates. CTN particles provide nuclei in all cell cycle phases. Doublets of G0/G1 nuclei can be discriminated from true G2/M singlets by pulse processing. Cells treated with 1µM nocodazol and 1-10µM staurosporin served as positive control for G2/M arrest and apoptosis. Nocodazol, an inhibitor of microtubule polymerization interferes with mitotic spindle formation and thus blocks cells in G2/M. The alkaloid staurosporin induces apoptosis by interaction with ATP-binding sites of various cellular kinases. Following treatment with TMZ, DEAB or a combination of both, cells were cultivated for 48 or 72 hours, harvested and adjusted to $1x10^6$ cells per tube. After a washing step with PBS, cells were fixed with 70% methanol and 30% PBS on ice for at least 1 hour. After fixation, cells were washed twice with PBS and RNA was digested with 100µg/ml RNase A for 20 minutes at 37°C in PBS (470µl PBS + 5µl RNase A (10mg/ml); V=475 µl). Staining was performed by addition of 50µg/ml PI (V=500 µl). Cell cycle was analyzed with a FACSCalibur flow cytometer with 10,000 events per determination. Fluorescence signals were detected with FL3 laser and linear gain settings.

Pulse processing was performed with FL3-Width (FL3-W) on X-axes and FL3-Area (FL3-A) on Y-axes; fluorescence intensity/DNA content was measured with FL3-Hight (FL3-H) histogram. Doublet discrimination and analysis of cell cycle distribution was performed with FlowJo analysis software.

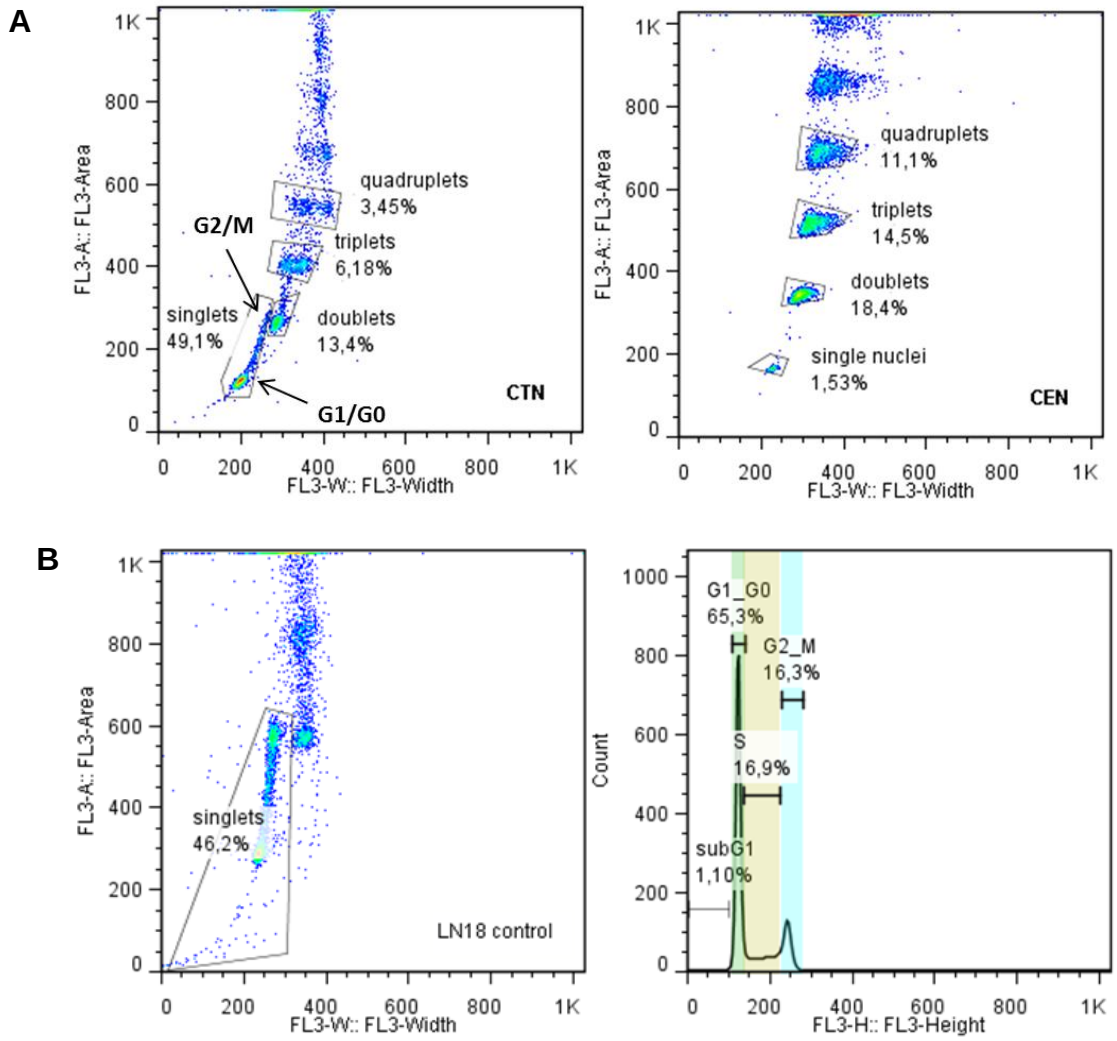

Figure 8: Cell cycle analysis with DNA quality control particles and LN18 cells

A, DNA quality control particles (Becton Dickinson) were applied to verify doublet discrimination function. CEN particles contain single nuclei, doublets triplets and some larger aggregates; CTN particles provide nuclei in all cell cycle phases. B, Representative pseudo-color dot-plot with pulse processing (left) and representative histogram of LN18 single cells, showing a subG1 fraction and cell cycle phases.

10. Analysis of nitric oxide and superoxide formation

To analyze oxidative stress following treatment with temozolomide, staining with DAF2/DA and dihydroethidium (DHE) was performed. DAF2/DA is a cell permeable fluorescent detector for nitric oxide (NO) (Ex_{max}495nm; Em_{max} 515nm). NONOate (10, 100µM) was used as positive control for nitric oxide in solution. The superoxide indicator DHE exhibits blue-fluorescence in the cytosol. After intracellular oxidation by superoxide radicals it intercalates with cellular DNA, staining the nucleus fluorescent red. H_2O_2 (100, 300µM) served as positive control for DHE staining. Cells were seeded at a density of $1x10^4$ cells per well on a 96 well plate and incubated ON. Prior to treatment with TMZ (200, 500µM), H_2O_2 or NONOate, medium was changed to MEM without phenol red and FBS. After the indicated incubation time (1 or 4 hours), cells were stained with 10µM DHE or 5µM DAF2/DA for 30 minutes at 37°C in MEM without FBS and phenol red. Following staining, cells were washed once and covered again with 100µl serumfree MEM. Fluorescence was measured with a fluorescent microplate reader (Infinite F200 PRO), with excitation and emission wavelengths set at 485 and 535nm (± 20nm) for DAF2/DA and at 535 and 635 (± 20nm) for red fluorescence after DHE staining. Fluorescence following staining with DAF2/DA and DHE was also analyzed by fluorescence microscopy with respective filters.

11. ALDH1A1 expression under hypoxic conditions

To analyze ALDH1A1 expression under hypoxia, cells were seeded to 10 cm-diameter culture dishes and incubated ON under standard cell culture conditions. To achieve hypoxic conditions, sub-confluent cells were placed into air-tight aluminum chambers at 37°C, connected to a vacuum pump and a gas cylinder containing a mixture of 95% N_2 and 5% CO_2. By alternating 11 times between oxygen evacuation and N_2 inflow, an oxygen concentration below 0.66% was reached after 22 minutes. Following incubation under hypoxia for 6 hours, proteins of hypoxic cells and normoxic control cells were isolated and analyzed for ALDH1A1 and HIF1A expression. Additional to real hypoxia, deferoxamine (DFX), a hypoxia-mimetic agent was applied. The iron chelator DFX inhibits prolylhydroxylases (PHDs) through the chelation of Fe^{2+} bound to the active site of PHD.

PHD hydoxylates conserved proline residues of HIF1A and marks it for ubiquitination and degradation under normoxic conditions. Under hypoxic conditions and after addition of DFX, PHDs are inhibited and the transcription factor HIF1A is stabilized.

12. Irradiation of GBM cell lines

To evaluate the impact of ALDH1A1 expression on resistance to irradiation, cells were seeded on 6-cm-diameter culture dishes ($5x10^5$ cells). Following incubation under standard cell culture conditions for 24 hours, cells were irradiated with 2 or 4 Gray (Gy) with RS225A irradiation device (Gulmay). Irradiation with X-rays (15mA, 200kV) was performed with a dose rate of 1Gy per 1.07 minutes. ALDH1A1 was inhibited by addition of 300µM 1 hour prior to irradiation. Following X-ray exposure and cultivation for 48 hours, cell cycle was analyzed by PI staining.

13. Cloning of EGFR constructs and ALDH1A1 into mammalian expression vectors

In order to analyze the role of EGFR alterations on a stem-like phenotype, EGFR constructs were cloned into mammalian expression vectors. The cDNA of dominant negative EGFR-CD533 was obtained from Prof. Dr. Axel Ullrich (Max Planck institute of Biochemistry, Martinsried, Germany). The constitutive active EGFRvIII variant in the mammalian expression vector pHβ Apr-1-neo was provided by Darell D. Bigner, MD, PhD (Duke University, Durham, NC, USA).

EGFR-CD533 is a variant with deletion of 533 C-terminal amino acids and thus missing the cytoplasmic part including tyrosin kinase domain (Livneh et al., 1986). The cDNA was present in pRK5RS/pLSX-NA8 via XbaI sites. Contrary to the sequence with accession number NM_005228, this cDNA contains no HindIII restriction site at position 1804-1809 (Ullrich et al., 1984). EGFR-CD533 cDNA was sub-cloned into pCDNA^{TM}3.1(-) (Life Technologies) for expression in eukaryotic cell lines. The mammalian expression vector pCMV6-AC carrying ALDH1A1 gene (NM_000689.3) was purchased from OriGene (OriGene Technologies, Rockville, MD, USA).

13.1 Media, buffers and solutions

LB medium	1% peptone (10 g), 0.05% yeast extract (5 g), 10 g NaCl, ad 1000 ml H_2O; sterilization and storage at 4°C
LB + Kan	5 mg Kan per 100 ml sterile LB-Medium
LB + Amp	7.5 mg Amp per 100 ml sterile LB-Medium
LB agar plate	1.5 mg agar per 100 ml LB-medium
S.O.C. medium	2% tryptone (10g), 0.05% yeast extract (2.5g), 10mMNaCl (0.3 g), 2.5 mMKCl (0.9 g), 10mM $MgCl_2$(1.02g), 10mM $MgSO_4$ (1.07 g) ad 500 ml H_2O; sterilization and addition of 20 mM glucose
Plasmid preparation	Solution 1: 50mM glucose (0.45 g), 25 mMTris (0.15 g), 10 mM EDTA (0.15 g) ad 50 ml H_2O; sterilization and storage at 4°C; addition of RNase prior to use (1 µg/ml) Solution 2: 0.2 M NaOH /1ml 1M NaOH), 1% SDS, ad 50ml H_2O; sterilization and storage at 4°C (max. 1 month) Solution 3: 3 M potassium acetate (30 ml 5M), 5.75 ml 100% acetic acid, ad 50 ml H_2O; sterilization and storage at 4°C

13.2 Preparation of plasmid stocks

First, a plasmid stock for each construct was prepared by transformation of MAX Efficiency® DH5α™ Competent Cells (Life Technologies). Transformation was carried out as described by the manufacturer in S.O.C. medium. Transformed bacteria were plated on LB plates supplemented with either kanamycin (EGFRvIII in pHβ Apr-1-neo) or ampicillin (EGFR-CD533 in pRK5RS/pLSX-NA8; pCDNA3; pCMV6-AC/ALDH1A1). Following overnight incubation at 37°C, single colonies were transferred to 2-5ml LB medium (+ antibiotics) and were grown ON shaking at 37°C. Plasmid preparation was performed with Miniprep-Plasmid-Kit (Seqlab Laboratories, Göttingen, Germany). Following elution with TE buffer, concentration was measured with a spectrophotometer. An absorbance of 1 unit at 260nm corresponds to 50µg of DNA per ml (A260 = 1 = 50µg/ml).

13.3 Restriction digest

Both, pCDNA3 target vector and EGFR-CD533cDNA were digested with the restriction enzyme XbaI (Roche) for sub-cloning. Following digestion for 2 hours at 37°C, the enzyme was inactivated for 20 minutes at 65°C. Digested DNA and linearized plasmids were stored at -20°C.

Restriction digestion:

Plasmid (500ng/µl)	5µl
Restriction enzyme (10U/µl))	1µl
10xbuffer	2µl
H_2O	ad 20µl

For preparative agarose gel electrophoresis, 8 x 2.5µg digested vector DNA were separated by electrophoresis through a 1% agarose gel containing ethidium bromide. Respective bands were excised with a scalpel under UV light and gel slices were purified with QIAquick® Gel Extraction Kit (Qiagen). Concentration of the digested DNA was estimated by loading to an agarose gel with GeneRuler™ 1 kb Plus DNA Ladder (Fermentas).

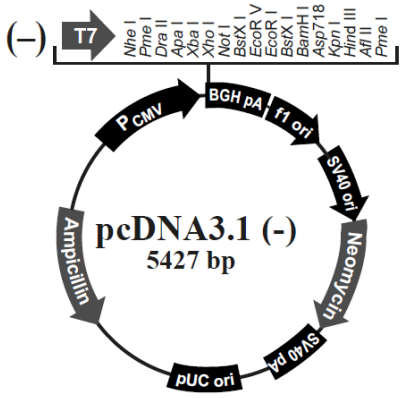

Figure 9: Scheme of pcDNA3.1(-) plasmid

13.4 Dephosphorylation of pCDNA3

In order to prevent self-ligation of the linearized and purified vector pCDNA3, 5' ends of DNA were dephosphorylated with rAPid Alkaline Phosphatase (Roche). Therefore 250ng of plasmid DNA were incubated with alkaline phosphatase for 10 minutes at 37°C followed by heat-inactivation of the enzyme for 2 minutes at 75°C.

Dephosphorylation mix:

Plasmid	250ng
Alkaline phosphatase	1µl
10xbuffer	2µl
H_2O	ad 20µl

13.5 Ligation of excised constructs and linearized pCDNA3

Ligation of EGFR-CD533 cDNA and XbaI linearized pCDNA3 was carried out with T4 DNA ligase (Life Technologies) for 1.5 hours at room temperature. The insert-vector ratio was calculated with the following formula:

$$ng_{Insert} = \frac{ng_{vector} \times kb_{Insert}}{kb_{vector}} \times 5$$

Ligation mix:

Vector DNA	25ng
Insert	x ng
5xbuffer (with ATP)	4µl
T4 DNA Ligase	1µl
H_2O	ad 20 µl

13.6 Transformation of competent E.coli

Transformation was performed with DH5α™ competent cells. Therefore 2µl of the plasmid ligation product were mixed with 50µl competent bacteria. Following incubation on ice for 30 minutes, competent cells were exposed to heatshock (42°C) for 45 seconds and incubated for 1 hour at 37°C and 225rpm in 900µl pre-warmed S.O.C. medium.

A volume of 200µl transformed DH5α™ competent cells was plated to pre-warmed LB + Amp plates and incubated ON at 37°C. LB plates with grown colonies were stored at 4°C. Single colonies were picked, transferred to 3ml LB + Amp and incubated ON at 37°C and 180 rpm.

13.7 Plasmid preparation to check for positive clones

Extrachromosomal DNA was isolated to select for plasmids carrying the insert. The overnight cultures (1.5 – 3ml) were collected by centrifugation for 1 minute at 13,000 rpm. The pellet was resuspended in 150µl of solution 1 supplemented with RNase A. After addition of 150µl lysis buffer (solution 2), the suspension was mixed head-over-head. Following neutralization with solution 3, 1ml 96% ethanol was added and the suspension was centrifuged for 10-15 minutes at 15,000g. The supernatant was removed and the dry pellet was resuspended in 50µl TE buffer. Purified plasmids were tested for correct insert orientation by control digestion. The construct pCDN3/EGFR-CD533 was digested with EcoRI (Roche) resulting in two fragments of ~1705 bp + ~5681 bp for inserts in right orientation and ~332 bp + ~7045 bp for inserts in wrong direction.

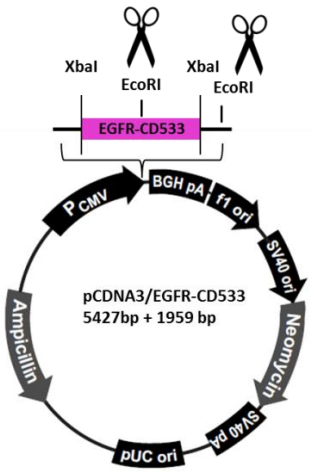

Figure 10: Scheme of EGFR-CD533 insertion via XbaI into pCDNA3

Correct insert orientation was tested by digestion with EcoRI.

Plasmid DNA of positive bacterial clones for transfection of eukaryotic cells was purified with Seqlab Miniprep-Plasmid-Kit.

Right orientation of inserts was further analyzed by sequencing of pCDN3/EGFR-CD533 construct with primers flanking the multiple cloning site on the DNA sequencer Genetic Analyzer 3130. Primer sequences were: T7 (forward), 5'-taatacgactcactataggg-3' and BGH (reverse), 5'-tagaaggcacagtcgagg-3'.

13.8 Stable transfection of eukaryotic cells

LN18 cells were transfected with mammalian expression vectors carrying ALDH1A1, EGFR-CD533 or EGFRvIII with the transfection reagent lipofectamine™ (Life Technologies) in Opti-MEM® medium on a 6-well dish. Cells were seeded 24 hours prior to transfection at a density of $1x10^5$ cells per well. Plasmid DNA (5µg) and transfection reagent (20µl) were mixed with 100µl Opti-MEM. Following incubation at RT for 35 minutes, diluted lipofectamine was added to the diluted plasmid. After 10 minutes at RT to allow for complex formation, LN18 cells were washed once with pre-warmed medium and transfection complexes were added in a total volume of 2ml Opti-MEM per well. Cells transfected with empty pCDNA3 plasmid, carrying neomycin/G418 resistance gene, served as mock control. Following ON incubation, medium was changed to DMEM + FBS. Selection with G418 started 48 hours after transfection. Therefore LN18 cells were transferred to a 10 cm-diameter dish with DMEM + 1mg/ml G418. Medium was changed twice weekly until all non-transfected control cells were dead. Single cell colonies were picked and transferred to a 12-well dish for further characterization.

Expression of wild-type EGFR (EGFRwt) and EGFR-CD533 on mRNA level was analyzed by RT-PCR. Amplification with EGFRvIII oligonucleotides (Table 3) resulted in a 1028bp band in case of expression of EGFRwt and a 227bp band after successful transfection with EGFRvIII plasmid. Western blot analysis with an EGFR antibody (Cocktail R19/48; Thermo Fisher Scientific, Waltham, MA, USA) specific to epitopes of extracellular and intracellular domain, allowed for discrimination between cells expressing only wild-type receptor (170kDa) and cells additionally featuring mutated EGFRvIII (140kDa) or truncated EGFR-CD533 (110kDa) on protein level. Positive single cell-clones were maintained in supplemented DMEM with 0.5mg/ml G418.

14. Statistical analysis

Differences between the results of experimental treatment as well as of average neurosphere size and number were assessed by one-way ANOVA followed by Bonferroni post-test with GraphPad Prism. Differences were approved as significant at values of $p < 0.05$ (* $p < 0.05$, ** $p < 0.01$, ***$p < 0.001$). If not further stated, all experiments were performed at least three times.

Patient data were analyzed with SPSS software program by the Institute of medical statistics and epidemiology, RDI, TUM. Kaplan-Meier models were applied to examine survival curves. Differences between the groups were analyzed using the log-rank (Mantel-Cox) test. Multivariate analysis using Cox's regression was applied to demonstrate that ALDH1A1 is an independent predictive factor. Single variables were age, sex, therapeutic modality and MGMT status.

D. Results

1. ALDH1A1 expression in primary and established glioblastoma cell lines

The ALDH1A1 status of primary and established GBM cell lines was assessed by Western blot analysis. All primary cell lines were collected with patient's consent from tumors diagnosed as astrocytomas WHO grade III and IV (Louis et al., 2007) and are referred to as "T#" in the following. Cells derived from freshly resected tumor tissue were cultured either in DMEM + FBS or under serum free conditions in neurobasal medium. From twenty analyzed primary tissue cultures, eleven showed high levels of ALDH1A1 including T30, T39 and T40, four expressed moderate levels and five were negative including T16 (Figure 11, 12). As we described recently (Rasper et al., 2010), expression of the cytosolic enzyme ALDH1A1 and the neuron specific marker beta-III-tubulin (Tuj1) correlated negatively: most cells showing high levels of ALDH1A1 featured low-level Tuj1 and vice versa (Figure 11 A).

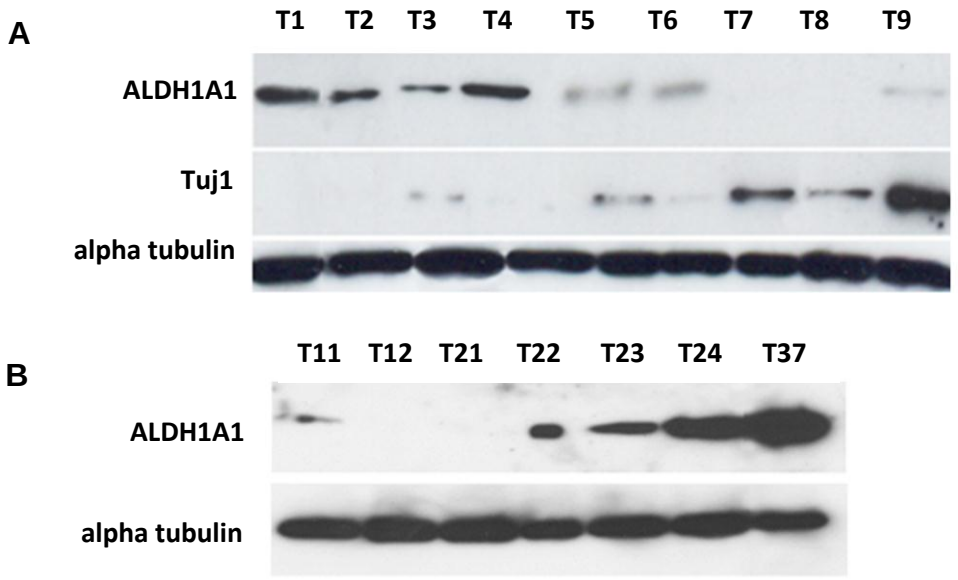

Figure 11: Western blot analysis of ALDH1A1 and Tuj1 levels in primary GBM cells

A, ALDH1A1 and Tuj1 levels of nine primary human GBM cell lines; ALDH1A1 and Tuj1 levels correlated negatively. B, Further primary GBM cell cultures were analyzed for ALDH1A1 expression.

To explore the role of this cytosolic enzyme in human GBM, six ALDH1A1 positive and three ALDH1A1 negative primary and established cell lines were used for further experiments (Figure 12). LN18, T98G, T30, T39, T40 and R28 cells express high levels of ALDH1A1 (ALDH1A1+) while T16, LN229 and G139 are negative for this enzyme (ALDH1A1-).

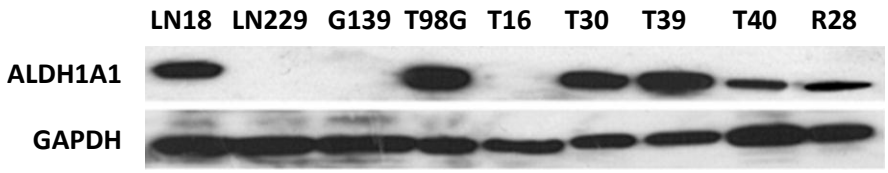

Figure 12: Western blot analysis of ALDH1A1

ALDH1A1 protein expression in primary (T39, T16, T30, T40 and R28) and established GBM cell lines (LN18, G139, T98G) was analyzed by Western blotting.

R28 cells are permenantly maintained in neurospheres and highly express the neural stem cell marker CD133 (Beier et al., 2007). This ALDH1A1 positive cell line could be differentiated into all three neural lineages by cultivation in differentiation medium for 10 days, as indicated by expression of GFAP (astrocytic lineage), Tuj1 (neuronal lineage) and GalC (oligodendroglial lineage) (Figure 13).

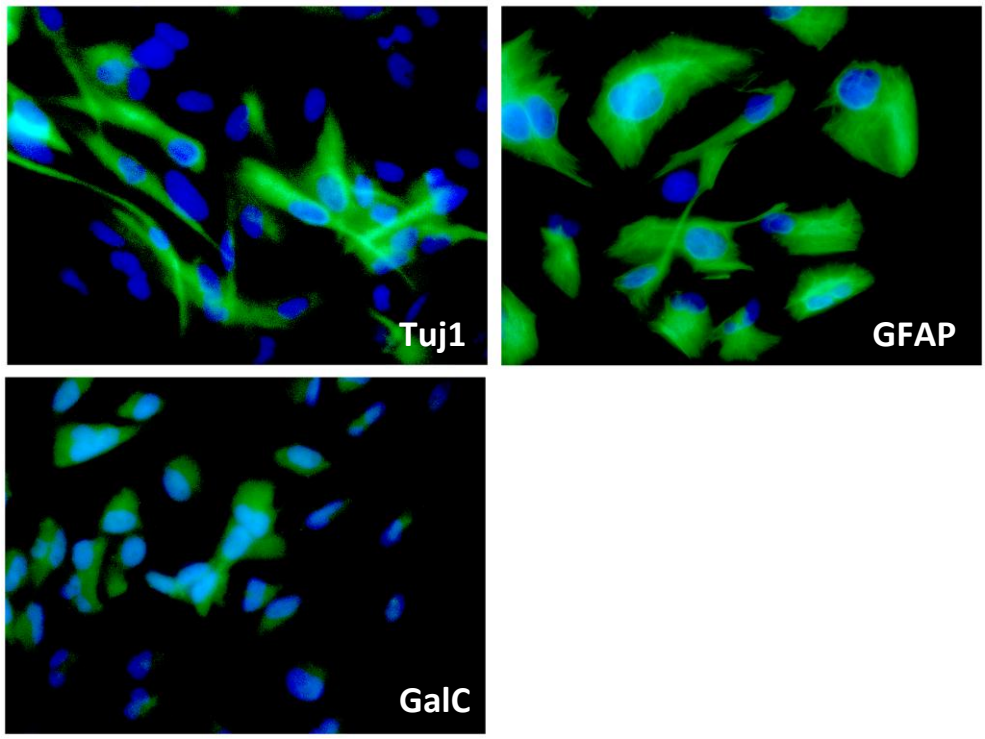

Figure 13: Immunofluorescence of R28 cells in differentiation medium

Expression of Tuj1, GFAP and GalC was determined following cultivation in differentiation medium.

The human ALDH1 superfamily is a group of highly conserved enzymes. The isoforms ALDH1A1, ALDH1A3 and ALDH8A1 have retinoic acid as their preferred substrate. The isoenzymes ALDH1A1, ALDH1A3 and ALDH3A1 are associated with cancer stem cells.

To ensure specificity of the applied antibody for the isoform ALDH1A1, expression of ALDH1A3, ALDH3A1, ALDH7A1, ALDH8A1 and ALDH2 was analyzed on mRNA level by RT-PCR (Figure 14). Mitochondrial ALDH2 and ALDH7A1 were expressed ubiquitously. ALDH8A1 was only expressed by T39, T16 and T30 cells. Isoform ALDH1A3 was not detectable in LN18 cells, while no ALDH3A1 mRNA was expressed by LN229. T16 cells for instance featured all tested isoforms on mRNA level apart from ALDH1A1 and displayed no reactivity with anti-ALDH1A1 antibody in Western blot analysis. The diverse expression pattern of various ALDH isoenzymes in GBM cell lines revealed specificity of the applied antibody to ALDH1A1.

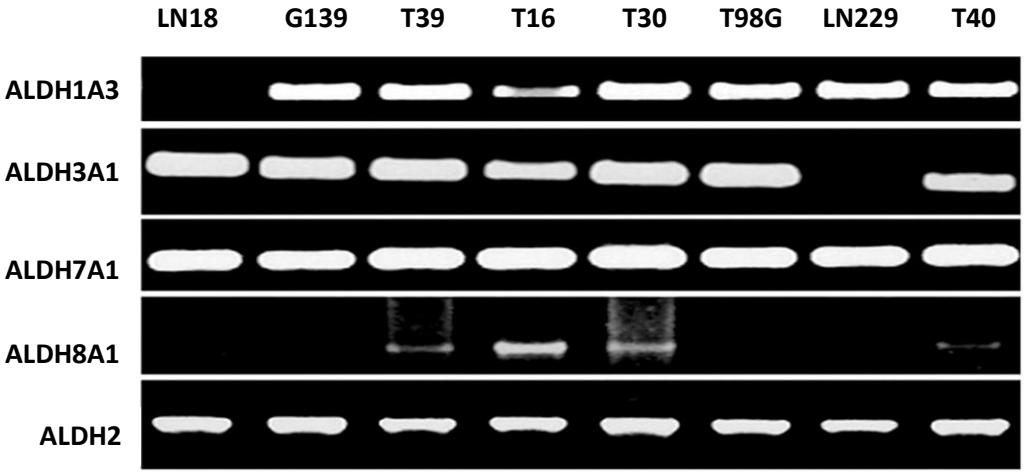

Figure 14: Analysis of ALDH isoforms in GBM cell lines by RT-PCR

2. Stable and specific knockdown of ALDH1A1 in glioblastoma cell lines by shRNA transduction

Stable knockdown of ALDH1A1 in LN18, T98G and R28 cells was obtained by transduction with shRNA lentiviral transduction particles. The clones ID TRCN0000026415 and TRCN0000026502 performed best regarding ALDH1A1 silencing (data not shown). In the following, cell clones transduced with the plasmid TRCN0000026415 are referred to as “shALDH1A1” and cells carrying the pLKO.1-puro control plasmid as “mock”. Analysis by qPCR showed a knockdown of ALDH1A1 mRNA of 99% in LN18 cells, of 80% in T98G cells and of 88-95% in R28 cells after lentiviral transduction (Figure 15 A). Specificity of shRNA to the isoenzymes ALDH1A1 was proven by RT-PCR (Figure 15 B).

Densitometric normalization to alpha-tubulin revealed a more than 90% knockdown of ALDH1A1 in shRNA transfected clones (shALDH1A1A1) on protein level compared to control cells (wild-type or mock) (Figure 15 C). Morphological changes were observed when R28 cells were transduced with the two different shRNAs to ALDH1A1. Impaired neurosphere formation was characterized by decreased sphere size and initiation of adherent growth under serum free conditions in neurobasal medium (Figure 15 D).

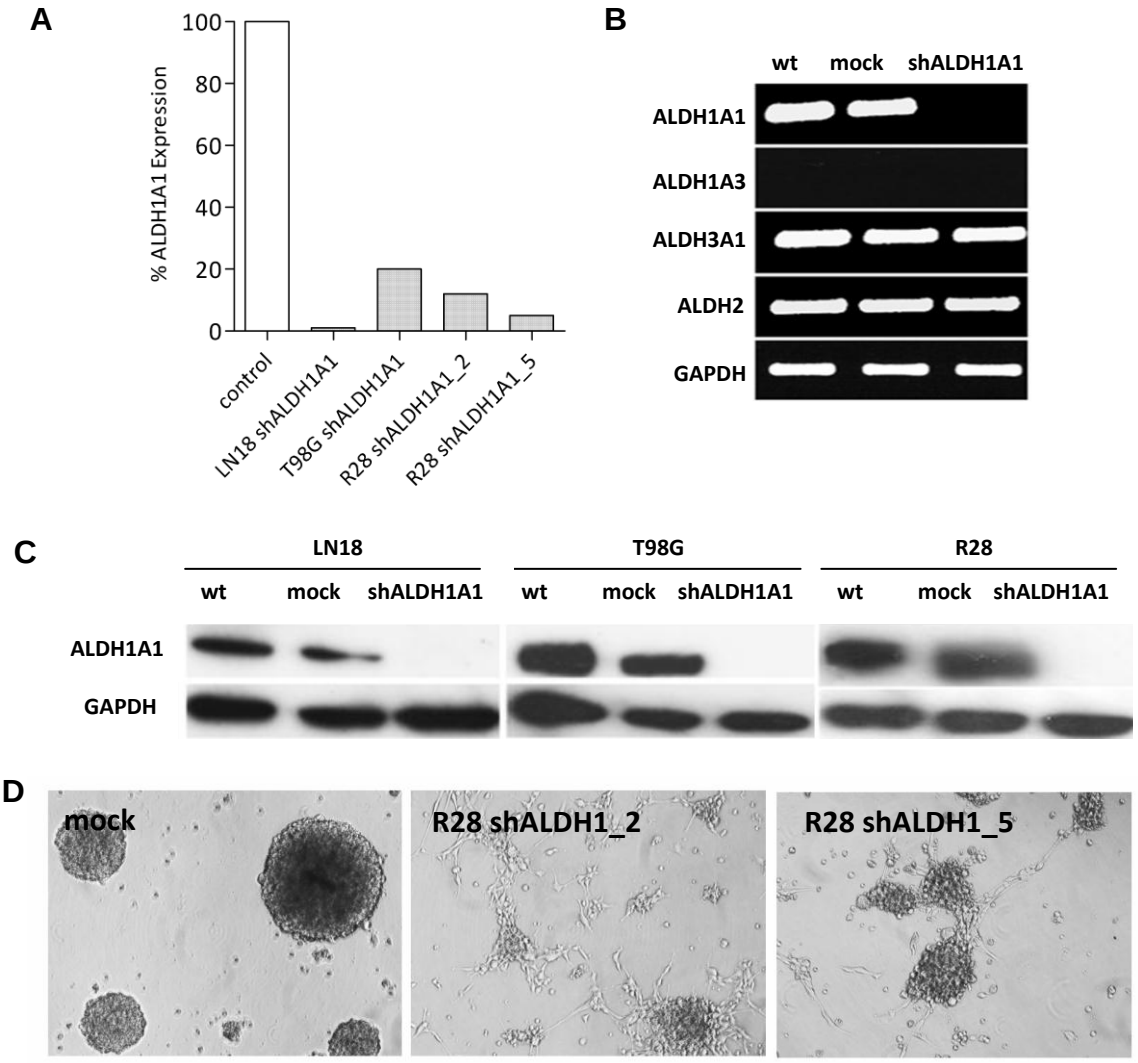

Figure 15: Stable knockdown of ALDH1A1 in LN18, T98G and R28 cells with shRNA

A, ALDH1A1 mRNA level following knockdown with shRNA was quantified by qPCR. B, Specificity of ALDH1A1 knockdown was proven by RT-PCR. C, Western blot analysis showed down-regulation of ALDH1A1 on protein level. D, Reduced neurosphere formation of R28 cells after knockdown of ALDH1A1 with shRNA; shALDH1A1: cells transfected with clone ID TRCN0000026415, shALDH1A1_2: R28 cells transfected with TRCN0000026415; shALDH1A1_5: R28 cells transfected with TRCN0000026502 (10x objective).

Results I: ALDH1A1 and PTEN/PI3K/Akt signaling

1. PTEN status of glioblastoma cell lines correlates with neurosphere formation

Recently, we could show that ALDH1A1 expression correlates with neurosphere formation. Further, inhibition of ALDH1A1 with DEAB or retinoic acid decreased neurospheres in size and number (Rasper et al., 2010). In GBM cell culture, PTEN and EGFR status are known to have a substantial impact on neurosphere formation (Bleau et al., 2009; Chen et al., 2010). To better understand the role of genetic variations on a stem cell-like phenotype, the PTEN status of nine GBM cell lines was determined by Western blot analysis (Figure 16). The cell lines LN18, LN229, T98G, T16 and T30 expressed PTEN. High levels of phosphorylated PTEN protein were detected in LN18, LN229 and T98G cells (Figure 16). Phosphorylation of PTEN leads to stabilization and inactivation of the protein.

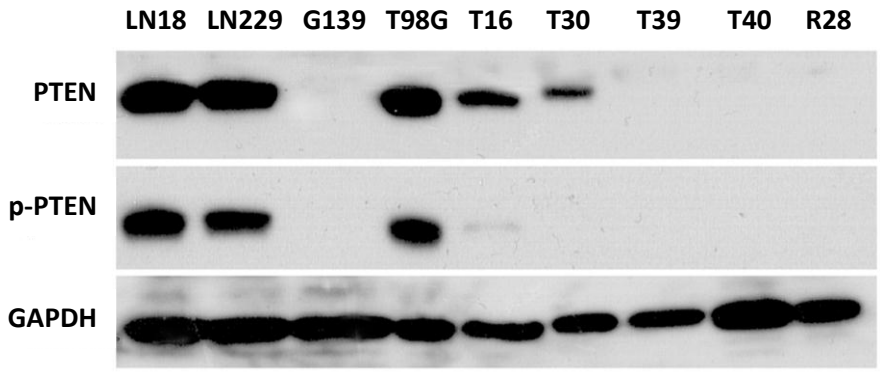

Figure 16: Western Blot analysis of PTEN expression in GBM cell lines

PTEN phosphorylation was detected with an antibody specific to PTEN, phosphorylated at Ser380/Thr382/383.

The PTEN gene of cell lines expressing the protein was sequenced by Kathrin Hock (Institute of Pathology, Technische Universität München) to screen for mutations. Cell lines that lack PTEN protein were not analyzed for PTEN gene mutations. Following sequencing, a correlation between PTEN status, ALDH1A1 protein levels and neurosphere formation was found (Table 10). Cell lines with mutated or absent PTEN in combination with high-level ALDH1A1 expression were capable of sphere formation (T98G, T30, T39, T40 and R28), while cell lines with wild-type PTEN that lack ALDH1A1 expression (LN229, T16) did not grow in neurospheres.

LN18 and G139 cells had an exceptional position: LN18 cells feature wild-type PTEN, high-level ALDH1A1 and form neurospheres; G139 showed a PTEN deletion, lack ALDH1A1 expression and are incapable of sphere formation. Strikingly, LN18 cells express high-levels of phosphorylated and therefore less active PTEN.

Table 10: PTEN status, ALDH1A1 expression and neurosphere formation of GBM cell lines

Cell line	*LN18*	*T98G*	*G139*	*LN229*	*T16*	*T30*	*T39*	*T40*	*R28*
PTEN status	+	+	-	+	+	+	-	-	-
PTEN mutation	-	Exon 2, codon 42, CTT→CGT	+	-	-	Exon 8, codon 321, AAA→GAA	+	+	+
Predicted effect	wild-type	Lys→Glu	deletion	wild-type	wild-type	Gly→Gln	deletion	deletion	deletion
ALDH1A1	+	+	-	-	-	+	+	+	+
Neurospheres	+	+	-	-	-	+	+	+	+

2. Akt activation and high-level ALDH1A1 expression are found in neurospheres

Further experiments were performed to illuminate whether ALDH1A1 expression or PTEN mutation is indispensable for neurosphere formation. The phosphatase PTEN inactivates PI3K and thereby negatively regulates Akt signaling pathway. Thus PTEN mutation, deletion or phosphorylation results in Akt activation. To analyze the impact of EGFR/PTEN/PI3K/Akt signaling and ALDH1A1 expression on neurosphere formation, LN18 cells with either mutated EGFR or an altered ALDH1A1 status were applied. LN18 cells transfected with ALDH1A1, dominant negative EGFR-CD533 or constitutively active EGFRvIII as well as ALDH1A1 knock-down cells (shALDH1A1) were grown under serumfree conditions in neurobasal medium. The capacity of these clones to form neurospheres was compared to wild-type (wt) and mock transfected control cells. Substantial neurosphere formation was observed for LN18 EGFRvIII and LN18 ALDH1A1 cells.

LN18 wt and mock cells initiated spheroid growth 72 hours after seeding to neurobasal medium, while neurosphere generation of LN18 EGFR-CD533 and LN18 shALDH1A1 cells was impaired (Figure 17 A). In addition, Western blot analysis of the respective cell clones following incubation in neurobasal medium suggested a correlation between ALDH1A1 expression, p-Akt protein level and the capacity to form spheres. Elevated levels of p-Akt and ALDH1A1 were detected in sphere-forming LN18 wt, mock, ALDH1A1 and EGFRvIII cells. In contrast, LN18 EGFR-CD533 and shALDH1A1 cells with impaired neurosphere formation showed minor Akt activation and lack of ALDH1A1 expression (Figure 17 B).

A

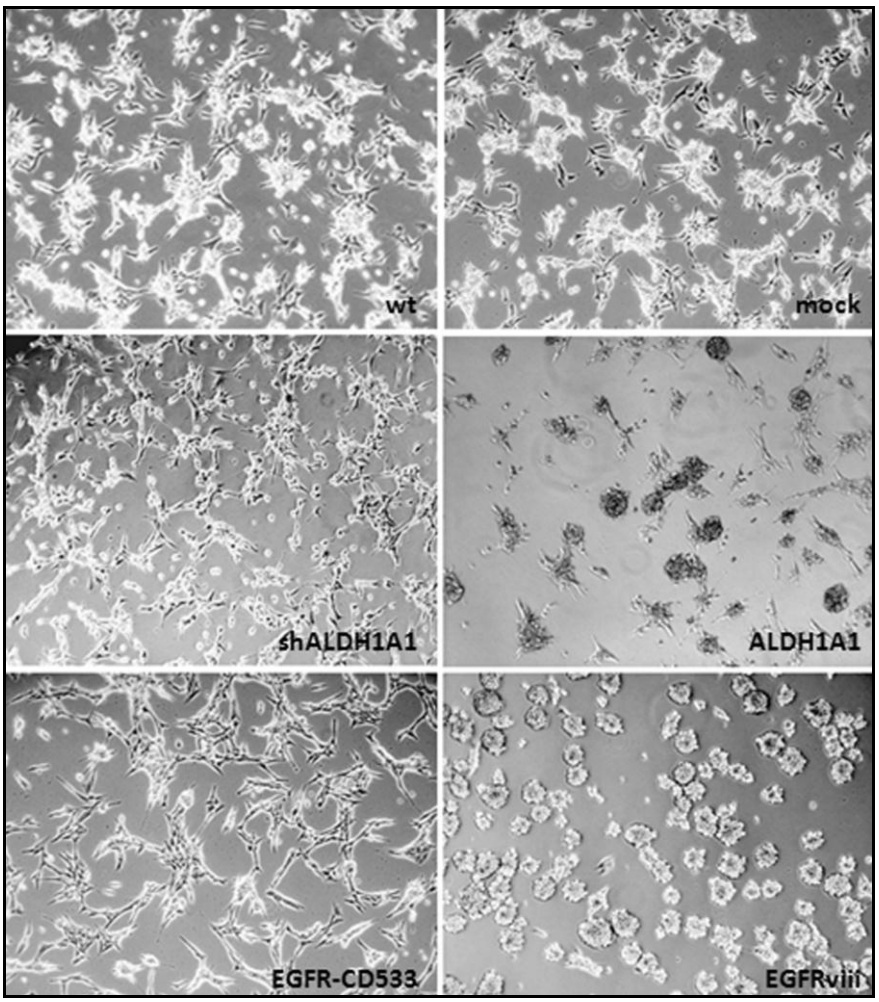

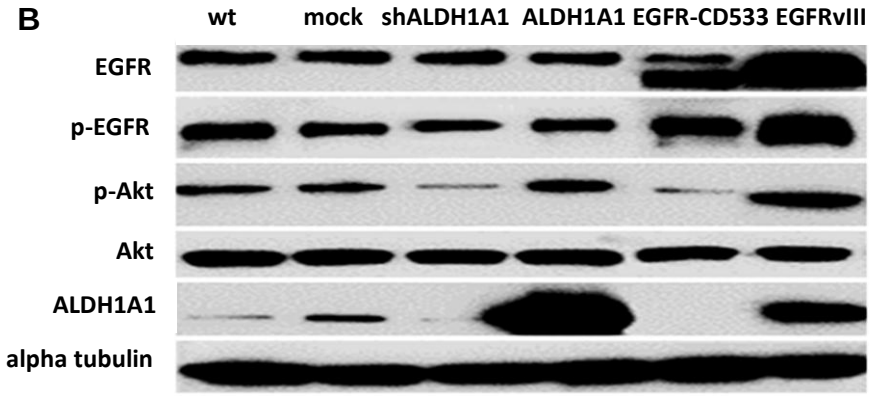

Figure 17: LN18 cell clones grown in neurobasal medium

A, LN18 EGFRvIII and LN18 ALDH1A1 cells generated neurospheres earlier and more frequently compared to EGFR-CD533 or shALDH1A1 cells. B, LN18 EGFRvIII and LN18 ALDH1A1 showed Akt activation (p-Akt) and elevated ALDH1A1 expression in neurobasal medium.

3. Inhibition of ALDH1A1 and Akt impairs neurosphere formation

In order to assess the connection between Akt activation and ALDH1A1 expression under normal cell culture conditions, LN18 cells were treated with 100ng/ml EGF, 50µM LY294002 (PI3K inhibitor), 10µM Akt1/2 kinase inhibitor (Akti) or 100µM DEAB (ALDH1A1 inhibitor) for 1, 6, 24, 48h in DMEM + FBS. The minimum dose of the Akt1/2 inhibitor that resulted in maximum inhibition and minimum cytotoxicity was tested before; inhibition of Akt with 10µM Akti was stable over 48 hours. Western blot analysis showed slightly decreased ALDH1A1 levels 48 hours after ALDH1A1 and PI3K/Akt inhibition. No effect of DEAB on Akt activation was observed, when cells were treated in serum containing cell culture medium (Figure 18).

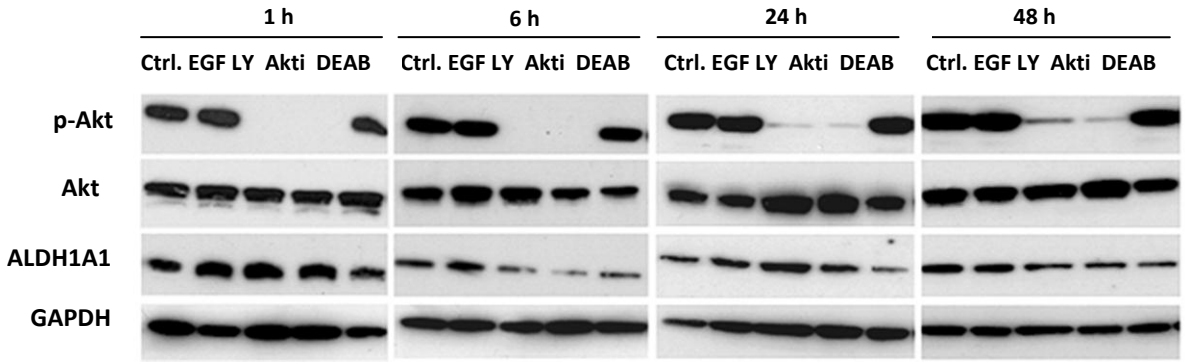

Figure 18: Western blot analysis of LN18 cells treated in DMEM + FBS

Cells were treated with 100ng/ml EGF (EGF), 50µM PI3K inhibitor LY294002 (LY), 10µM Akt 1/2 inhibitor (Akti), or 100µM ALDH1A1 inhibitor (DEAB) for 1, 6, 24 and 48 hours.

To yield confirmation that both, ALDH1A1 and Akt are involved in neurosphere formation, LN18 wt/mock/shALDH1A1 and R28 cells were treated in neurobasal medium for 10 days every 48 hours with 10µM Akti or 100µM DEAB as described above. In LN18 cells, activation of Akt was significantly attenuated following treatment with Akti or with the ALDH1A1 inhibitor DEAB. Corresponding to these results, LN18 shALDH1A1 cells showed low phospho-Akt levels when grown in neurobasal medium. In addition, inhibition of Akt led to lowered ALDH1A1 protein levels (Figure 19 A). In line with these findings, neurospheres decreased in size and number after exposure to DEAB or Akt 1/2 inhibitor (Figure 19 B, C).

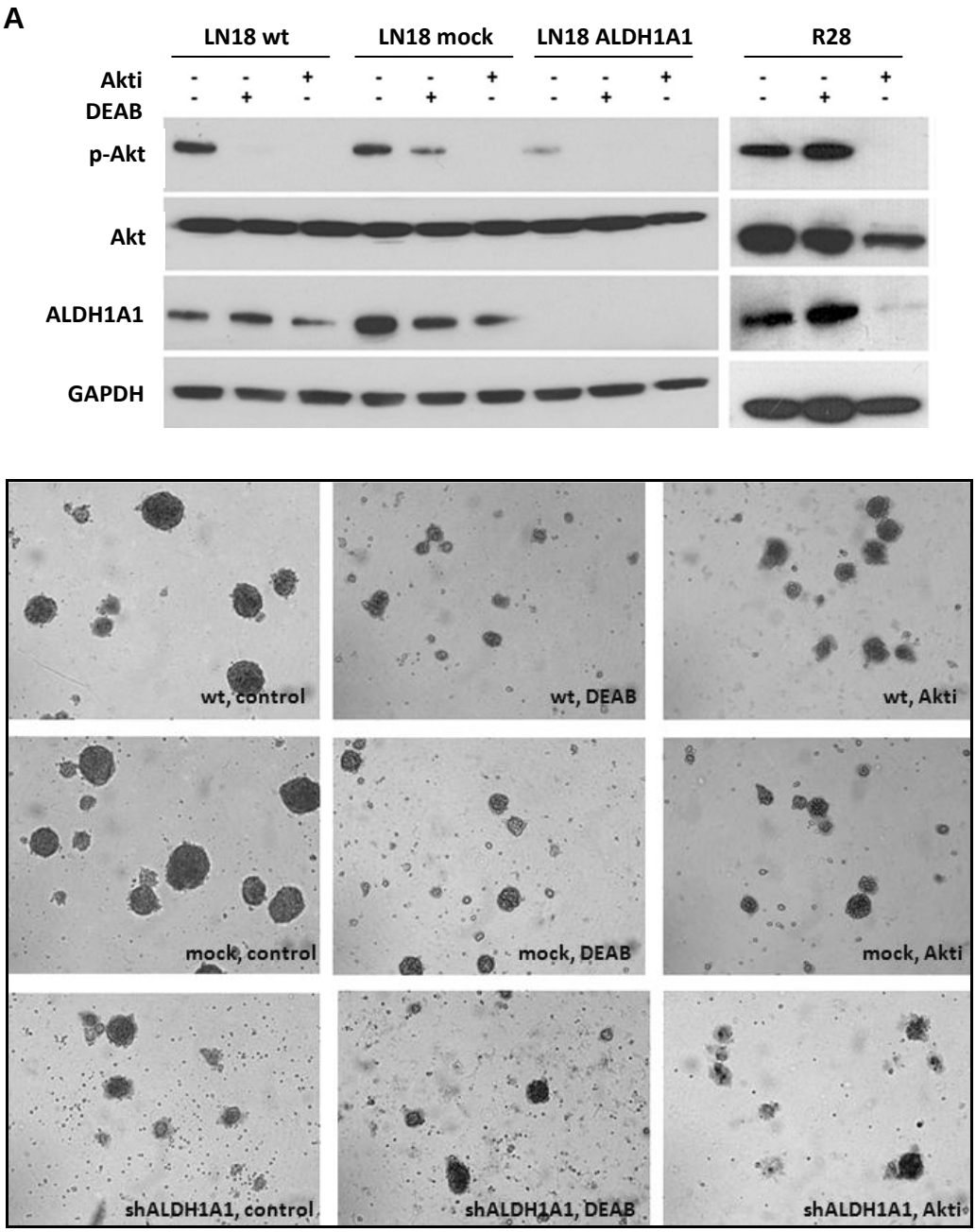

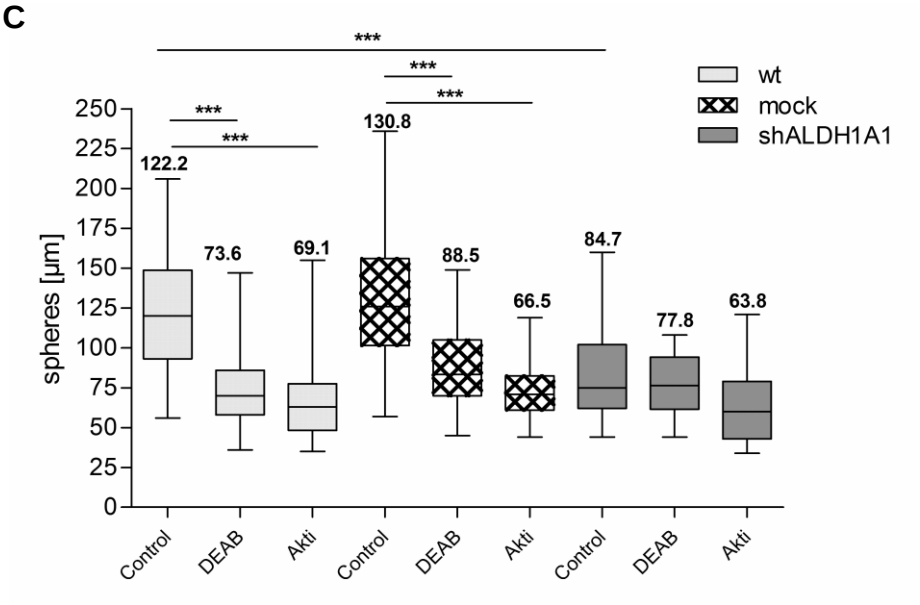

Figure 19: Treatment of LN18 and R28 cells with DEAB or Akti in neurobasal medium

A, Western blot analysis of p-Akt/Akt and ALDH1A1 in LN18 and R28 neurospheres following inhibition with Akti or DEAB. B-C, Neurosphere formation of LN18 wt (light grey bar), mock (cross-hatch) and shALDH1A1 (dark grey) following treatment with Akt 1/2 inhibitor (Akti), ALDH1A1 inhibitor (DEAB) or knockdown with shRNA (shALDH1A1) (10x objective).

Sphere formation of R28 cells was also strongly attenuated by exposure to DEAB or Akti. However, Akt activation was not affected by treatment with DEAB. Strikingly, ALDH1A1 protein levels strongly decreased after Akt inhibition (Figure 19 A).

To highlight the mechanism of Akt and ALDH1A1 mediated sphere formation, downstream targets of PTEN/PI3K/Akt pathway were analyzed. No change in phospho-mTOR level was observed following ALDH1A1 knockdown or exposure to DEAB or Akti. In contrast, dephosphorylation and thereby activation of GSK-3α/β was observed after treatment with Akt1/2 inhibitor (Figure 20). Activated GSK-3α/β is able to inhibit activation and nuclear translocation of β-catenin, a key downstream effector in the Wnt signaling pathway. GSK-3 destabilizes β-catenin by phosphorylating it at Ser33, Ser37, and Thr41. Total β-catenin protein level did not significantly change following incubation with DEAB or Akti. Strikingly, phospho-β-catenin expression decreased when transferred from adherent growth (FBS) to neurosphere growth conditions (Figure 20), indicating activation of β-catenin signaling in stem-cell preserving medium. However, it is necessary to analyze cellular localization of β-catenin and the transcription of target genes in order to conclude whether Wnt signaling is involved in ALDH1A1 and Akt mediated neurosphere formation.

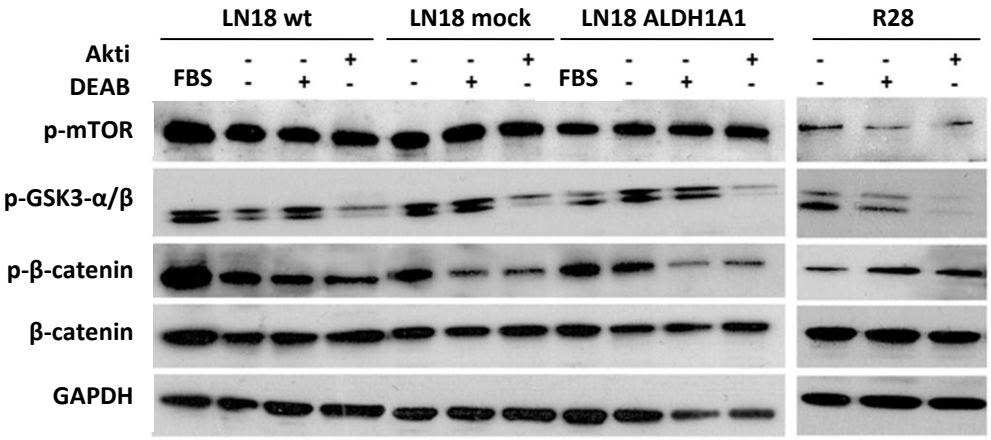

Figure 20: Western blot analysis following treatment with Akti or DEAB

Phospho-mTor, phosho-GSK-3α/β and (phospho-) β-catenin expression in LN18 and R28 neurospheres following treatment with Akti or DEAB, respectively. FBS: LN18 cells, grown adherent under normal cell culture conditions

4. Inhibition of ALDH1A1 and Akt under serumfree conditions induces apoptosis and G1 arrest

Strikingly, inhibition of ALDH1A1 under serumfree conditions induced apoptosis, as indicated by an elevated subG1 fraction in cell cycle analysis and by increased caspase 3 cleavage. In general, apoptosis took place to some extent after prolonged cultivation in neurobasal medium. In contrast, Akt inhibition in neurobasal medium led to G1 arrest and a decrease of the apoptotic fraction, as shown by absent caspase 3 cleavage. Apoptosis following treatment with Akti was only found in LN18 shALDH1A1 cells, as indicated by an elevated subG1 peak and caspase 3 cleavage. No PARP1 cleavage was detected in LN18 shALDH1A1 cells (Figure 21).

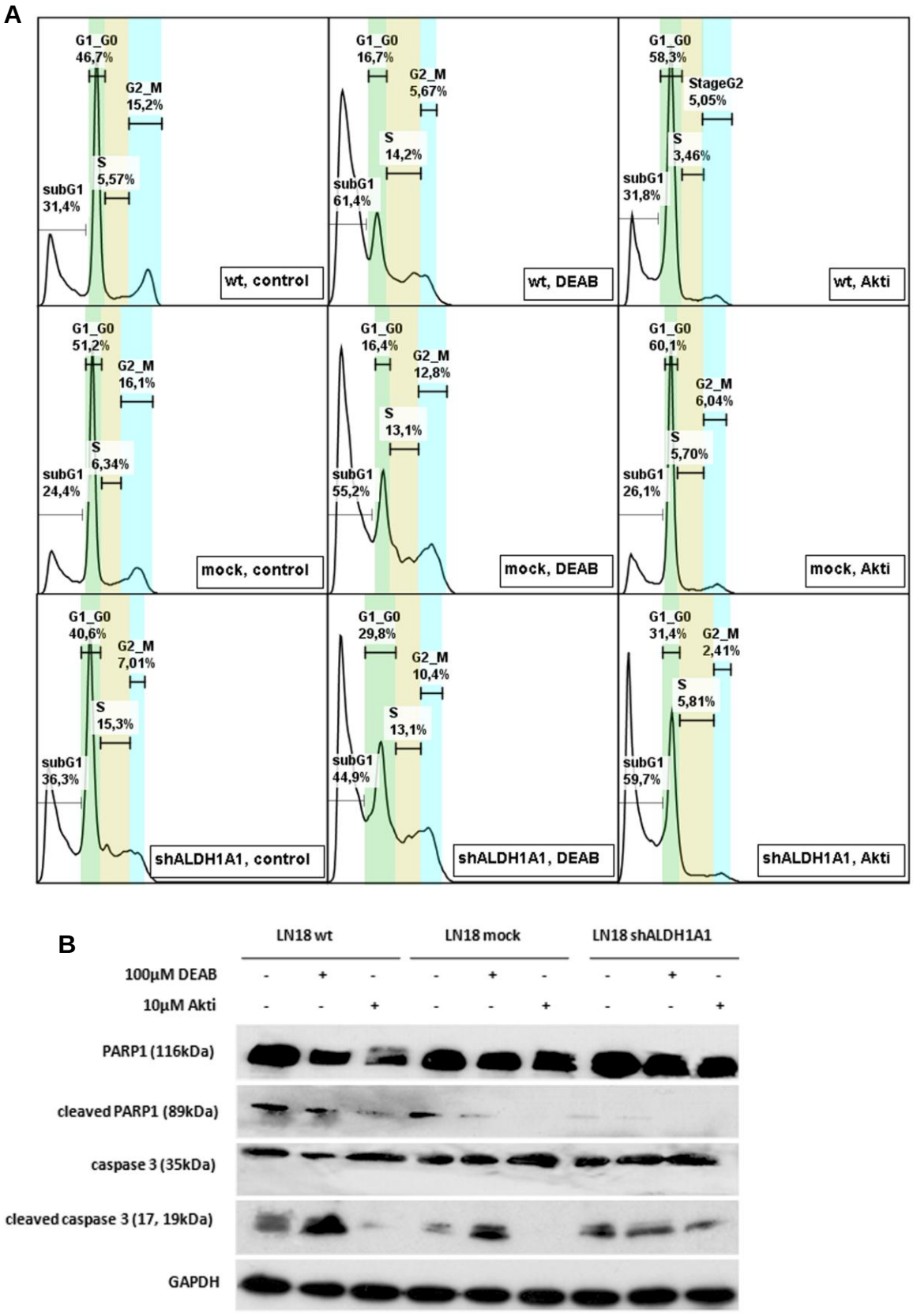

Figure 21: Cell cycle and Western blot analysis of neurospheres after treatment with Akti or DEAB

A, Cell cycle analysis of LN18 neurospheres treated with DEAB or Akt1/2 inhibitor; B, Western blot analysis of PARP1 and caspase 3 cleavage following exposure to Akti or DEAB for 10 days;

Results II: ALDH1A1 and chemoresistance

1. ALDH1A1 expression in MGMT+ and MGMT- glioblastoma cell lines correlates with resistance to temozolomide

To assess the role of ALDH1A1 in mediating resistance to temozolomide, cytotoxicity of this cytostatic drug was determined by colorimetric MTT assay. As MGMT represents a major mechanism in TMZ resistance, MGMT status of nine GBM cell lines was analyzed before by Western blot analysis (Supplementary figure S1) and by specific relative quantitative real-time PCR technique named MethyQESD (Bettstetter et al., 2008). In the following, cells with MGMT expression are referred to as MGMT negative (MGMT-) and cells without as MGMT positive (MGMT+). No relevant promoter-methylation was observed in LN18, T98G, T39, T40, R28 and G139 cells (MGMT+). The MGMT promoter of the cell lines T16, T30, LN229 was methylated to 60%, 30% and 100% (MGMT-), respectively (Table 11). Despite of cell line G139, MGMT protein expression was detected in all cell lines that had no epigenetically silenced MGMT promoter (Supplementary figure S1). Therefore, in the following G139 cells are stated as (ALDH1A1-/MGMT-*).

Table 11: ALDH1A1 and MGMT status of GBM cell lines

	LN18	*LN229*	*G139*	*T98G*	*T16*	*T30*	*T39*	*T40*	*R28*
ALDH1A1	+	-	-	+	-	+	+	+	+
MGMT promoter methylation	-	+	-	-	+	+	-	-	-
MGMT protein	+	-	-	+	-	-	+	+	+

Following daily treatment with 100, 200 and 300µM TMZ in DMEM + FBS, response of GBM cell lines to TMZ was analyzed by metabolic assay (Figure 22). The cell line R28 was additionally treated in neurobasal medium + B27 every 48 hours (R28, B27). ALDH1A1-/MGMT- T16 and LN229 were most sensitive to TMZ (IC_{50} < 100µM). The cell line G139 (ALDH1A1-/MGMT-*) responded in a comparable way to temozolomide as T30 (ALDH1A1+/MGMT-), when doses of ≥ 200µM were applied. Notably, at TMZ concentrations of ≤ 100µM, ALDH1A1- G139 cells were more sensitive to TMZ than ALDH1A1+ T30 cells.

ALDH1A1+/MGMT+ LN18, T98G, T39, T40 and R28 were resistant to TMZ with an IC_{50} of > 200µM. The marginal cytotoxicity levels of the primary cell lines T40 and R28 in the metabolic MTT assay partially resulted from a lower proliferation rate compared to LN18 or T98G cells.

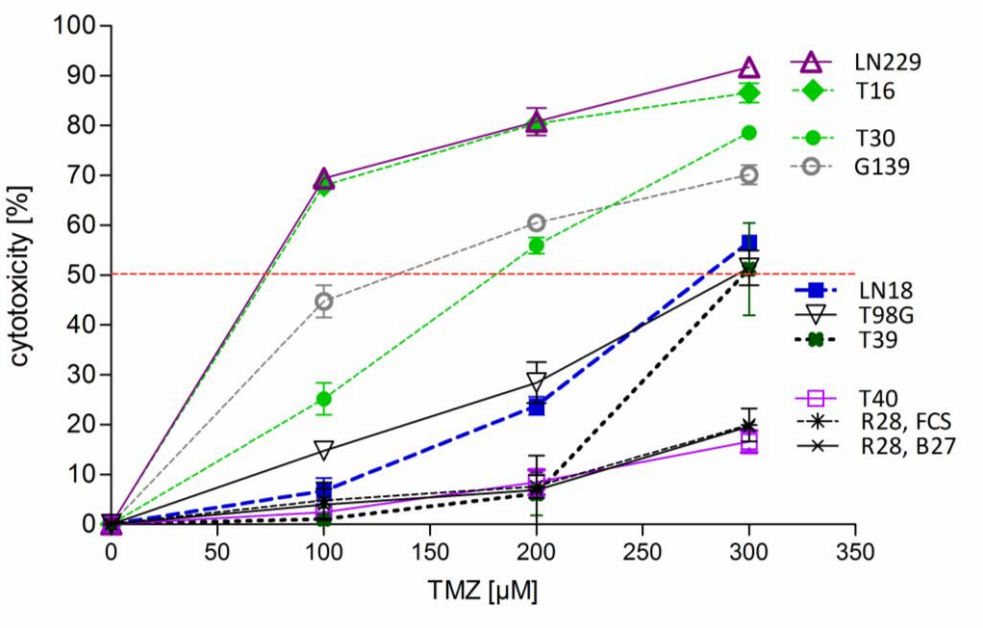

Figure 22: MTT analysis of GBM cell lines following treatment with TMZ for 7 days

ALDH1A1+/MGMT+ cell lines LN18, T98G, T39, T40 and R28 were resistant to TMZ, while ALDH1A1-/MGMT- LN229 and T16 cells were sensitive.

2. Combination of TMZ and ALDH1A1 depletion reduces the clonogenic potential of ALDH1A1+ glioblastoma cell lines

To further explore the impact of ALDH1A1 expression on TMZ resistance, the non-responding cell line LN18 (ALDH1A1+/MGMT+) was treated twice with 200µM or 500µM TMZ alone or in combination with 300µM DEAB. In addition, LN18 shALDH1A1 cells were treated twice with 200µM or 500µM TMZ. Following treatment, a colony formation assay was performed by seeding 150 or 300 viable cells. After cultivation for 14 days, staining with diff-quick revealed that the clonogenic capacity of ALDH1A1+ cells exposed to TMZ in combination with DEAB was significantly attenuated. Strikingly, clonogenicity of LN18 shALDH1A1 cells was significantly decreased following exposure to mere TMZ (Figure 23).

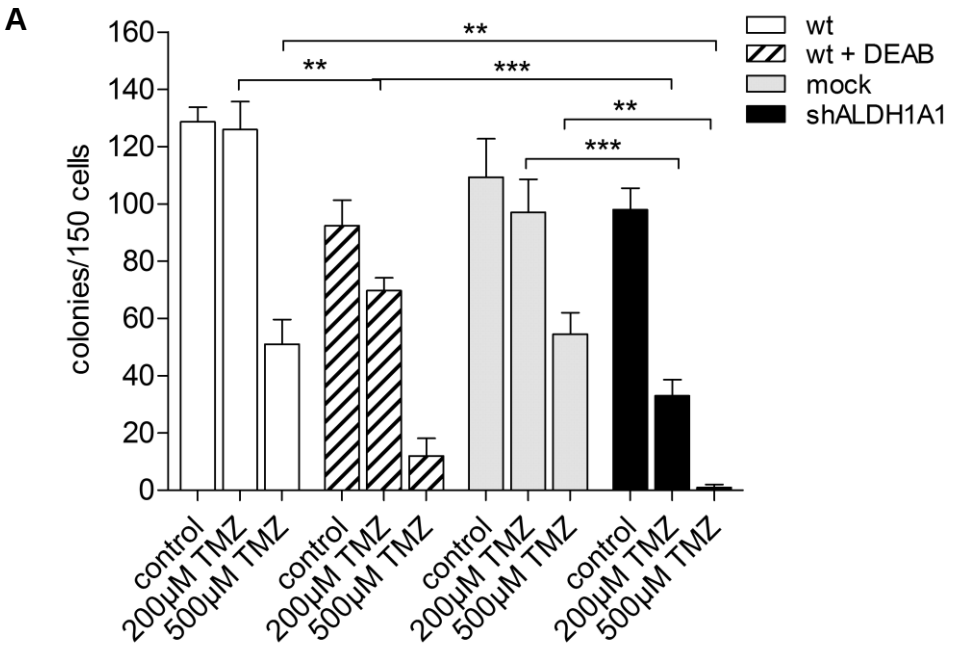

Figure 23: Colony formation assay with LN18 cells

Clonogenicity was significantly reduced when cells were treated with DEAB and 200µM TMZ (wt + DEAB, striped bar) compared to LN18 control cells (wt, white bar). Clonogenicity of ALDH1A1 knockdown cells (shALDH1A1, black bar) was significantly reduced following exposure to 200µM or 500µM TMZ compared to control cells (wt, white bar or mock, grey bar). Column bar graph shows mean number of colonies per 150 seeded cells of two different experiments. $^{**}p < 0.01$, $^{***}p < 0.001$;

In addition, neurosphere generation of LN18, T98G and R28 was analyzed to determine clonogenicity of sphere forming cell lines following treatment with concomitant TMZ and DEAB (Figure 24). Neurosphere formation was affected in ALDH1A1+/MGMT+ LN18 and T98G cell lines when the cells were pre-incubated with TMZ and DEAB; spheres were significantly decreased in size and number by combination therapy. Concomitant application of DEAB and TMZ lowered the neurosphere formation frequency from about 50% (TMZ alone) to 8% (TMZ + DEAB) and the average size to less than 50µM. Similar results were obtained with T98G cells. The cell line R28 is permanently maintained in neurospheres. As we described previously, neurosphere formation is impaired by ALDH1A1 inhibition in neurobasal medium (Rasper et al., 2010). Beier *et al.* showed decreased neurosphere capacity following treatment with mere TMZ (Beier et al., 2008).

These finding are consistent with the present results. Strikingly, concomitant treatment with DEAB and TMZ in neurobasal medium further decreased size (~ 1.6 fold) and number of neurospheres (4.3 fold and 2.3 fold, respectively).

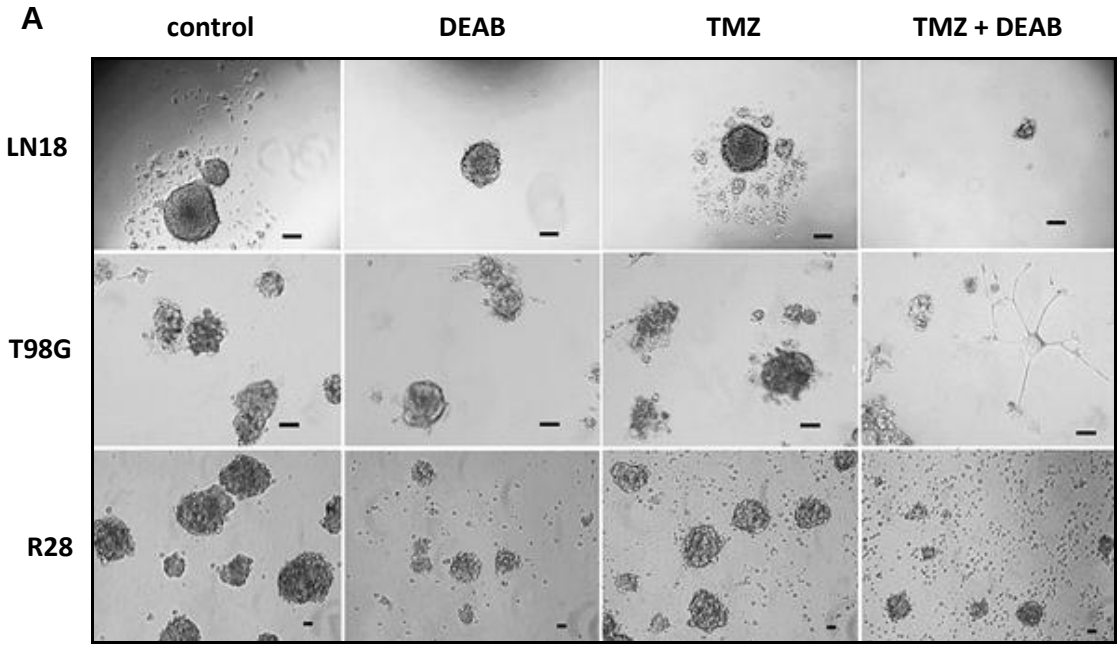

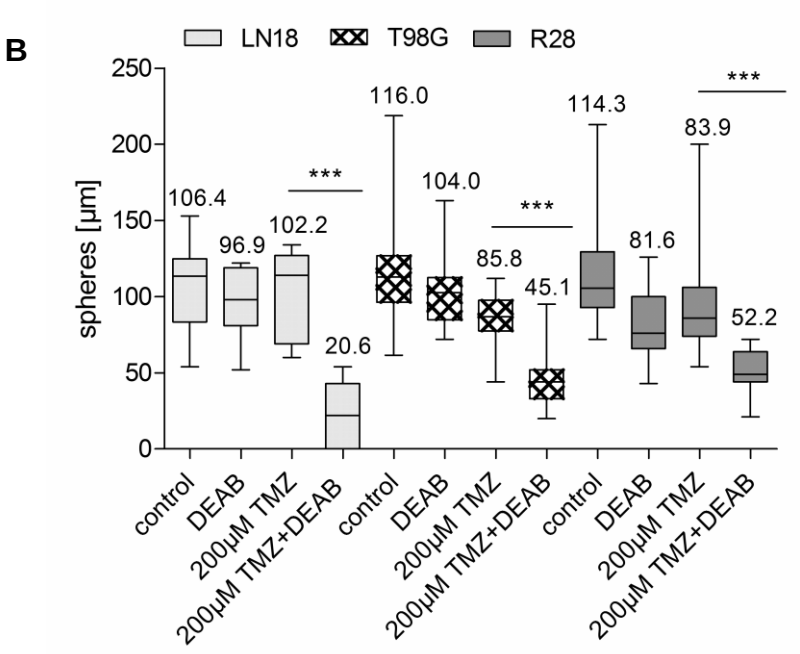

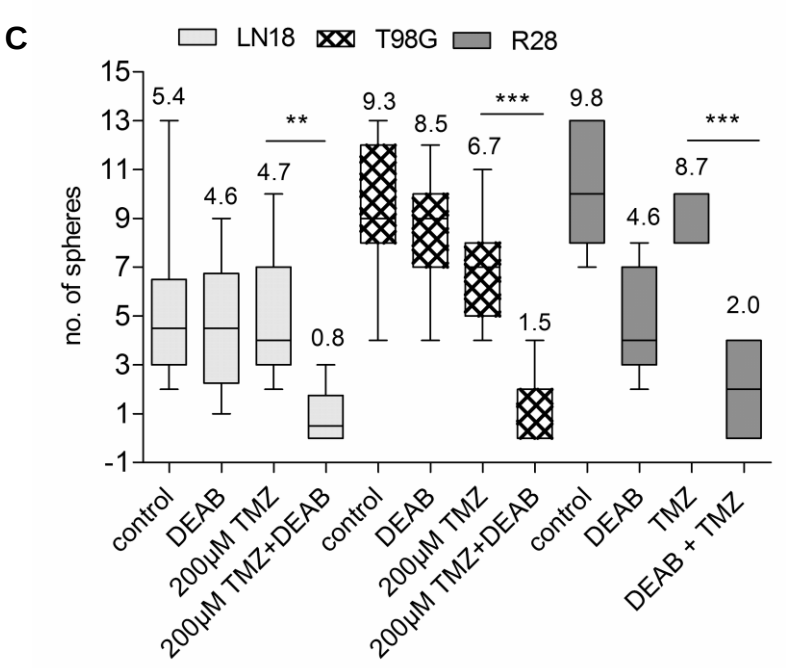

Figure 24: Neurosphere formation after treatment with TMZ, DEAB or TMZ + DEAB

A-C, Neurospheres of LN18 (grey boxplot), T98G (crosshatch) and R28 (dark grey) cells decreased in size and number after concomitant TMZ and DEAB administration (**p < 0.01, ***p < 0.001). Spheres per 10 seeded cells (LN18) or spheres per field (T98G, R28) were counted (scale bar represents 100µM). Mean values of the neurosphere- diameters are shown above the box blots.

3. Sensitivity to TMZ in MGMT+/ALDH1A1+ cells is restored by inhibition or knockdown of ALDH1A1 *in vitro*

In order to exclude potential off-target effects of DEAB and to prove the pivotal role of ALDH1A1 in mediating TMZ resistance, specific shRNA was applied (Figure 15). Cytotoxicity of TMZ in combination with ALDH1A1 inhibition or knockdown was analyzed by metabolic MTT assay (Figure 25). Notably, treatment of LN18 and T98G shALDH1A1 cells with mere TMZ induced a response comparable to the combination therapy with DEAB in ALDH1A1+ wild-type and control cells. Treatment of LN18 cells with 200µM TMZ in combination with ALDH1A1 inhibition or ALDH1A1 knockdown increased the cytotoxicity significantly from approximately 25% to about 50% (DEAB) or more than 70% (shALDH1A1). T98G cells were also more sensitive to TMZ when ALDH1A1 was inhibited or depleted as indicated by 2-fold increased cytotoxicity.

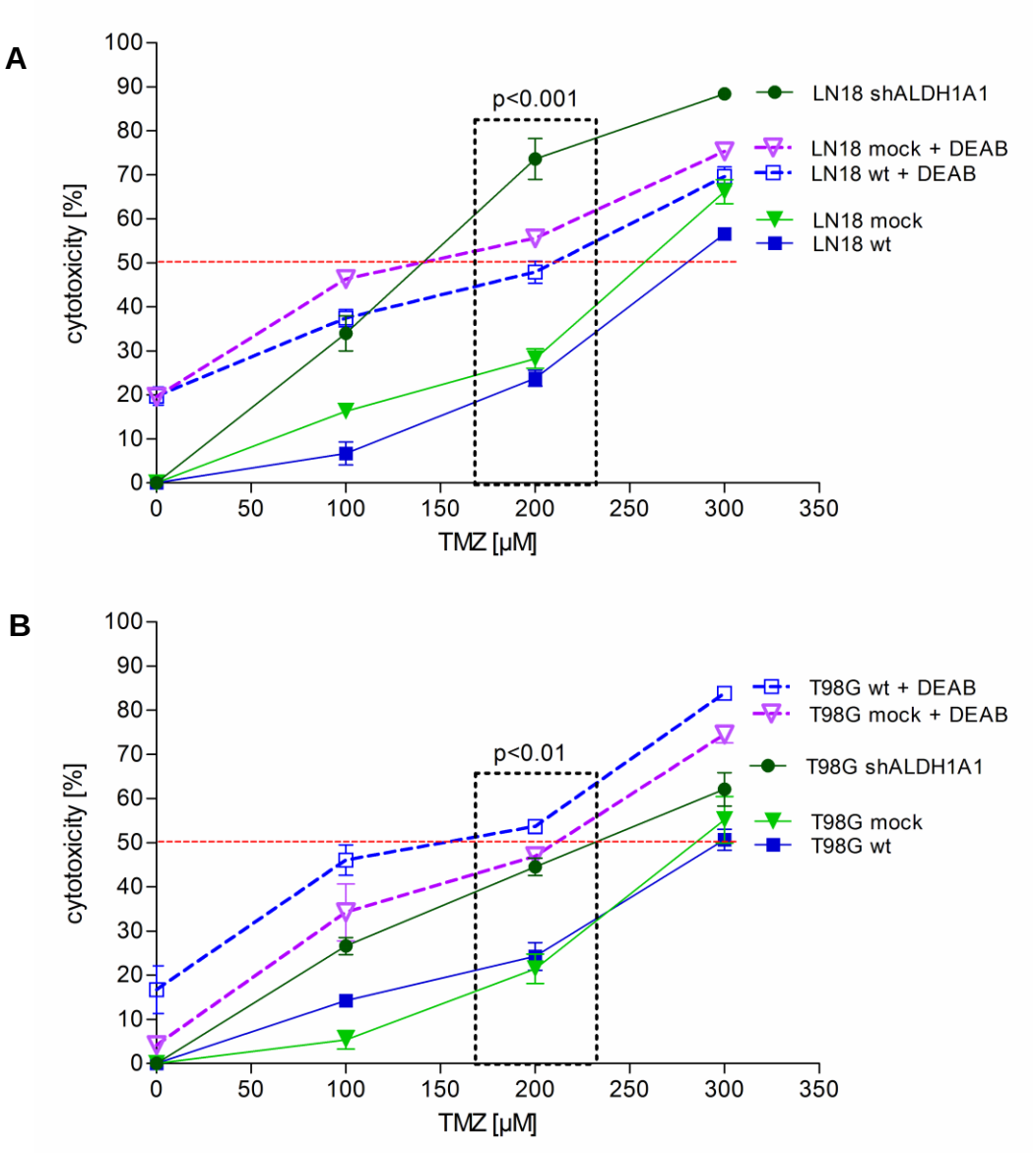

Figure 25: MTT assay of ALDH1A1 inhibited or depleted cells after treatment with TMZ

Cells were treated with mere TMZ or TMZ + DEAB for 7 days. Following inhibition or depletion of ALDH1A1, cell were more sensitive to TMZ compared to wild-type and mock transfected control cells. A, LN18 wt/mock/shALDH1A1 cells; B, T98G wt/mock/shALDH1A1 cells;

4. TMZ induces prolonged G2/M cell cycle arrest in ALDH1A1+/MGMT+ GBM cells after inhibition or knockdown of ALDH1A1

Temozolomide is known to induce DNA lesions leading to cell cycle arrest at the G2/M boundary and to rather induce senescence than direct apoptosis in glioblastomas (Hirose et al., 2001; Karran and Bignami, 1994; Karran et al., 1993). As indicated by flow cytometry following PI staining, treatment with 200µM TMZ for 7 days led to G2/M arrest in LN18 shALDH1A1 cells while the cell cycle of wild-type and mock cells was not affected (Figure 26).

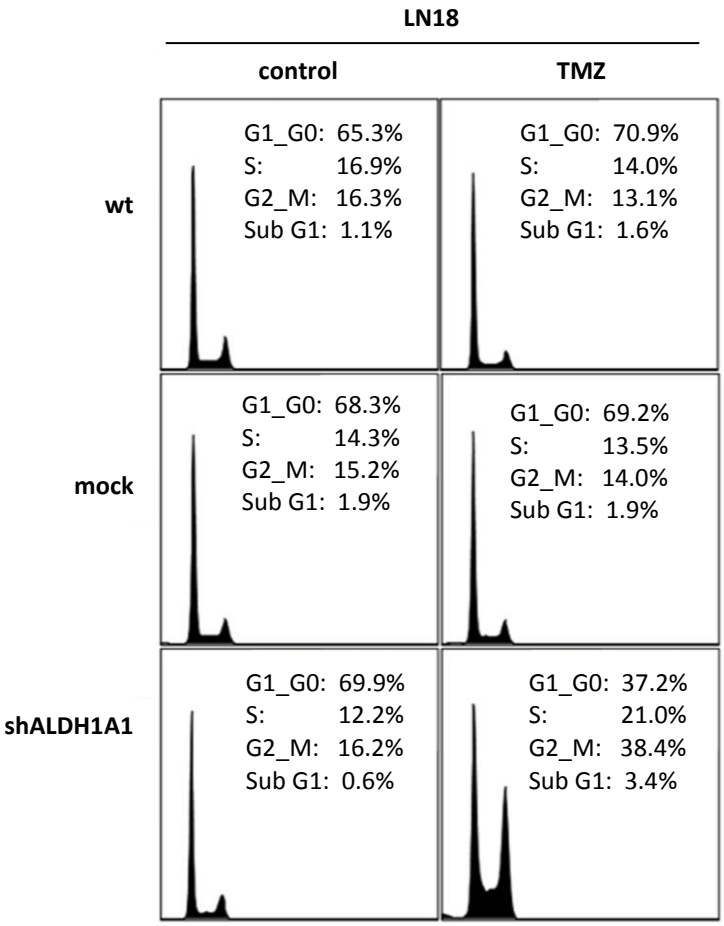

Figure 26: Cell cycle analysis after treatment with TMZ for 7 days

Representative flow cytometry histograms of LN18 wt, mock and shALDH1A1 cells after exposure to 200µM TMZ for 7 days; Y-axes: DNA content, X-axes: FL3-H

In addition, LN18 and T98G cells were treated with a single dose of 500µM TMZ, 300µM DEAB or a combination of both and cell cycle distribution was analyzed after 48 and 72 hours. Results indicate that repeated treatment with median doses TMZ (200µM) or exposure to a single high dose (500µM) induced G2/M arrest. Notably, ALDH1A1 positive cells (LN18 wt/mock, T98G wt/mock) showed a cell cycle distribution comparable to untreated control cells 48 hours after high-dose TMZ application. In contrast, ALDH1A1 negative cells (LN18 shALDH1A1, T98G shALDH1A1) or cells with inhibited ALDH1A1 (LN18 wt + DEAB, T98G wt + DEAB) accumulated in G2/M following treatment with TMZ (Figure 27 A, see supplementary figure S 2 for histograms of T98G cells). The proportion of LN18 cells in G2/M 48 hours after TMZ treatment increased from 15.4% to 40% by concomitant ALDH1A1 inhibition and to 45.6% by knockdown of ALDH1A1 (Figure 27 B).

The median proportion of T98G cells in G2/M following treatment with mere TMZ was 22.2% compared to 53.2% in combination with DEAB. After stable knockdown of ALDH1A1, 41.1% T98G cells accumulated in G2/M following exposure to TMZ (Figure 27 B; Supplementary figure S 2). Increase of subG1 population after treatment with TMZ demonstrated apoptosis of ALDH1A1 negative LN18 and T98G cells (Table 12).

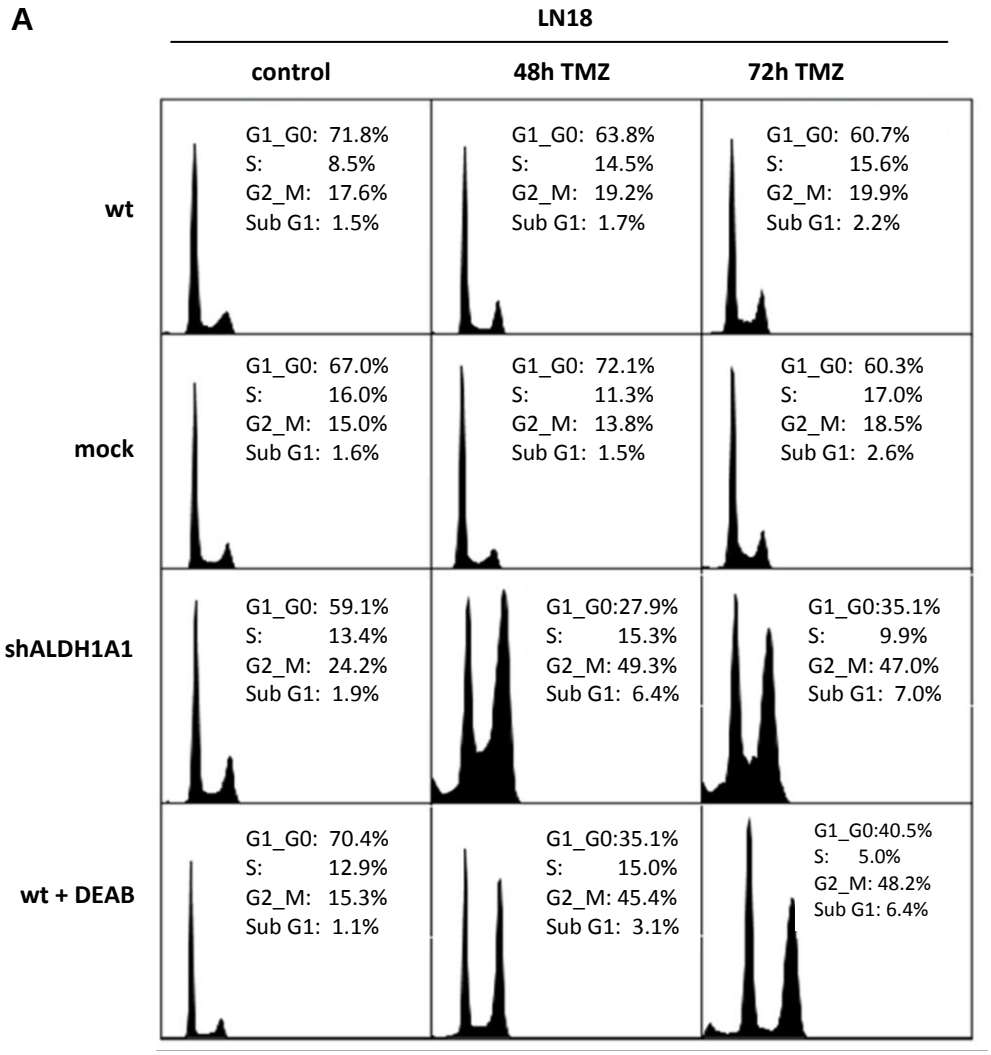

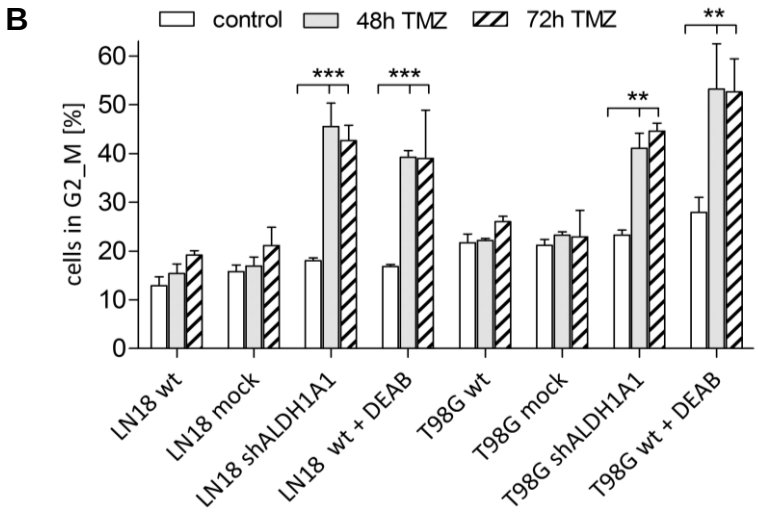

Figure 27: Cell cycle analysis after treatment with TMZ for 48 or 72 hours

A, Representative flow cytometry histograms of LN18 cells after treatment with 500µM TMZ, 300µM DEAB or a combination of both for 48 and 72 hours (Y-axes: DNA content, X-axes: FL3-H). B, Mean proportion of LN18 and T98G cells in G2/M after three independent experiments; (**$p < 0.01$, ***$p < 0.001$); White bar: control (DMSO or DEAB), grey: 48 hours treated (TMZ or TMZ + DEAB), striped: 72 hours treated (TMZ or TMZ + DEAB);

Table 12: Percentage of LN18 and T98G cells in the subG1 fraction following treatment with TMZ or TMZ + DEAB for 48 or 72 hours.

sub G1 (%)		LN18 wt	mock	shALDH1A1	+ DEAB	T98G wt	mock	shALDH1A1	+ DEAB
control	**mean**	1.07	1.3	1.53	1.77	2.07	1.9	0.95	4.33
	SD	0.83	0.4	0.86	0.55	1.33	0.87	0.21	1.45
48h TMZ	**mean**	1.73	1.5	4.17	2.9	3.46	4.0	7.15	8.95
	SD	1.5	0.7	1.36	0.95	1.17	0.4	0.78	2.76
72h TMZ	**mean**	2.4	2.53	6.6	6.9	2.1	3.85	5.3	8.6
	SD	0.17	0.37	0.65	0.71	1.3	0.35	1.9	0.35

In the present cell cycle analysis experiments, dosages of TMZ and DEAB were applied that had no effect on cell cycle distribution of control cells. The ALDH1A1+/MGMT+ cell lines T40 and R28 as well as ALDH1A1-/MGMT- LN229 cells were treated with a single dose of 200µM TMZ, 300µM DEAB or a combination of both in DMEM + FBS. Cell cycle was analyzed after 48 hours by PI staining and flow cytometry. ALDH1A1 negative cells showed strong accumulation in G2/M following treatment with single doses of ≤ 200µM TMZ, while DEAB administration had no impact on cell cycle distribution.

In line with the results obtained after treatment of LN18 and T98G cells, ALDH1A1+/MGMT+ R28 and T40 cells showed a G2/M arrest following combined treatment with TMZ and DEAB while mere TMZ did not influence cell cycle (Figure 28, see supplementary figure S3 for histograms of cell cycle analysis). In addition to accumulation in G2/M, an increased subG1 fraction was observed after treatment of ALDH1A1+ R28 and T40 cells with TMZ + DEAB (Table 13). R28 cells were treated in DMEM + FBS and neurobasal medium + B27. When treated under serumfree, stem cell preserving conditions, single doses of 100µM DEAB were used as described before (Rasper et al., 2010). When grown in DMEM + FBS, R28 cells showed only G2/M arrest after combination of TMZ and ALDH1A1 inhibition. Under stem cell-maintaining conditions, severe accumulation in G2/M and an increased subG1 peak were detected after addition of mere DEAB (Figure 28, Table 13). R28 shALDH1A1 were also relatively more sensitive to TMZ compared to ALDH1A1 positive control cells (Supplementary figure S4). As described before, an elevated subG1 fraction was also observed, when LN18 shALDH1A1 cells were cultivated in neurobasal medium (Figure 21).

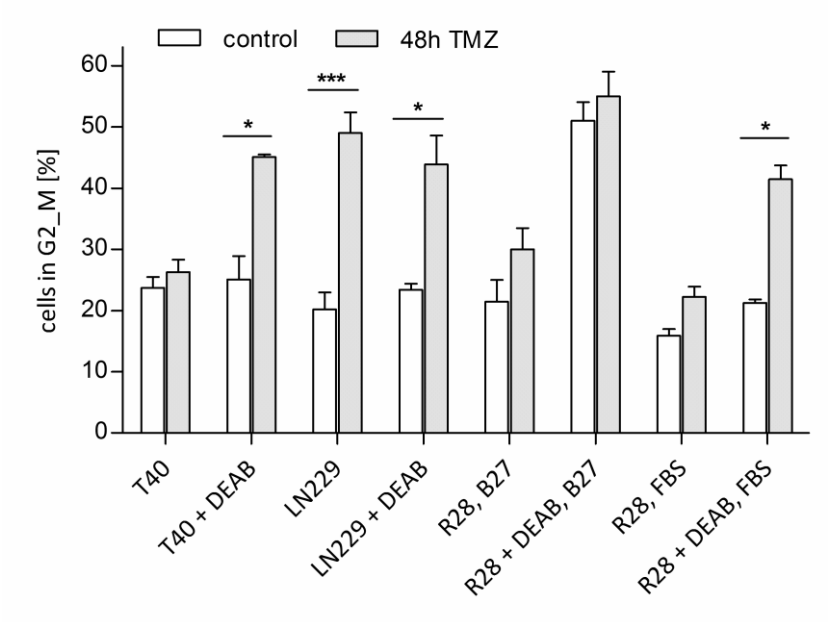

Figure 28: Percentage of LN229, T40 and R28 cells in G2/M

Cell cycle analysis of LN229, T40 and R28 (R28, FBS) cells treated in DMEM + FBS with 200µM TMZ, 300µM DEAB or a combination of both for 48 hours. R28 cells were also analyzed after treatment with 200µM TMZ and 100µM DEAB in neurobasal medium (R28, B27); white bar: control (DMSO or DEAB), grey: 48 hours treated (TMZ or TMZ + DEAB); *p < 0.05, **p < 0.01, ***p < 0.001

Table 13: Percentage of LN229, T40 and R28 cells in the subG1 fraction following treatment with mere TMZ or in combination with DEAB for 48 hours

sub G1 (%)		LN229	+ DEAB	T40	+ DEAB	R28, FCS	+ DEAB	R28, B27	+ DEAB
control	mean	1.17	1.25	0.85	2.0	3.25	4.6	10.2	11.5
	SD	0.32	0.49	0.21	0.98	0.21	0.28	3.25	4.24
48h TMZ	mean	1.15	1.3	2.75	5.0	3.7	9.53	8.3	20.15
	SD	0.35	0.28	0.35	0.42	0.61	1.85	0.85	1.63

ALDH1A1-/MGMT- LN229 cells showed no subG1 peak following TMZ administration but distinct cell cycle arrest and senescence as indicated by β-galactosidase staining (Figure 29).

Figure 29: β-galactosidase staining of senescent LN229 cells after treatment with TMZ

5. Cell cycle arrest following exposure to TMZ and DEAB is accompanied by neural differentiation of ALDH1A1 positive glioblastoma cells

As indicated by flow cytometry, treatment with 200µM TMZ led to a G2/M arrest in LN18 shALDH1A1A1 cells while the cell cycle of wild-type and mock cells was not affected (Figure 26, 27). LN18 shALDH1A1A1 cells blocked at the G2/M boundary by TMZ showed increased levels of neuron specific beta-III-tubulin (Tuj1), while no effect on LN18 control cells was observed (Figure 30 A). Corresponding results were obtained with other ALDH1A1+/MGMT+ cell lines (LN18, T98G, T40 and R28). Combination of TMZ and ALDH1A1 inhibition led to increased expression of Tuj1. In contrast, ALDH1A1 negative cell lines showed elevated Tuj1 levels after treatment with TMZ alone (T16), or no neural differentiation at all (LN229) (Figure 30 B).

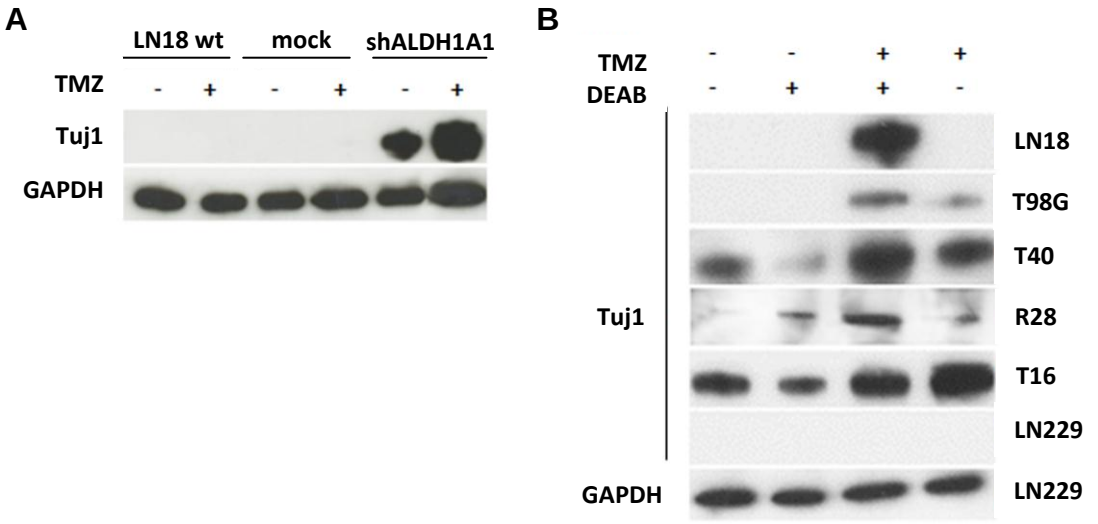

Figure 30: Tuj1 expression following treatment with TMZ, DEAB or TMZ + DEAB in DMEM + FBS

A, Increased Tuj1 expression was detected in LN18 shALDH1A1 cells following exposure to TMZ for 7 days. B, Up-regulation of Tuj1 in ALDH1A1 positive cell lines was observed after treatment with TMZ + DEAB.

6. ALDH1A1 inhibition or knockdown leads to phosphorylation of H2AX after TMZ treatment

Besides MGMT expression, other known mechanisms of TMZ resistance include deficiencies in the MMR pathway, which render cells tolerant to O^6-MG lesions and the base excision repair pathway (BER). Following activation, PARP1, an enzyme involved in BER, recruits DNA repair proteins to DNA lesions. TMZ induced DNA-adducts may result in futile cycles of mismatch repair and double-strand breaks (DSBs) (Karran and Bignami, 1994; Karran et al., 1993); DSBs induce rapid histone H2AX phosphorylation at serine 139 (γ-H2AX), serving as a surrogate marker for DNA damage (Meador et al., 2008). LN18 shALDH1A1 cells showed high levels of γ-H2AX 48 hours after TMZ treatment, while the respective wild-type and mock cells showed no significantly increased γ-H2AX level. Notably, γ-H2AX was strongly increased in LN18 wt cells when TMZ was added in combination with DEAB. LN18 cells feature MGMT activity and thus are able to repair O^6-MG lesion; elevated PARP1 cleavage after TMZ application in LN18 wt and mock cells argues for activation of a caspase-cascade. In contrast, PARP1 cleavage in LN18 shALDH1A1 cells did not increase under TMZ treatment (Figure 31 A).

Similar results were obtained with T98G cells, apart from PARP1 cleavage being first detectable 72 hours after treatment. T98G shALDH1A1 cells featured elevated γ-H2AX 48 hours after TMZ exposure (Figure 31 B). Apoptosis, as analyzed by caspase-3 cleavage was observed neither in treated LN18/T98G wt nor in LN18/T98G shALDH1A1 cells (data not shown).

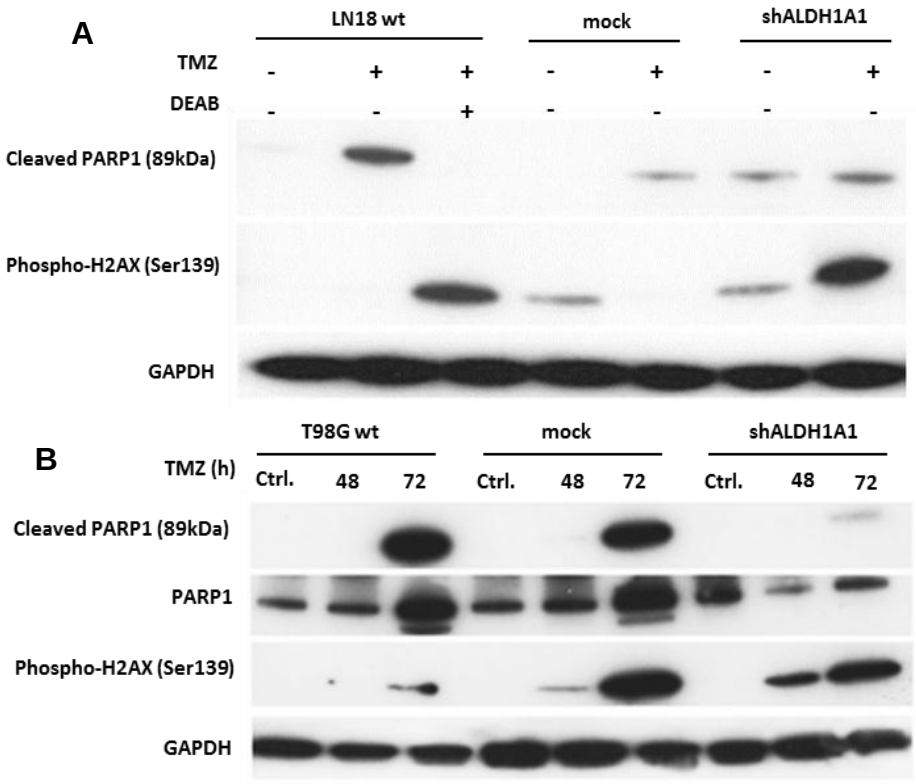

Figure 31: Protein levels of cleaved PARP1 and γ-H2AX after treatment with TMZ, DEAB or TMZ + DEAB

A, Western blot analysis of PARP1 cleavage and γ-H2AX foci in LN18 cells (wt/mock/shALDH1A1) treated with mere TMZ or TMZ + DEAB for 48 hours; B, T98G cells (wt/mock/shALDH1A1) were treated with mere TMZ for 48 or 72 hours.

7. ALDH1A1 plays no major role in mediating resistance to radiotherapy

LN18 cells were irradiated with and without addition of DEAB to further explore the role of ALDH1A1 in the repair or prevention of therapy-induced DNA damage. Application of 2 or 4 Gray (Gy) had no major effect on cell cycle distribution. Apoptotic subG1 fraction increased after irradiation with 4 Gy. Following combined ALDH1A1 inhibition, G2/M peak only slightly increased while no changes in subG1 were observed (Figure 32).

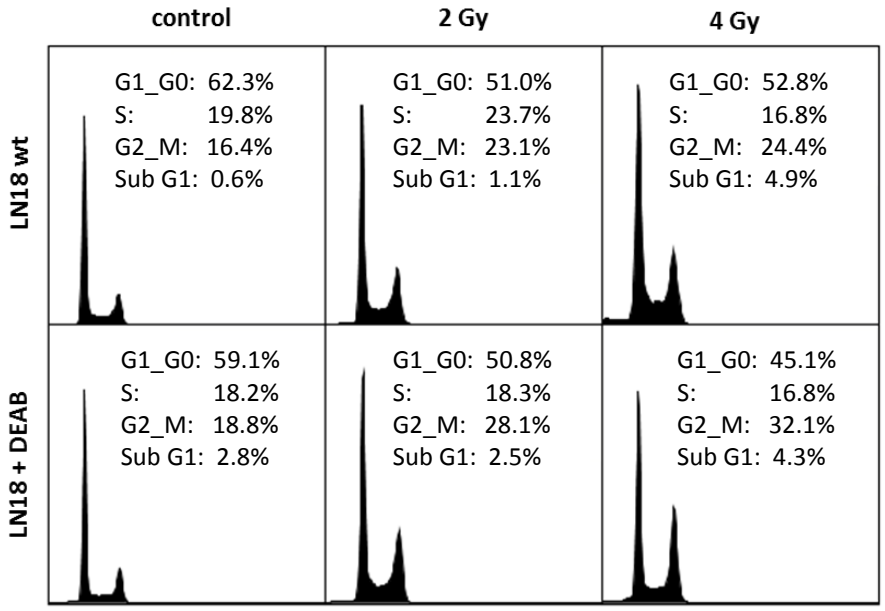

Figure 32: Cycle analysis of irradiated LN18 cells

Representative flow cytometry histograms of LN18 cells following irradiation (alone or in combination with DEAB); Y-axes: DNA content, X-axes: FL3-H

8. ALDH1A1 plays a pivotal role in the protection against oxidative stress

ALDHs are able to catalyze the oxidation of a wide range of aldehydes and a variety of data demonstrate the role of ALDHs in handling oxidative stress and in the protection against DNA-damaging agents (Colvin et al., 1988; Hilton, 1984; Magni et al., 1996; Pappa et al., 2005). To examine the protective role of ALDH1A1 in glioblastoma, oxidative stress was induced by cultivation under hypoxic conditions or by treatment with TMZ.

8.1 ALDH1A1 protein levels increase under hypoxic conditions

Up-regulation of various markers associated with CSCs such as CD133, Oct4, or Nanog under hypoxia was shown before (Heddleston et al., 2009; Li et al., 2009; Soeda et al., 2009). To explore the role of ALDH1A1 in a hypoxic microenvironment, cells were incubated for 6 hours under real hypoxia or with the hypoxia-mimetic agent DFX. Following incubation, ALDH1A1 expression was detected by Western blot analysis. As control for efficient deoxygenation, HIF1A stabilization was analyzed. ALDH1A1 protein level of ALDH1A1+ LN18, T30 and T40 cells was strongly elevated after incubation under hypoxia (Figure 33 A, B).

In contrast, ALDH1A1 negative T12 cells showed no ALDH1A1 expression following exposure to <1% oxygen conditions (Figure 33 B). Strikingly, cultivation under serumfree conditions also resulted in higher ALDH1A1 levels, independently of the oxygen status of the microenvironment (Figure 33 C). Serumfree medium promotes oxidative stress in cell culture as anti-oxidation properties of serum are missing. This substantiates the pivotal role of ALDH1A1 in handling oxidative stress.

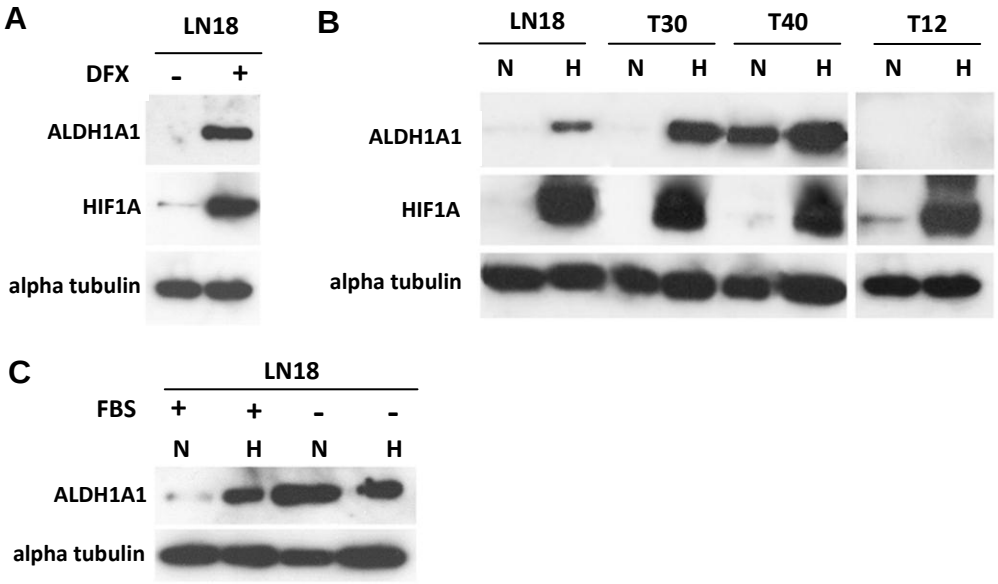

Figure 33: Western blot analysis of ALDH1A1 expression under hypoxic conditions

A, LN18 cells were treated for 6 hours with DFX. B, ALDH1A1 protein level in primary (T30, T40, T12) and established cell lines (LN18) following exposure to hypoxia for 6 hours; C, LN18 cells incubated under hypoxia in DMEM with or without FBS; N: normoxia, H: hypoxia

8.2 Oxidative stress is induced by treatment with temozolomide

In order to assess whether oxidative stress is induced by treatment with temozolomide, nitric oxide and superoxide anion levels in LN18 cells treated with this alkylating agent were analyzed. DAF2/DA staining revealed no significant nitric oxide production after incubation with TMZ (data not shown). In contrast, increased amounts of superoxide radicals were detected after TMZ application. Superoxide levels following incubation with 500µM TMZ were comparable to those in cells treated with 100µM H_2O_2 (Figure 34 A). Microscopic analysis demonstrated a deep red staining of LN18 cells treated with TMZ or H_2O_2. This indicates intercalation of the red fluorescent product (ethidium or 2-hydroxyethidium) with DNA upon reaction of DHE with superoxide anions (Figure 34 B).

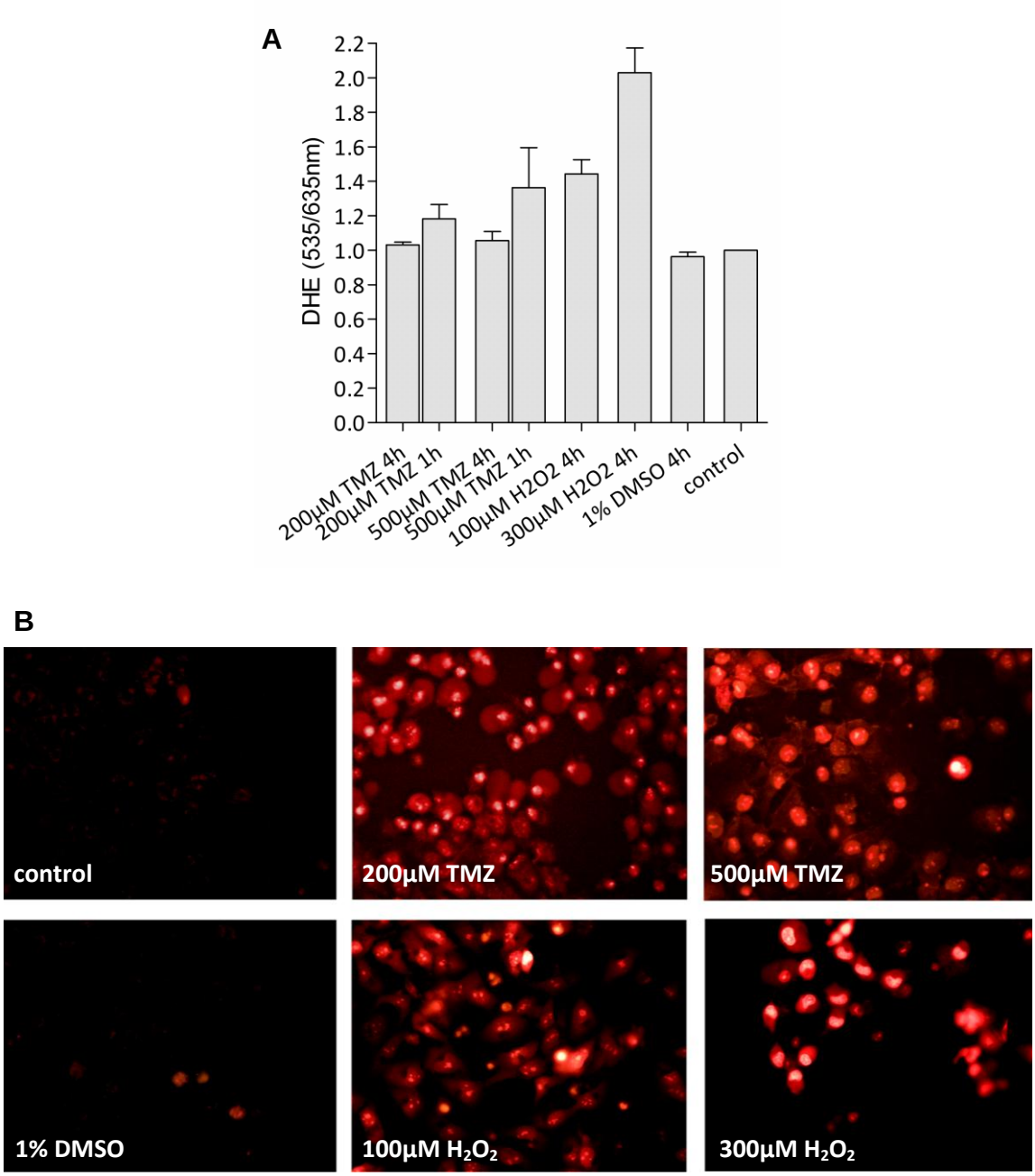

Figure 34: Detection of TMZ induced oxidative stress in LN18 cells

A, Increased fluorescence of DHE at 535/635nm corresponds to superoxide formation following treatment with TMZ or H_2O_2. B, Microscopic analysis of superoxide radicals after exposure to TMZ or H_2O_2 for 1 hour;

Superoxide radicals are well known to induce peroxidation of lipids in the membrane, resulting in highly reactive aldehydes such as 4-HNE or MDA. 4-HNE is the primary α,β-unsaturated aldehyde formed after reaction of radicals with membrane lipids and it is found in higher amounts under oxidative stress. This aldehyde reacts rapidly with nucleophilic functional groups of proteins and DNA leading to etheno-DNA adducts.

To further clarify the role of the isoform ALDH1A1 in handling oxidative stress especially in the context of superoxide anions, LN18 wt/mock/shALDH1A1 cells were treated with 5µM 4-HNE. Cell cycle analysis 48 hours after exposure to 4-HNE indicated accumulation of ALDH1A1 knockdown cells in G2/M, while ALDH1A1 positive wt and mock cells were not affected (Figure 35 A). Western blot analysis of H2AX phosphorylation in 4-HNE treated cells demonstrated elevated γ-H2AX protein level in LN18 shALDH1A1 cells but not in LN18 wt or mock cells (Figure 35 B). These results are corresponding to increased γ-H2AX levels in ALDH1A1 knockdown cells after treatment with mere TMZ or in wt and mock cells after exposure to TMZ + DEAB (Figure 31 A, B). No PARP1 cleavage was observed following exposure to 4-HNE in wt, mock or ALDH1A1 depleted cells.

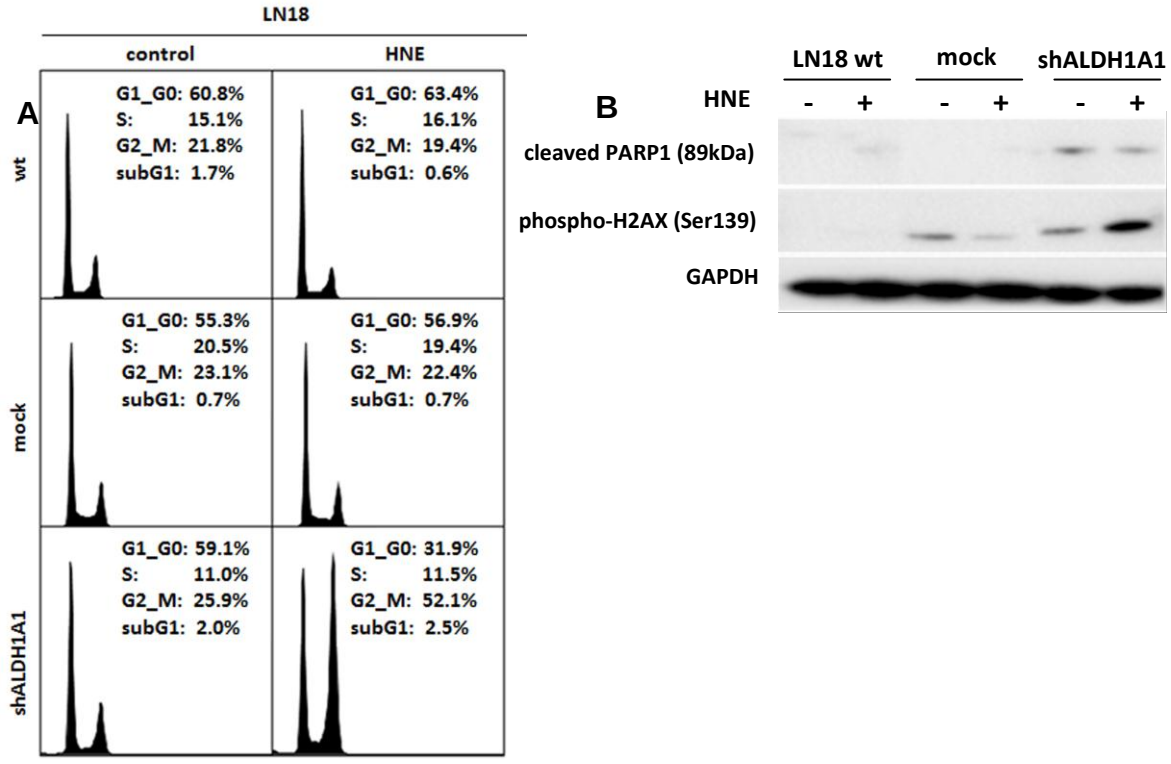

Figure 35: Cell cycle and Western blot analysis of LN18 cells treated with 4-HNE

A, Cell cycle analysis of LN18 wt/mock/shALDH1A1 cells 48 hours after treatment with 5µM 4-HNE; B, Western blot analysis of PARP1 cleavage and γ-H2AX levels 48 hours after exposure to 5µM 4-HNE.

9. High-level ALDH1A1 expression is associated with an unfavorable prognosis in glioblastoma patients

A major role of ALDH1A1 in mediating TMZ resistance was observed *in vitro*. To explore the impact of ALDH1A1 on chemoresistance *in vivo*, ALDH1A1 expression was analyzed by immunohistochemistry (IHC) in seventy surgical specimens of primary glioblastoma patients. ALDH1A1 IHC staining was performed by Julian Teufel and Ingrid Hoepner (Institute of Pathology, Technische Universität München). IHC analysis of IDH1 with R132H point mutation in this cohort underlined the diagnosis as primary GBM, with only one positive tumor sample out of seventy cases (Figure 36).

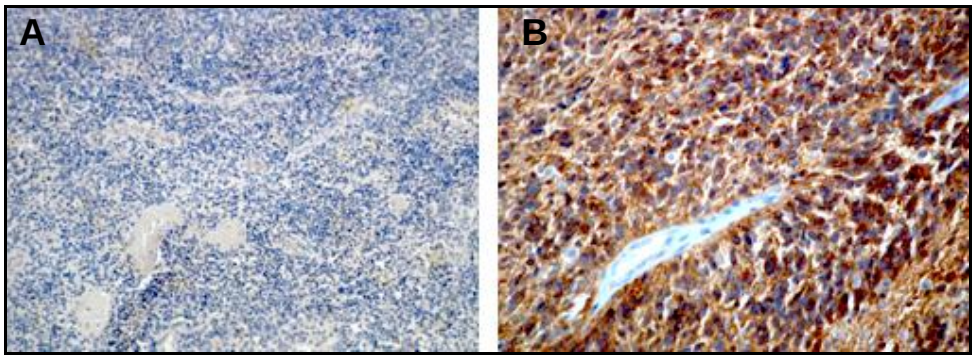

Figure 36: IHC staining of IDH1 with R132H point mutation

A, Tissue specimen of glioblastoma without R132H mutation in IDH1; B, Positive staining for IDH1 with R132H mutation;

As MGMT promoter status was shown to be a predictive factor in TMZ therapy, MGMT status of GBM specimens was assessed by MethyQESD. The cut-off for MGMT positive and MGMT negative tumors was determined by analysis of the martingale residuals (Therneau TM, 1990). Tumor tissues with ≤ 20% MGMT promoter methylation were considered to be MGMT positive (MGMT+); specimens with > 20% MGMT promoter methylation were referred to as MGMT negative (MGMT-). Within the cohort of patients receiving standard therapeutic regimen, the median survival of patients with MGMT- and MGMT+ tumors was 24.3 and 19.2 months, respectively ($p = 0.21$).

Univariate analysis according to the Cox regression model showed that variables such as age and gender were not significantly associated with longer survival.

In the present investigation, clinical outcome was dependent on the therapeutic regimen and the ALDH1A1 status ($p < 0.0001$). Patients treated with radiotherapy plus concomitant and adjuvant temozolomide as described by Stupp *et al*. (Stupp et al., 2005) had a better prognosis than patients that did not receive standard therapy, with a median survival of 20.5 and 8.0 months, respectively ($p < 0.0001$). Multivariate analysis revealed that ALDH1A1 levels were independent of age and gender. Liver tissue served as positive control for ALDH1A1 expression. The cut-off for ALDH1A1 high and low tumors was determined by analysis of the martingale residuals (Therneau TM, 1990). Tumor tissues with ≤ 10% positive cells were considered to be ALDH1A1 low, specimens with > 10% ALDH1A1 positive cells were referred to as ALDH1A1 high (Figure 37).

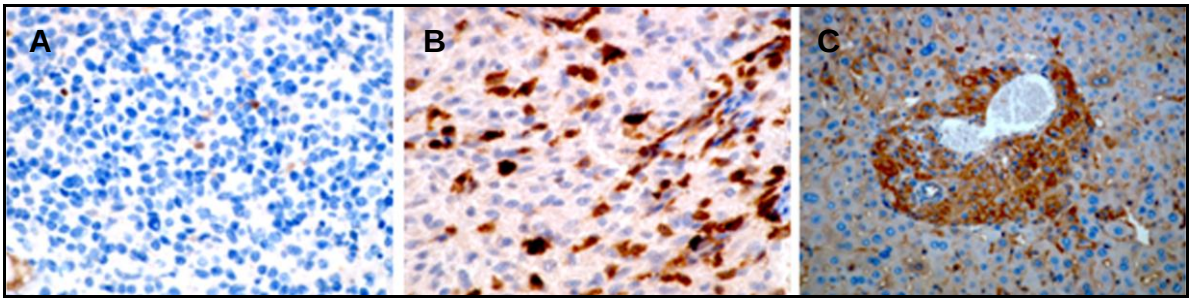

Figure 37: IHC staining of ALDH1A1 in human glioblastomas

A, Tumor tissue with a low percentage of ALDH1A1 positive cells (≤ 10%). B, FFPE section of glioblastoma with a high number of ALDH1A1 positive cells (> 10%). C, Liver tissue served as positive control.

Kaplan-Meier analysis demonstrated that the median survival of patients with low ALDH1A1 expression ($n = 42$) was 21.0 months, compared to 9.8 months of patients with a high percentage of ALDH1A1 positive cells ($n = 28$; $p < 0.0001$) (Figure 38 A). Comparable differences in the median survival were observed when only patients receiving standard therapeutic regimen as described by Stupp *et al.* (Stupp et al., 2005) were analyzed ($n = 50$), with 24.3 and 13.3 months median survival, respectively (Figure 38 B). Within the cohort of patients receiving no standard treatment ($n = 20$), prognosis of patients with low levels of ALDH1A1 was not significantly better compared to patients with high levels, with a median survival of 8.6 and 6.7 months, respectively ($p = 0.217$) (Figure 38 C).

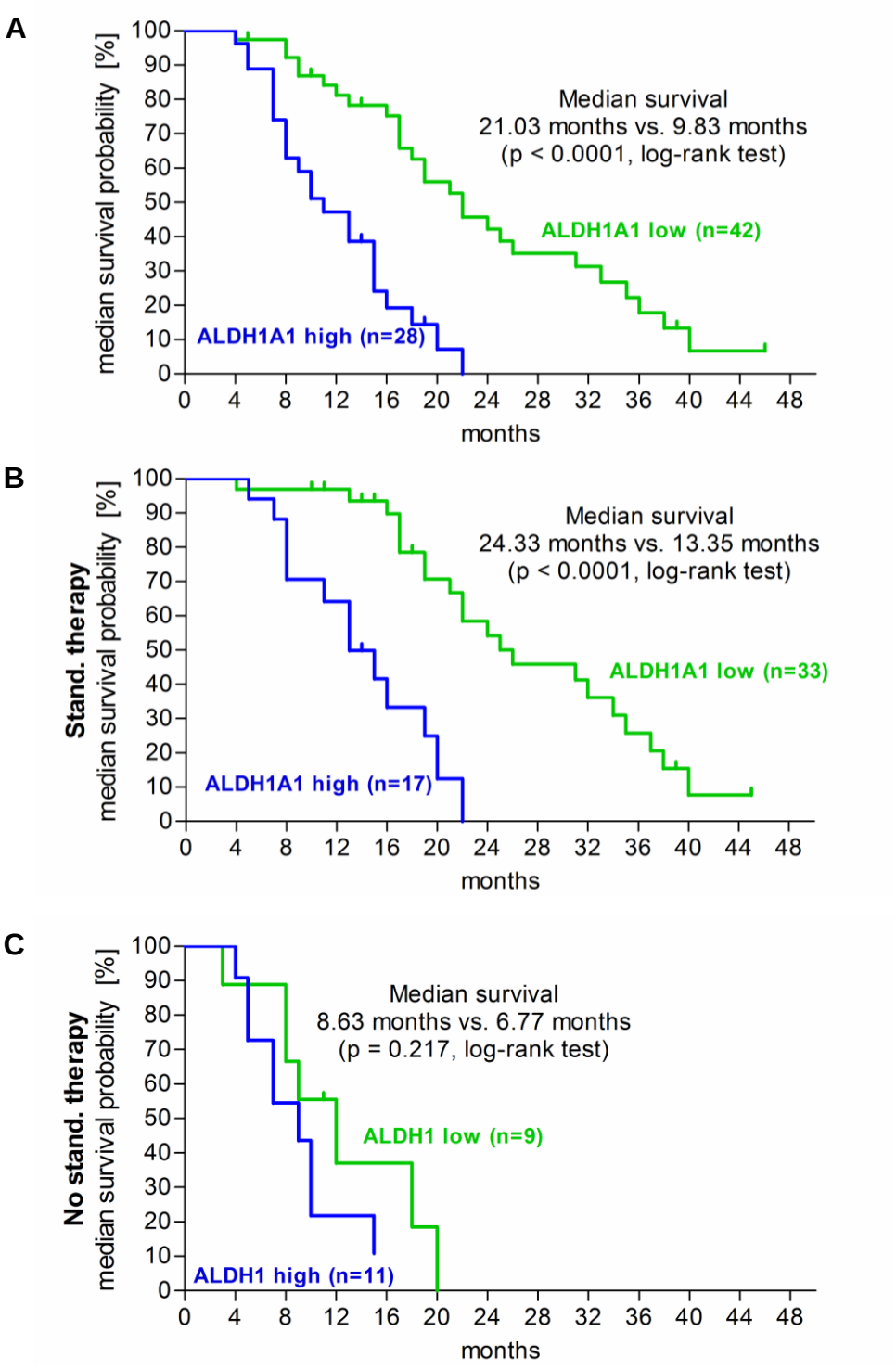

Figure 38: Kaplan-Meier plot of patient median survival

Patients with tumors showing a high level of ALDH1A1 positive cells (blue curve) had a significant shorter median survival compared to patients with low-level tumors (green curve) ($p < 0.0001$). A, All patients were included. B, Only patients receiving standard therapeutic regimen as described by Stupp *et al.* (Stupp et al., 2005); C, Kaplan-Meier plot of patients receiving no standard therapy;

Patients receiving standard therapeutic regimen were further classified regarding the MGMT promoter status within the tumor. The median survival of patients with MGMT- and MGMT+ glioblastomas was 24.3 months and 19.2 months, respectively (p = 0.21). In the group of patients with MGMT- tumors, median survival was 32.9 months and 14.6 months, respectively (p = 0.0004) (Figure 39 A). In the cohort of MGMT+ patients, median survival was 21.4 months and 12.6 months for ALDH1A1 low and high glioblastomas, respectively (p = 0.005) (Figure 39 B).

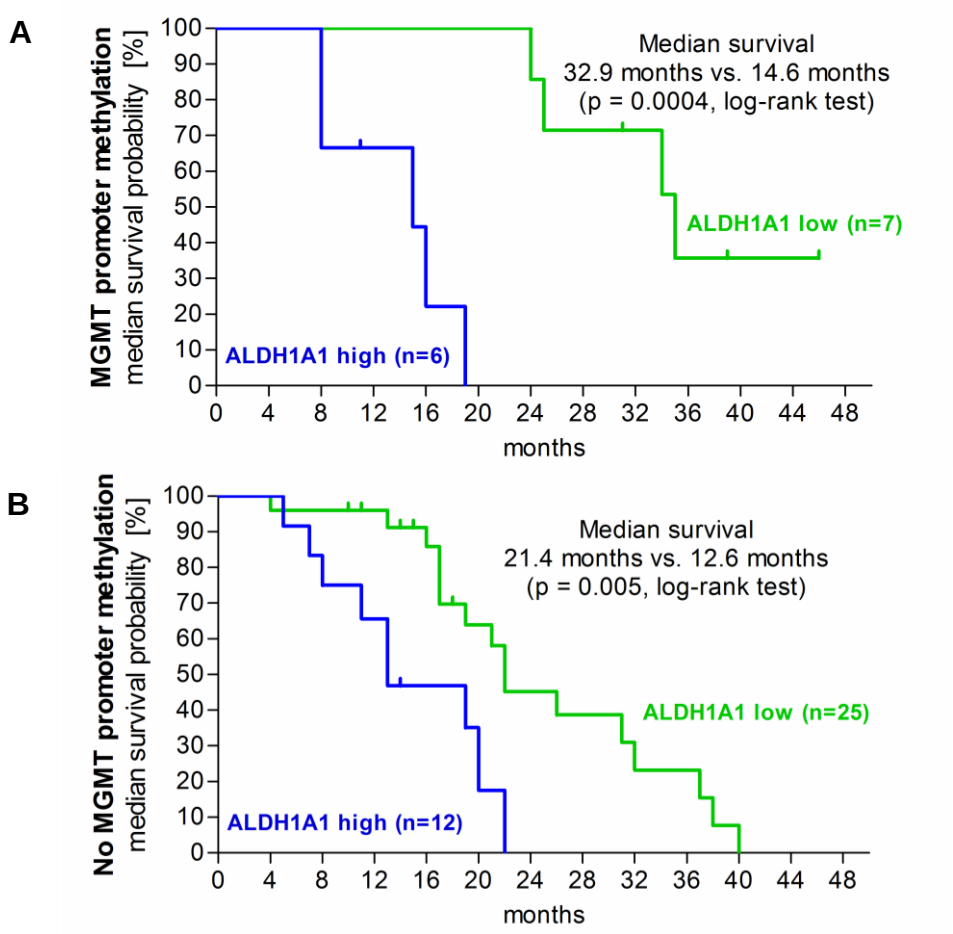

Figure 39: M**edian survival of patients with MGMT+ or MGMT- glioblastomas**

Kaplan-Meier plot demonstrates poor clinical outcome of patients with tumors showing a high level of ALDH1A1 positive cells (blue curve) compared to patients with low-level tumors (green curve) independently of the MGMT status. A, Patients with glioblastomas showing MGMT promoter methylation (p = 0.004); B, Patients with neoplasms without MGMT promoter methylation (p = 0.005).

10. Relapsed glioblastomas show a high percentage of ALDH1A1 positive cells

ALDH1A1 expression levels of primary and relapsed tumors from fourteen primary GBM patients were compared by IHC staining. Remarkably, specimens of recurrent GBM demonstrated significantly higher ALDH1A1 expression levels than the respective primary tumors. The mean ALDH1A1 level increased from 8.5% to 28.6% positive cells in relapsed tumors.

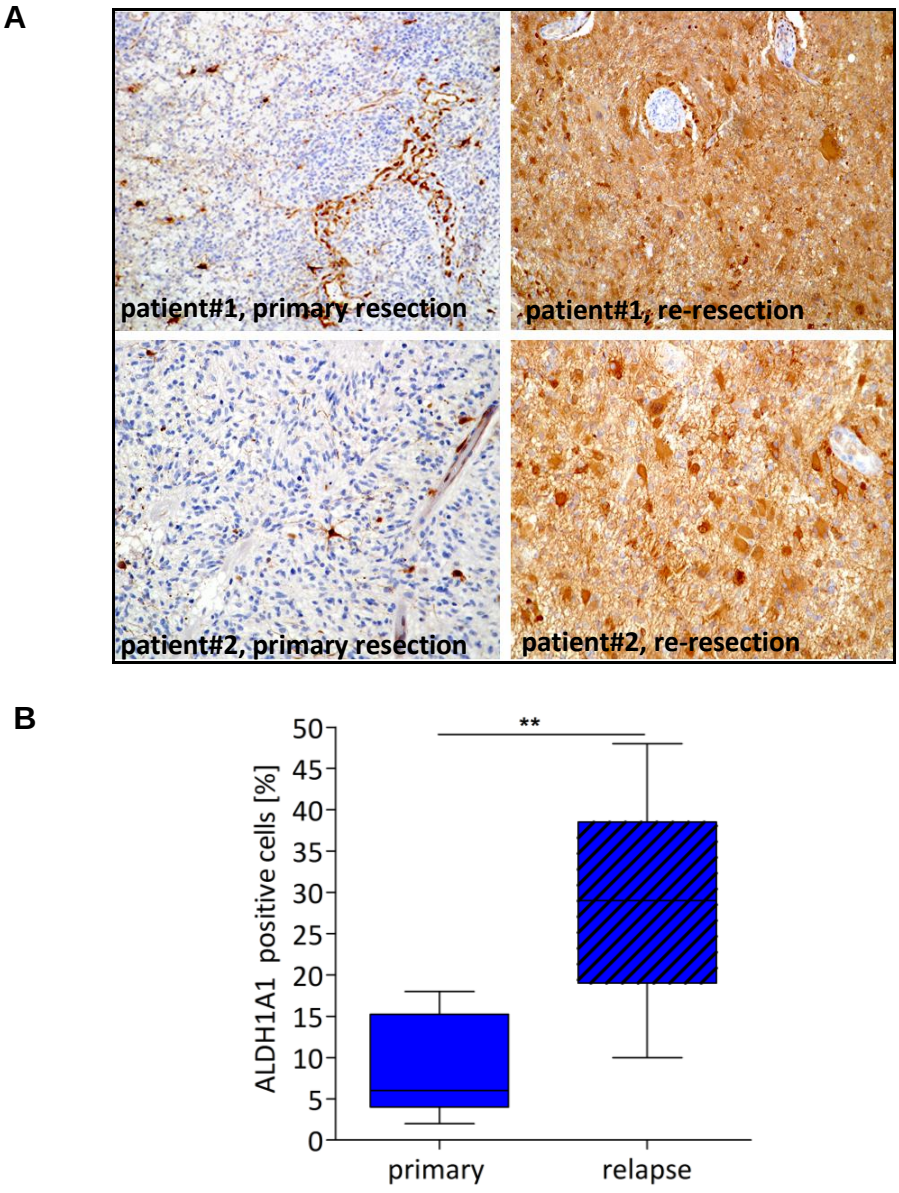

Figure 40: ALDH1A1 expression in recurrent glioblastomas

A, Representative tumor specimens from re-resection (right) showed a significant higher amount of ALDH1A1 positive cells compared to specimens from the respective primary resection (left). B, The median percentage of ALDH1A1 positive cells in relapsed GBMs was significantly higher compared to the respective primary tumors ($p = 0.002$).

E. Discussion

Glioblastoma (GBM) is a WHO grade IV astrocytic tumor and the most common primary brain tumor, accounting for approximately 50% of all gliomas. Application of temozolomide as standard treatment in addition to surgical resection and radiotherapy increased the overall survival of patients with newly diagnosed glioblastoma from 12.1 to 14.6 months (Friedman et al., 2000; Stupp et al., 2005). The orally administered alkylating agent temozolomide transfers methyl groups to the DNA, including the O^6 position of guanine; the repair protein MGMT is able to remove these O^6-methylguanine (O^6-MG) DNA lesions. Hegi and colleagues demonstrated that patients with an epigenetically silenced MGMT promoter (MGMT-) have an improved median overall survival following combined radio-chemotherapy (Hegi et al., 2005). However, despite aggressive therapy the prognosis of glioblastoma patients remains devastating and tumor relapse occurs regularly. A therapy-resistant subpopulation of cells, often described as cancer stem cells seems to be responsible for tumor re-growth. Therefore, additional predictive biomarkers and targets for glioblastoma therapy are of highest clinical interest.

Since the first description of a stem cell-like subpopulation within brain tumors by Singh *et al*. (Singh et al., 2003), the integrity of CD133 as the only robust CSC marker in gliomas has been challenged. For example, Beier *et al.* reported on CD133 positive and negative glioblastoma derived stem-like cells (Beier et al., 2007). In 2007, Ginestier *et al.* described ALDH1 as a marker of breast cancer stem cells (Ginestier et al., 2007). Since then, ALDH1A1 expression was found to characterize stem cells and to correlate with poor clinical prognosis in various solid tumors, including colon carcinoma, prostate cancer, ovarian cancer and lung adenocarcinoma (Ginestier et al., 2007; Huang et al., 2009; Landen et al., 2010; Li et al., 2010; Sullivan et al., 2010). The cytoplasmic enzyme ALDH1A1 belongs to a group of $NAD(P)^+$ dependent dehydrogenases. ALDH1A1 plays an essential role in multiple biological processes including oxidative stress response (Marchitti et al., 2008), cell differentiation (Chute et al., 2006) and drug resistance (Hilton, 1984; Muramoto et al., 2010). Recently, we presented ALDH1A1 as a novel marker for GBM cells with stem cell characteristics (Rasper et al., 2010). Based on the present investigation ALDH1A1 seems to be a new mediator of chemoresistance in glioblastoma.

Sensitivity to temozolomide of ALDH1A1+/MGMT+ cells could be restored by inhibition or by knockdown of ALDH1A1, as indicated by increased cytotoxicity, reduced clonogenicity, accumulation in G2/M cell cycle phase and partial differentiation. Further, the prognosis of patients with high-level ALDH1A1 expression was poor compared to those with low-level. The hypothesis, that ALDH1A1 is a marker for therapy resistant glioblastoma cells is also supported by the observation, that the percentage of ALDH1A1 positive cells was significantly higher in recurrent GBMs compared to the respective primary tumors. Even though the mechanism could not be clarified completely, the present results indicate that oxidative stress plays a critical role in ALDH1A1 mediated temozolomide resistance.

1. ALDH1A1 is expressed by stem-like glioblastoma cells

A broadly used method for the selection of viable ALDH1A1 positive cells in the context of cancer stem cells is flow cytometry with aldefluor®. This assay is based on the conversion of the substrate BAAA (BODIPY-aminoacetaldehyde) by ALDHs into the negatively charged fluorescent reaction product BAA^- (BODIPY-aminoacetate). However, BAAA is not a substrate specific to the isoenzyme ALDH1A1, but is also converted by other isoforms such as ALDH1A3 (Marcato et al., 2011). In prostate cancer cell lines, ALDH7A1 was found to contribute to aldefluor activity. In line with these results, a high aldefluor activity was detected in the ALDH1A3+, ALDH1A1- cell line LN229 (FACS data are not shown). Therefore an antibody specific to the isoform ALDH1A1 was applied in the present experiments. Specificity of the antibody was proven by RT-PCR of various ALDH isoforms; mRNA levels of isoenzymes being associated with cancer stem cells (ALDH3A1, ALDH1A3), having retinal as preferred substrate (ALDH1A3, ALDH8A1), as well as the ubiquitously expressed isoenzymes ALDH7A1 and ALDH2 were determined (Figure 14). Immunoreactivity of the antibody only correlated with expression of the isoform ALDH1A1.

In 2006, Corti *et al*. demonstrated the isolation of neural stem cells by ALDH1 activity. ALDH1 positive cells were able to self-renew, form neurospheres and gave rise to mature neurons when transplanted into the mouse brain (Corti et al., 2006). In 2007, ALDH1 was introduced as a marker of normal and cancerous mammary epithelial cells with stem cell properties; positive cells generated mammospheres, could be differentiated and were highly tumorigenic (Ginestier et al., 2007).

Recently, we described the functional role of ALDH1A1 in the maintenance and expansion of a stem-like phenotype in glioblastoma (Rasper et al., 2010). Only ALDH1A1 positive cell lines were able to generate neurospheres when transferred into neurobasal medium. In addition, inhibition of ALDH1A1 attenuated neurosphere formation. Notably, in the present investigation, knockdown of ALDH1A1 with two different shRNAs induced morphological changes in sphere-forming R28 cells. Following ALDH1A1 depletion, floating neurospheres attached to the cell culture flask (Figure 15 D). Thus, ALDH1A1 seems to play a substantial role in the maintenance of an undifferentiated cellular pool with stem cell characteristics. Primary cell cultures expressing high levels of ALDH1A1 featured low levels of neuron specific beta-III-tubulin (Tuj1) and vice versa (Figure 11). When neurospheres were exposed to the ALDH1A1 inhibitor DEAB or to retinoic acid, increased protein levels of Tuj1 indicated initial neural differentiation. In addition, ALDH1A1 positive cells could be differentiated into all three neural lineages: oligodendroglial, astrocytic and neuronal, as shown by expression of GalC, GFAP or Tuj1 (Figure 13).

Within the last years, various works analyzed the potential of retinoic acid to induce cellular differentiation in gliomas (Campos et al., 2011; Zeng et al., 2009). ALDH1A1 converts the precursor retinal to biologically effective retinoic acid which leads to hetero-dimerization of RAR and RXR upon translocation to the nucleus. Heterodimeric retinoic acid receptors subsequently induce transcription of genes related to differentiation. It was shown, that differentiated glioma cells are sensitive to radio- and chemotherapy (Campos et al., 2010). Campos *et al*. also demonstrated the influence of aberrant retinoic acid signaling on the outcome of patients with astrocytic tumors. They suggested the retinoic acid binding protein FABP5 (fatty acid binding protein 5) to play a crucial role in this context; FABP5 can inhibit retinoic acid induced differentiation by activation of Akt upon binding to retinoic acid. Hereby, FABP5 converts the differentiation potential of the ALDH1A1 product retinoic acid into an anti-apoptotic one. This might explain, why ALDH1A1 overexpression predicts adverse patient survival despite the differentiating potential of its product retinoic acid. In contrast, Adam *et al*. described co-expression of ALDH1A1 with GFAP and therefore suggested ALDH1A1 to be a marker of astrocytic differentiation. Our immunohistochemical analysis of glioblastoma specimens revealed that ALDH1A1 and GFAP expression are rather mutually exclusive.

In addition, ALDH1A1 positive cells were found in the subependymal ribbon of the subventricular zone (Rasper et al., 2010), where several types of astrocytes, including multipotent neural stem cells, reside (Quinones-Hinojosa et al., 2006).

Furthermore, elevated ALDH1A1 protein levels were found under hypoxia. While the physiological oxygen concentration in normal brain tissue ranges from 12.5% to 2.5%, glioblastomas exhibit a hypoxic microenvironment with oxygen concentrations ranging from 2.5% to 0.1%. Up-regulation of various markers associated with cancer stem cells such as CD133, Oct4, or Nanog under hypoxia was shown before (Heddleston et al., 2009; Li et al., 2009; Soeda et al., 2009). Our results indicate that cellular ALDH1A1 protein levels increase under hypoxia in ALDH1A1 positive cells lines (LN18, T30, T40), while ALDH1A1 expression was not inducible in cells negative for ALDH1A1 under normal cell culture conditions (T12) (Figure 33 B, C). An elevated enzyme level under stress conditions such as hypoxia or serum-deprivation seems to protect cells against reactive oxygen species.

Taken together, ALDH1A1 positive GBM cells were capable to form neurospheres and could be differentiated into all three neural lineages. Inhibition of ALDH1A1 impaired sphere formation and induced neural differentiation. In addition, ALDH1A1 protein levels increased under oxygen stress conditions, offering a mechanism to protect cells against a toxic microenvironment.

2. PTEN/PI3K/Akt pathway and ALDH1A1 expression play a substantial role in neurosphere formation

In 1992, Reynolds and Weiss described the growth of neural stem cells in neurospheres in serum free cell culture medium supplemented with EGF and bFGF (Reynolds and Weiss, 1992). Since then, formation and serial passaging of neurospheres has become a widely accepted assay to functionally characterize normal and malignant cells with stem cell capacity. As described above, a correlation between ALDH1A1 expression and neurosphere formation was observed in established and primary GBM cell lines. However, little is known about the mechanism of ALDH1A1 controlled sphere formation. Aberrations in EGFR and PTEN represent a genetic hallmark of primary glioblastoma.

A strong correlation between mutations in the EGFR/PTEN/PI3K/Akt signaling and a stem cell phenotype was found in different malignancies such as breast cancer or glioma (Bleau et al., 2009; Korkaya et al., 2009). Therefore, the interaction of ALDH1A1 with this pathway was analyzed in glioblastoma cell lines.

Amplification of the EGFR gene is found in 30-40% of primary GBM. Recently, it was shown that EGFR gene amplification as well as expression of the constitutive active, truncated EGFRvIII variant could be preserved by cultivation in neurobasal medium (Witusik-Perkowska et al., 2011). Moreover, treatment with the EGFR inhibitor AG1478 or the PI3K inhibitor LY294002 significantly reduced sphere formation (Torroglosa et al., 2007). In the present investigation, LN18 cells carrying the EGFRvIII variant generated neurospheres faster and more frequently compared to control cells or to cells with the dominant negative construct EGFR-CD533 (Figure 17 A). Cells growing in neurospheres shared high levels of ALDH1A1 and Akt activation, indicating that both factors are relevant for sphere formation (Figure 17 B). Furthermore, all analyzed sphere forming GBM cell lines showed PTEN aberrations such as mutation, depletion or phosphorylation and thus inactivation of the protein (Vazquez et al., 2000) (Figure 16). In 2010, Chen and colleagues analyzed the correlation of various factors, including CD133 expression, MGMT promoter methylation, p53 mutation, EGFR amplification and PTEN status with the capacity to generate neurospheres in primary GBM. Exclusively the PTEN status correlated with neurosphere formation (Chen et al., 2010). Several other works addressed the role of an aberrant PTEN status and thus activated Akt in the maintenance of a stem cell phenotype. Bleau *et al*. described the role of the PTEN/PI3K/Akt pathway in the regulation of the side population (SP) of glioma stem-like cells. Exposure of neurospheres to the PI3K inhibitor LY294002 reduced the proportion of SP cells. In addition, loss of PTEN increased the SP fraction and led to greater temozolomide resistance (Bleau et al., 2009). However, the authors could not explain how PI3K/Akt signaling regulates the SP phenotype.

Our data highlight a major role of ALDH1A1 expression and activated Akt in neurosphere growth following aberrant EGFR signaling or PTEN deactivation. Inhibition of both, ALDH1A1 and Akt decreased neurospheres in size and number. Further, sphere growth of cells with an ALDH1A1 knockdown was reduced, with an average sphere size comparable to DEAB treated control cells (Figure 19 B, C).

In line with these findings, levels of activated Akt were lower in ALDH1A1 inhibited or depleted cells compared to ALDH1A1+ control cells (Figure 19 A). Even though, R28 neurosphere formation was strongly affected by treatment with DEAB or by knockdown of ALDH1A1 (Figure 15, 24), Akt activation was not attenuated. Cell cycle analysis of LN18 and R28 cells, following treatment with DEAB or Akti (Figure 21, 28; Table 12, 13) also hint to different mechanisms. Inhibition of ALDH1A1 led to increased apoptosis and G2/M arrest, while a G1 arrest was observed after exposure to the Akt1/2 inhibitor. Caspase 3 cleavage confirmed apoptosis after DEAB treatment (Figure 21 B). In accordance, only ALDH1A1 depleted cells exhibited apoptosis and G1 arrest after incubation with the Akt1/2 inhibitor. Due to this additive effect, ALDH1A1 depletion and Akt inhibition might serve as an efficient combination therapy in glioblastoma.

Notably, ALDH1A1 protein level was significantly reduced after treatment with the Akt1/2 inhibitor in both, LN18 and R28 cells. These findings suggest that ALDH1A1 is a downstream target of Akt signaling (Figure 41). Similar results were recently described in breast cancer: the authors found an enrichment of ALDH1 positive cells after knockdown of PTEN in mammospheres (Korkaya et al., 2009). The present data indicate that vice versa, activation of PI3K/Akt signaling is necessary for the maintenance of an ALDH1A1 positive cell pool in suspension culture.

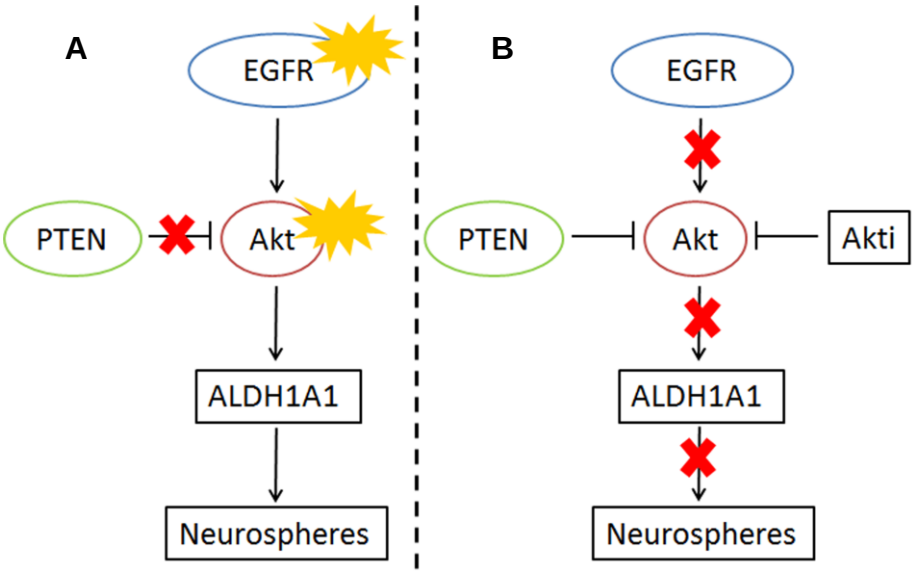

Figure 41: The role of PTEN/PI3K/Akt signaling in the maintenance of a self-renewing ALDH1A1 positive cell pool

A, EGFR activation (EGFRvIII variant) or non-functional PTEN protein (deletion or mutation) induce Akt activation (phospho-Akt). Activated Akt leads to increased ALDH1A1 protein levels and neurosphere generation. B, Akt phosphorylation is inhibited by attenuated EGFR signaling (EGFR-CD533 variant), wild-type PTEN or addition of an Akt1/2 inhibitor (Akti). Following Akt inhibition, ALDH1A1 protein levels decrease and neurosphere formation is impaired.

Analysis of downstream effectors of PTEN/PI3K/Akt signaling provided evidence, that GSK-3 but not mTor was involved in neurosphere formation (Figure 20). GSK-3 activity is inhibited by Akt-mediated phosphorylation at Ser21 of GSK-3α and Ser9 of GSK-3β. As a consequence, GSK-3α/β is dephosphorylated and activated following inhibition of Akt (Figure 20). Activated GSK-3 has been shown to regulate cyclin D1 proteolysis by phosphorylation (Diehl et al., 1998). In the presence of growth factors, D-type cyclins (D1, D2, and D3) assemble with either CDK4 or CDK6 to active holoenzymes that allow G1/S transition. A G1 cell cycle arrest was observed in LN18 cells following inactivation of Akt and thus activation of GSK-3α/β. This might be explained by GSK-3α/β mediated phosphorylation and degradation of cyclin D1, leading to checkpoint activation. Furthermore, GSK-3α/β is a critical effector of the Wnt signaling pathway, involved in embryonic development and tumorigenesis. Following inhibition of Akt, activated GSK-3β can destabilize β-catenin, a key downstream factor in the Wnt signaling pathway by phosphorylation, as it was observed in R28 neurospheres.

In general, reduced levels of phosphorylated β-catenin were detected when cells were transferred from adherent growth conditions to stem cell preserving suspension cultures, indicating β-catenin activation (Figure 20). Korkaya *et al.* described that PTEN/Akt driven mammary stem cell enrichment is mediated by phosphorylation of GSK-3α/β and subsequent activation of Wnt/β-catenin pathway (Korkaya et al., 2009). Further studies should determine whether the Wnt signaling pathway is involved in the maintenance of a stem-like cell pool in glioblastoma. As phosphorylation sites of β-catenin are often mutated in cancer cell lines, activity of GSK-3α/β and β-catenin must be analyzed by determining cellular localization. When translocated into the nucleus, β-catenin activates transcription of a wide range of genes. Little is known about the transcriptional regulation of ALDH1A1 in tumors and further experiments should be done to elucidate whether β-catenin or other transcription factors downstream of PTEN/PI3K/Akt pathway are involved in ALDH1A1 gene regulation. In addition, comparison of ALDH1A1 negative cell lines such as LN229 and G139 that grow adherent in neurobasal medium with sphere forming ALDH1A1+ cells, might give a hint on pathways involved in the enrichment of stem-like glioblastoma cells.

Recent studies report on therapy resistant cellular subpopulations within tumors that display stem-like properties. The PTEN/PI3K/Akt pathway seems to be involved in the regulation of a stem cell phenotype. Applying neurosphere growth as a functional assay to characterize stem-like glioblastoma cells, a correlation between neurosphere generation, PTEN/Akt status and ALDH1A1 expression was found in the present investigation. PTEN/PI3K/Akt signaling seems to maintain a self-renewing ALDH1A1 positive cell pool *in vitro*.

3. ALDH1A1 overexpression predicts temozolomide resistance *in vitro*

Therapy resistance is often associated with a subpopulation of cells that is able to escape therapy and to re-induce tumor growth. These cells share some properties with (cancer) stem cells: i) they are slow-growing and therefore resistant to drugs targeting highly proliferative cells, ii) the ability to activate specific repair mechanisms or to inactivate cell cycle check points, iii) they express ATP-binding cassette transporters (ABC transporters) that facilitate efflux of chemotherapeutic drugs (Dean et al., 2005). Characterization of these resistant subpopulations within glioblastomas is essential for the development of more efficient therapeutic strategies.

To date, MGMT represents a major mechanism of resistance to temozolomide. Hegi *et al*. demonstrated that patients with an epigenetically silenced MGMT promoter (MGMT-) have an improved median overall survival (Hegi et al., 2005). However, to date there is no alternative treatment option for patients with an unfavorable MGMT promoter status (MGMT+). In addition, there are patients profiting from TMZ treatment despite expression of MGMT as well as patients with an epigenetically silenced MGMT promoter showing no response (Gaspar et al.; Hegi et al., 2008). These observations might be explained by glioblastoma cells that feature additional mechanisms of TMZ resistance.

The enzyme ALDH1A1 has been associated with drug resistance and cellular detoxification. It was first described in the early 1980s, that ALDH1A1 positive leukemic and hematopoietic stem cells are able to metabolize and detoxify the alkylating agent cyclophosphamide (Eyler and Rich, 2008; Hilton, 1984). In a retrospective study of 171 human breast cancer patients, ALDH1A1 expression predicted response to cyclophosphamide (Sladek et al., 2002). In the present investigation, the enzyme ALDH1A1 is introduced as a new mediator of resistance to TMZ. High levels of ALDH1A1 were associated with resistance to TMZ *in vitro*, in particular in MGMT+ GBM cells. ALDH1A1-/MGMT- cells (T16, LN229) were most sensitive to TMZ while cell lines expressing ALDH1A1 and MGMT (ALDH1A1+/MGMT+; LN18, T98G, T39, T40, R28) were highly resistant to treatment with TMZ. ALDH1A1-/MGMT-* (G139) cells were more sensitive to low doses (≤ 100µM) TMZ as ALDH1A1+/MGMT- (T30) cells (Figure 22).

Data of Mihatsch *et al*. described ALDH1 as a mediator of resistance to radiotherapy *in vitro*. While Sox2, Oct4 and CD133 expression was not prevalent in radioresistant breast cancer cells, a strong correlation with ALDH1 expression was found (Mihatsch et al., 2011). Preliminary analysis of LN18 cells, irradiated with or without DEAB, did not clearly indicate a correlation between ALDH1A1 expression and radioresistance (Figure 32).

In conclusion, ALDH1A1 expression predicted resistance of glioblastoma cells to TMZ independently of the MGMT status. As MGMT+ glioblastomas are in general highly resistant to TMZ treatment, the present investigation focused on finding new methods to sensitize these cells to therapy.

4. Sensitivity of ALDH1A1+/MGMT+ glioblastoma cells to temozolomide is restored by inhibition or knockdown of ALDH1A1

The present results indicate that inhibition and knockdown of ALDH1A1 are efficient mechanisms to overcome chemoresistance in MGMT+ GBM cells. Colony and neurosphere formation assay revealed significantly attenuated clonogenicity of ALDH1A1+/MGMT+ cells after exposure to TMZ in combination with ALDH1A1 inhibition or depletion (Figure 23). Concomitant treatment with TMZ and DEAB in ALDH1A1+/MGMT+ cells (LN18, T98G, R28) significantly decreased neurospheres in size and number, demonstrating both inhibition of proliferation (decreased neurosphere-size) and reduction of clonogenicity (reduced number of neurospheres) (Figure 24). Recently, it was shown that TMZ was efficient to block neurosphere formation of MGMT- human GBM cells (Mihaliak et al., 2010). The present data indicate that neurosphere formation of MGMT+ cells is not attenuated by pre-treatment with mere TMZ but clonogenic capacity was strongly decreased by combined ALDH1A1 inhibition (Figure 24). ALDH1A1+/MGMT+ R28 cells showed impaired neurosphere formation when treated in neurobasal medium with mere TMZ or DEAB. These observations are in line with previous studies demonstrating attenuated neurosphere development following exposure to DEAB or TMZ under serum free conditions (Beier et al., 2008; Rasper et al., 2010). Strikingly, combination of TMZ and DEAB led to a stronger decrease of clonogenic capacity under both, normal and stem cell-maintaining conditions. Further, MTT assay revealed a synergistic cytotoxic effect of ALDH1A1 inhibition with DEAB or knockdown by shRNA and TMZ in ALDH1A1+/MGMT+ cells (Figure 25).

It is important to notice that temozolomide concentrations in the plasma of glioblastoma patients do not exceed 50µM while in the cerebrospinal fluid only levels of 5µM are reached (Ostermann et al., 2004). However, after oral administration, the prodrug TMZ is rapidly hydrolyzed to its reactive methylating agent MTIC. In order to evaluate efficacy of treatment and to compare experimental concentrations with clinical practice, determination of MTIC levels in plasma and cerebrospinal fluid would be more reasonable. In cell culture experiments, a broad range of temozolomide concentrations are applied; while a dosage of 50µM TMZ is efficient to inhibit MGMT- human GBM cells (Mihaliak et al., 2010), the IC_{50} of MGMT+ cells is often more than 10 fold higher (Hermisson et al., 2006).

Since the aim was to overcome temozolomide resistance in MGMT+ GBM cells, concentrations of ≥ 200µM were applied. In cell cycle experiments, dosages that had no cytostatic effect on ALDH1A1+/MGMT+ control cells were used.

TMZ is known to induce DNA lesions leading to cell cycle arrest at the G2/M boundary and to rather induce senescence than direct apoptosis in GBM. Hirose *et al.* described the role of p53 on cell cycle arrest under TMZ treatment; cells with mutated p53 or p53 deficient cells were relatively more resistant to TMZ and underwent only transient G2/M arrest, while cells with wild-type p53 showed prolonged arrest. Nevertheless, the fraction of apoptotic cells did not exceed 10% (Hirose et al., 2001). In the present investigation, most cell lines used in cell cycle experiments had mutated p53 (LN18, LN229, G139, T98G). The p53 status of the respective primary cell lines was not assessed. Furthermore, Hirose *et al*. demonstrated a pivotal role of activated Akt in bypassing temozolomide induced G2/M arrest. Akt activation suppressed G2/M arrest and protected GBM cells from senescence following exposure to TMZ (Hirose et al., 2005). All cell lines used in the present cell cycle experiments featured aberrant PTEN status; they either had PTEN mutations (T98G), absent PTEN protein (T40, R28) or showed high levels of phosphorylated less active PTEN (LN18, LN229) (Figure 16). In general, GBM cells feature a very heterogeneous profile of genetic alterations. In the present investigation, all cell lines shared the most common mutations, so that conclusions could be drawn on the role of ALDH1A1 in mediating response to temozolomide. Analysis of cell cycle distribution following TMZ treatment indicated that prolonged G2/M arrest was dependent on ALDH1A1 expression and MGMT status. ALDH1A1 positive LN18, T98G, T40 and R28 cells exhibited no or only slight G2/M accumulation in response to TMZ, while the respective shALDH1A1 or ALDH1A1 inhibited cells showed prolonged G2/M arrest (Figure 26, 27, 28).

In addition to cell cycle arrest, induction of apoptosis was detected in DEAB treated or ALDH1A1 knockdown cells following TMZ exposure (Table 12, 13). ALDH1A1-/MGMT- LN229 cells showed prolonged G2/M arrest and became senescent following treatment with TMZ, as indicated by β-galactosidase staining (Figure 29). ALDH1A1-/MGMT-* G139 cells responded comparable to LN229 cells after exposure to TMZ (data not shown). The reason for this behavior is absent MGMT repair protein in G139 cells, despite an unmethylated MGMT promoter.

As previously described, sphere formation was attenuated following exposure to DEAB (Rasper et al., 2010); spheres grown in neurobasal medium were strongly affected by treatment with DEAB while under normal cell culture conditions no response to ALDH1A1 inhibition was observed. When grown in DMEM + FBS, R28 cells showed only G2/M arrest after combination of TMZ and ALDH1A1 inhibition. Under serumfree stem cell maintaining conditions, substantial accumulation in G2/M and increase of subG1 peak was detected after addition of mere DEAB (supplementary figure S3). Cell cycle arrest and an elevated subG1 fraction after cultivation of LN18 shALDH1A1 cells in neurobasal medium (supplementary figure S5) demonstrate once more the pivotal role of ALDH1A1 in the protection against oxidative stress under serumfree conditions.

In addition, accumulation in G2/M was accompanied by neural differentiation of ALDH1A1 inhibited or knockdown cells following treatment with TMZ. Since ALDH1A1+ control cells showed no Tuj1 expression, cell cycle arrest might be necessary for differentiation, as already shown for other cell types (Zanet et al., 2010). Cellular differentiation following TMZ application was demonstrated in leukemia and GBM cell lines (Beier et al., 2008; Zucchetti et al., 1989). Considering the present results, TMZ induced neural differentiation only occurred in ALDH1A1 negative or inhibited cells. However, further markers such as GalC or GFAP should be examined to support the hypothesis of temozolomide induced differentiation.

In principle, concomitant inhibition by DEAB or knockdown of ALDH1A1 by short hairpin RNA re-sensitized MGMT+ cell lines to TMZ treatment, as indicated by increased cytotoxicity, reduced clonogenicity and accumulation in G2/M.

5. High-level ALDH1A1 expression correlates with an unfavorable prognosis in GBM patients

Our present *in vitro* data demonstrate an important role of ALDH1A1 in mediating TMZ resistance additionally to MGMT. To compare these experimental findings with clinical practice, ALDH1A1 expression was investigated retrospectively in seventy tumor specimens from patients with primary GBM. IHC staining of isocitrate dehydrogenase 1 (IDH1) with R132H point mutation supported the diagnosis as primary GBM with only one positive sample out of seventy cases (Figure 36) (Nobusawa et al., 2009).

Martingale residuals were plotted versus the percentage of ALDH1A1 positive cells or versus the percentage of MGMT promoter methylation to determine the cut-off, respectively (Therneau TM, 1990). This analysis offers an adequate way to find a statistically relevant cut-off. A significant link between ALDH1A1 expression and median survival probability was found *in vivo*. Patients with tumors expressing high levels of ALDH1A1 (> 10% ALDH1A1 positive cells) had a poor clinical prognosis, compared to patients with low levels (≤ 10%), in both MGMT+ and MGMT- cohorts (Figure 38, 39). Even though ALDH1A1 overexpression was shown to correlate with a poor survival in most solid tumor entities, data on the predictive value of ALDH1A1 are contradictory. In breast, lung, prostate, ovarian and pancreatic cancer, ALDH1 expression correlated with a worse outcome and more aggressive tumors (Deng et al., 2010; Ginestier et al., 2007; Jiang et al., 2009; Li et al., 2010; Rasheed et al., 2010). Other studies on pancreatic and ovarian cancer showed an association with a favorable outcome (Chang et al., 2009; Kahlert et al., 2011).

There are also contradictory data on the predictive value of ALDH1A1 expression in glioblastoma: Adam *et al*. postulated a better survival in glioblastoma patients with a high percentage of ALDH1A1 positive cells, while Campos *et al*. found ALDH1A1 to be an independent prognostic marker for adverse patient survival (Adam et al., 2012; Campos et al., 2011). Our data clearly contradict the work of Adam and colleagues. Analysis of the clinical data provided by the authors revealed, that in their setting ALDH1A1 was not an independent factor, but dependent on the type of sampling. Significant higher levels of ALDH1A1 were found in samples analyzed after stereotactic biopsy compared to specimens from total resection. Apparently the sampling type was prognostically relevant, since patients with stereotactic biopsy had a significant lower median overall survival time compared to the cohort receiving total resection. This is in line with our findings that ALDH1A1 expression was not predictive in the group of patients that did not receive standard therapy as described by Stupp *et al*. (Stupp et al., 2005) (Figure 38 C). Further, it demonstrates the importance of standardized therapeutic regimens in the evaluation of biomarkers. The present results on the predictive value of ALDH1A1 in glioblastoma are consistent with the work by Campos *et al.*; the authors showed that the percentage of ALDH1A1 positive cells increases with the malignancy in astrocytic gliomas.

In GBM, high ALDH1A1 levels were significantly associated with poor patient survival (Campos et al., 2011). Nevertheless, the authors did not state whether primary or secondary glioblastomas were analyzed and they did not propose a cut-off for clinical practice.

The present results indicate that ALDH1A1 is a feasible predictor of clinical outcome complementary to MGMT status. IHC staining of ALDH1A1 along with a generally accepted cut-off for ALDH1A1+ and ALDH1A1- GBM would be practical for routine clinical histopathological diagnosis. Even though the outcome of patients with a methylated MGMT promoter was better compared to patients with MGMT+ glioblastoma, the MGMT status of the analyzed cohort was not significantly predictive. A prospective study with a larger cohort of patients receiving a standardized therapeutic regimen should be performed to verify the correlation of ALDH1A1 expression in MGMT+ and MGMT- glioblastomas with clinical prognosis and to validate the applicability of a 10% cut-off for routine diagnostic.

6. ALDH1A1 is extensively expressed in tumors of patients with recurrent GBM

Despite therapy, tumor relapse occurs regularly in GBM patients. As stated before, this clinical behavior might be associated with a resistant sub-population of cells (Bao et al., 2006; Frosina, 2009; Gaspar et al., 2010). Enrichment of ALDH1 positive colorectal stem-like cells was found in xenogeneic tumors following chemotherapy with cyclophosphamide (Dylla et al., 2008). In order to assess, whether ALDH1A1 positive cells are enriched following chemotherapy, ALDH1A1 expression was analyzed in specimens resected prior to therapy and in tissues of patients with relapsed GBM (Figure 40). Significantly increased ALDH1A1 levels in relapsed GBMs indicate that TMZ resistant ALDH1A1 positive cells are able to escape therapy and contribute to tumor re-growth. However, the present data allow no conclusions, whether the high percentage of ALDH1A1 positive cells in recurrent GBMs resulted from a therapeutic selection or whether ALDH1A1 expression was even induced by combined radio-chemotherapy. As illustrated in Figure 33, ALDH1A1 levels increased under extrinsic stress conditions such as hypoxia or serum deprivation. Thus, it must be pointed out that the predictive value of ALDH1A1 in a retrospective study can only be assessed when specimens from primary resection, prior to radio- or chemotherapy are analyzed.

7. Mechanisms of ALDH1A1 mediated resistance to temozolomide

In prior studies, expression of ALDH1A1 has been associated with drug resistance and cellular detoxification. To date the mechanism of ALDH1A1 mediated therapy resistance in various solid tumors is not completely understood. This enzyme is known to bind and detoxify aldehydes such as the alkylating agent cyclophosphamide (Hilton, 1984; Kastan et al., 1990) and non-aldehydes such as flavopiridol (Schnier et al., 1999). Regarding the chemical structure of TMZ and its reactive methylating agent MTIC, direct binding of these compounds by ALDH1A1 seems rather unlikely. In the following, two feasible mechanisms of ALDH1A1 mediated TMZ resistance are described.

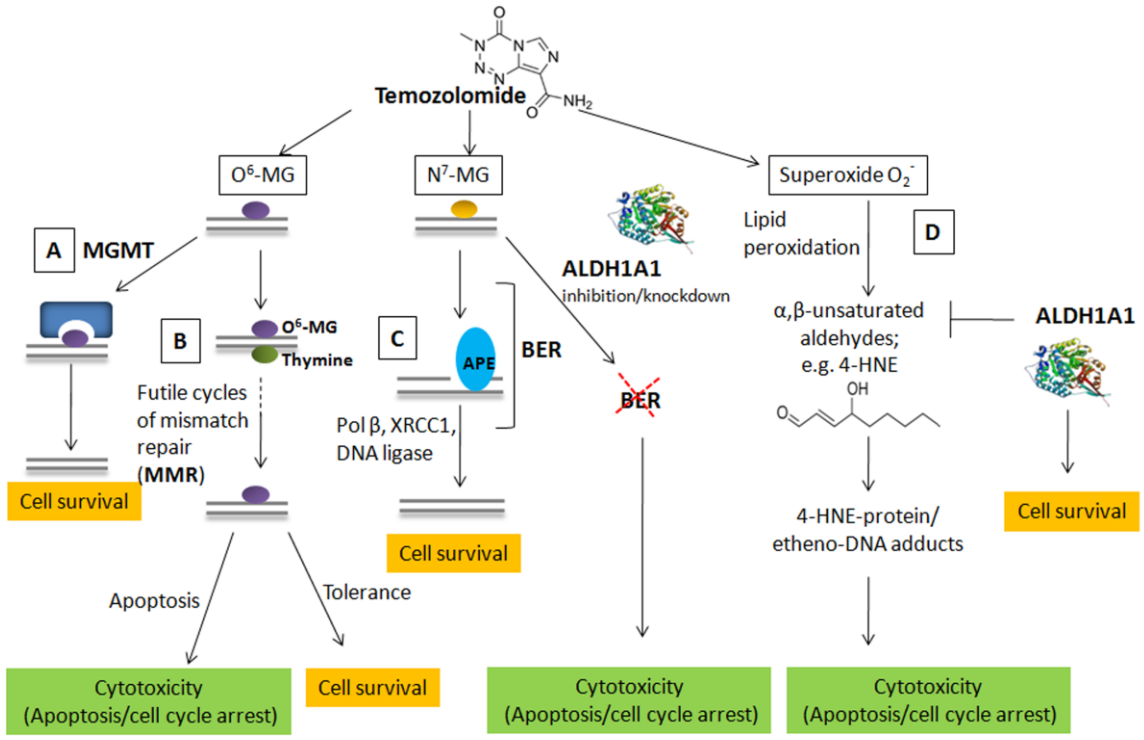

Figure 42: Mechanism of action of pathways mediating resistance to temozolomide

A, MGMT removes TMZ induced O^6-MG lesions. B, Non-repaired O^6-MG adducts mispair with thymine, resulting in futile cycles of mismatch repair (MMR). Alternatively, deficiencies in the MMR pathway can render cells tolerant to O^6-MG lesions. C, N^7-MG adducts, which account for >70% of all TMZ induced DNA lesions, are fixed by the base excision repair pathway (BER). Cleaved PARP1 recruits DNA repair proteins of the BER system to DNA lesions, which can be antagonized by inhibition or knockdown of ALDH1A1. D, TMZ induces the formation of superoxide radicals that peroxidize membrane lipids. The resulting aldehydes such as 4-hydroxynonenal (4-HNE) react with cellular proteins and DNA giving rise to cytotoxic protein and etheno-DNA adducts. ALDH1A1 is able to detoxify these aldehydes and thus prevents cell cycle arrest and apoptosis.

7.1 Depletion or inhibition of ALDH1A1 impairs base excision repair

TMZ transfers methyl groups to DNA, including the N^7 and O^6 position of guanine, and the O^3 position of adenine. These DNA adducts induce various repair pathways including MGMT protein, mismatch repair (MMR) and base excision repair (BER) (Figure 42). Double-strand breaks (DSBs) following DNA damage induce rapid histone H2AX phosphorylation at serine 139 (γ-H2AX). These γ-H2AX foci play an essential role in the recruitment of DNA repair factors (Meador et al., 2008) and can be used as a surrogate marker for DNA damage. While the O^6-MG adducts, which account for about 5% of all lesions are removed by MGMT, N^7 methylguanine (N^7-MG) and O^3 methyladenine (O^3-MA) lesions are repaired by the BER pathway. In brief, damaged bases are removed by N-methylpurine DNA glycosylase, leaving abasic sites (AP sites) that are hydrolyzed by AP endonuclease (APE). PARP1 recognizes these DNA strand interruptions and recruits DNA repair proteins to the lesions including BER scaffold protein XRCC1, DNA polymerase β and DNA ligase IIIα. Elevated PARP1 activity was found in various GBM cell lines following treatment with TMZ, while inhibition of PARP1 sensitized cells towards alkylating agents (Friedman et al., 2000). Tang *et al*. described an enhanced cytotoxic effect of TMZ in T98G cells treated concomitant with BER or PARP1 inhibitors (Tang et al., 2011). Various clinical trials on PARP1 inhibitors in combination with alkylating agents are ongoing (Ratnam and Low, 2007). Efficiency of PARP inhibitors can be evaluated by detecting poly ADP-ribosylation (PAR). Currently, the national cancer institute investigates γ-H2AX and PAR as clinical pharmacodynamic biomarkers (Redon et al., 2010).

Using γ-H2AX as a surrogate marker of DNA damage, it was shown that TMZ induced lesions occurred earlier and to a greater extent in ALDH1A1 inhibited or depleted cells, compared to ALDH1A1+ control cells (Figure 31). PARP activity upon treatment should be analyzed by measuring poly ADP-ribosylation in order to determine, whether TMZ induced DNA damage in ALDH1A1 depleted cells results from attenuated BER. Despite PARP1 cleavage in ALDH1A1+ cells, no activation of caspase-cascade (data not shown) or subG1 peak was observed, arguing against apoptosis. Even though to a lower extend, ALDH1A1+ cells also exhibited TMZ induced DNA damage. Contrary to ALDH1A1 depleted cells, ALDH1A1+ cells proceeded with cell cycle despite DNA lesions. This might be due to repair of DSBs below the threshold for checkpoint initiation (Deckbar et al., 2007), or to checkpoint adaption of ALDH1A1+ cells as observed after radiation therapy (Syljuasen et al., 2006).

Thus, attenuation of the BER pathway may be one explanation for the restored sensitivity of ALDH1A1+/MGMT+ GBM cells to temozolomide following depletion of ALDH1A1; pathways for the repair of common N^7-MG and O^3-MA lesions, which are not removed by MGMT, might be impaired after inhibition or knockdown of ALDH1A1.

7.2 Temozolomide treatment causes oxidative stress

A variety of data demonstrate the role of ALDHs in the protection against DNA-damaging agents such as cyclophosphamide, mitomycin c or Vp-16 and in handling oxidative stress (Hilton, 1984; Magni et al., 1996; Pappa et al., 2005). Notably, recent studies described an increase of reactive oxygen species (ROS) after treatment with TMZ. The authors found a correlation between the potential to reduce oxidative stress and chemoresistance *in vitro* (Oliva et al., 2011; Zhang et al., 2010). DHE staining of glioblastoma cells following exposure to TMZ confirmed the formation of superoxide radicals (O^{2-}) (Figure 34), while no increase in nitric oxide was observed by DAF2/DA staining (data not shown). Superoxide radicals lead to peroxidation of membrane lipids. The resulting aldehydes such as malondialdehyde (MDA) and 4-hydroxynonenal (4-HNE) are highly reactive and bind to cellular proteins and DNA, giving rise to etheno-DNA adducts (Gago-Dominguez et al., 2005). Treatment of LN18 cells with 4-HNE showed that ALDH1A1 is able to detoxify these reactive aldehydes, as described before (Lassen et al., 2007); while ALDH1A1+ cells were not affected by exposure to 4-HNE, ALDH1A1 depleted cells arrested in G2/M and showed elevated levels of γ-H2AX. Normal cell cycle progression along with absence DNA damage in ALDH1A1+ cells hints at a predominant role of ALDH1A1 in managing oxidative stress induced by TMZ (Figure 31, 35 A, B). Western blot analysis of 4-HNE-protein adducts showed no significant difference between 4-HNE treated ALDH1A1 knockdown and ALDH1A1+ control cells (data not shown). Thus, 4-HNE induced cell cycle arrest must result from etheno-DNA lesions.

In the past, ROS were considered to induce carcinogenesis upon DNA damage. However, recent studies describe their potential to enhance the cytotoxicity of various chemotherapeutic drugs. ROS and lipid peroxides were shown to generate apoptosis and necrosis of tumor cells (Fruehauf and Meyskens, 2007; Pettazzoni et al., 2011).

Oxidative damage lesions are mainly repaired by BER, while etheno-DNA adducts are principally removed by nucleotide excision repair (Feng et al., 2004; Maynard et al., 2009). Notably, Maynard *et al*. showed that 4-HNE does not only induce DNA lesions but also inhibits the respective repair pathways. The present experiments demonstrate increased DNA lesions in ALDH1A1 depleted cells after both, treatment with TMZ and with 4-HNE (Figure 31, 35).

In addition, inhibition of ALDH1A1 did not only enhance cytotoxicity when applied concomitant with TMZ but also up to 12 hours after TMZ treatment (Supplementary figure S 6). Since half-life of temozolomide in plasma or PBS is only 1.8 hours (Friedman et al., 2000), interaction of ALDH1A1 with side products of the temozolomide metabolism such as superoxide radicals and membrane peroxides is more likely than direct reaction with TMZ or MTIC. Further experiments are required to prove our hypothesis on TMZ induced etheno-DNA lesions in ALDH1A1 negative GBM cells. A sensitive method to analyze DNA damage products would be liquid chromatographic tandem mass spectrometry (LC/MS-MS) as described by Taghizadeh and colleagues (Taghizadeh et al., 2008).

Taken together, the present results implicate a pivotal role of ALDH1A1 in the prevention and repair of TMZ induced DNA lesions that are not removed by MGMT (Figure 42).

8. Outlook

The data of the thesis demonstrate that ALDH1A1 is not only a marker for therapy resistant GBM cells with stem cell characteristics, but also a direct mediator of chemoresistance. ALDH1A1 predicted temozolomide resistance *in vitro* and clinical outcome *in vivo*, independently of the MGMT status. Nevertheless, further experiments are required to prove our hypothesis on the mechanism of ALDH1A1 mediated chemoresistance.

Since inhibition or depletion of ALDH1A1 re-sensitized chemoresistant MGMT positive GBM cells to temozolomide, this enzyme might serve as a potential therapeutic target in the future treatment of human malignancies. Indeed, our *in vitro* data must be confirmed in a mouse model to prove the effect of combined ALDH1A1 inhibition and temozolomide application *in vivo*. Therefore, an inhibitor specific to the isoform ALDH1A1 is in high demand.

Disulfiram, a drug formerly used in the treatment of chronic alcoholism is an irreversible inhibitor of ALDHs. Lately, the potential of disulfiram to reduce chemoresistance *in vitro* and *in vivo* was shown in melanoma and colorectal cancer (Cen et al., 2002; Wang et al., 2003). As a well-tolerated orally active drug, disulfiram might be also a promising compound in human glioma therapy. Nevertheless, disulfiram is not an inhibitor specific to ALDH1A1; in order to prevent side-effects and to further clarify the role of ALDH1A1 in mediating chemoresistance, a specific inhibitor is required.

In addition, the present data demonstrate ALDH1A1 as a potential down-stream target of the PTEN/PI3K/Akt signaling pathway. This pathway is apparently involved in the maintenance of a self-renewing ALDH1A1 positive cell pool. In order to better understand the role of ALDH1A1 in therapy resistant cells, more effort should be made to highlight the regulatory mechanisms of ALDH1A1 in normal and cancerous cells.

Recently, molecular subclasses of glioblastomas were defined by the activity of different signaling pathways and by genetic alterations. These subclasses differ in their clinical prognosis and response to aggressive radio-chemotherapy. Hence, it would be of highest interest to assign ALDH1A1 expression to a distinct molecular subclass.

F. Danksagung

Diese Arbeit wäre ohne den wissenschaftlichen und persönlichen Beitrag vieler Personen nicht möglich gewesen. Daher möchte ich an dieser Stelle meinen Dank all denen aussprechen, die mich während meiner Dissertation begleitet und unterstütz haben.

Mein besonderer Dank gilt Prof. Dr. Jürgen Schlegel, der mir die Möglichkeit bot mich mit diesem spannenden Thema zu beschäftigen. Neben den zur Verfügung gestellten finanziellen Mitteln durch den SFB 824 konnte ich immer auf seine persönliche Unterstützung zählen. Ich möchte mich für das in mich gesetzte Vertrauen bedanken, welches mir ein kreatives und eigeninitiiertes Arbeiten in einem sehr angenehmen Umfeld ermöglichte.

Ich danke Prof. Dr. Höfler, an dessen Institut für Pathologie und pathologische Anatomie ich diese Arbeit fertigstellen konnte. Einen besonders herzlichen Dank möchte ich auch an Frau Krummeck richten, die bei allen administrativen Fragestellungen ein sehr hilfsbereiter und kompetenter Ansprechpartner war.

Bei Prof. Dr. Wolfgang Wurst möchte ich mich herzlich dafür bedanken, dass er meine Arbeit als erster Prüfer vor der Fakultät Wissenschaftszentrum Weihenstephan für Ernährung, Landnutzung und Umwelt der Technischen Universität München vertritt. Mein besonderer Dank gilt hierbei auch Elisabeth Güll, die bei den mit der Dissertation verbundenen administrativen Angelegenheiten ein zuverlässiger Ansprechpartner war.

Ich danke meinen Kolleginnen und Kollegen für eine schöne und lehrreiche Zeit. Julian Teufel und Michael Rasper danke ich für wertvolle und bereichernde Diskussionen, welche sicher auch entscheidend zum Gelingen dieser Arbeit beigetragen haben. Bei Michael Rasper möchte ich mich zudem von ganzem Herzen für seine persönliche Unterstützung und sein Verständnis bedanken. Mein herzlicher Dank gilt auch Ingrid Hoepner, die nicht nur tatkräftig bei der Immunhistochemie und den MGMT-Promotormethylierungs-Analysen mitgewirkte, sondern auch für ein sehr angenehmes Arbeitsklima sorgte. Meinen lieben Kolleginnen Veronika Boxhammer, Claire Delbridge, Velia Hülsmeyer, Julia Köritzer, Liza Pill, Kathrin Hock und Vanessa Röhrig danke ich nicht nur für anregende wissenschaftliche Diskussionen, sondern auch für viele gute Gespräche und unterhaltsame Stunden. Dank dieses tollen Teams habe ich trotz diverser Rückschläge nie die Motivation verloren.

Außerdem gilt mein Dank Dr. Christoph Beier, der mich bei dem Verfassen der Publikation „Aldehyde dehydrogenase 1 A1 – a new mediator of resistance to temozolomide in glioblastoma“ unterstützte und die R28 Zellen zur Verfügung stellte. Dr. Gero Brockhoff danke ich herzlich für die Hilfe bei der Etablierung der Zellzyklusanalysen, Dr. Gisela Keller für Ihre Unterstützung bei den Zell-Authentifizierungen.

Ich danke Michael Rasper, Luisa Hohlefelder, Vanessa Röhrig und insbesondere Dr. Birgit Schäfer für das kritische Lesen des Manuskripts. Claire Delbridge sowie Steven Verhelst danke ich zudem für sprachliche und strukturelle Korrekturen.

Zuletzt möchte ich mich von ganzem Herzen bei meinen Eltern bedanken, die mich immer in allen Belangen großzügig unterstützt und an mich geglaubt haben.

Danke

G. References

Adam, S. A., Schnell, O., Poschl, J., Eigenbrod, S., Kretzschmar, H. A., Tonn, J. C., and Schuller, U. (2012). ALDH1A1 is a Marker of Astrocytic Differentiation during Brain Development and Correlates with Better Survival in Glioblastoma Patients. Brain Pathol.

Al-Hajj, M., Wicha, M. S., Benito-Hernandez, A., Morrison, S. J., and Clarke, M. F. (2003). Prospective identification of tumorigenic breast cancer cells. Proc Natl Acad Sci U S A *100*, 3983-3988.

Aldape, K. D., Ballman, K., Furth, A., Buckner, J. C., Giannini, C., Burger, P. C., Scheithauer, B. W., Jenkins, R. B., and James, C. D. (2004). Immunohistochemical detection of EGFRvIII in high malignancy grade astrocytomas and evaluation of prognostic significance. J Neuropathol Exp Neurol *63*, 700-707.

Appel, B., and Eisen, J. S. (2003). Retinoids run rampant: multiple roles during spinal cord and motor neuron development. Neuron *40*, 461-464.

Avgeropoulos, N. G., and Batchelor, T. T. (1999). New treatment strategies for malignant gliomas. Oncologist *4*, 209-224.

Bao, S., Wu, Q., McLendon, R. E., Hao, Y., Shi, Q., Hjelmeland, A. B., Dewhirst, M. W., Bigner, D. D., and Rich, J. N. (2006). Glioma stem cells promote radioresistance by preferential activation of the DNA damage response. Nature *444*, 756-760.

Beier, D., Hau, P., Proescholdt, M., Lohmeier, A., Wischhusen, J., Oefner, P. J., Aigner, L., Brawanski, A., Bogdahn, U., and Beier, C. P. (2007). CD133(+) and CD133(-) glioblastoma-derived cancer stem cells show differential growth characteristics and molecular profiles. Cancer Res *67*, 4010-4015.

Beier, D., Rohrl, S., Pillai, D. R., Schwarz, S., Kunz-Schughart, L. A., Leukel, P., Proescholdt, M., Brawanski, A., Bogdahn, U., Trampe-Kieslich, A*., et al.* (2008). Temozolomide preferentially depletes cancer stem cells in glioblastoma. Cancer Res *68*, 5706-5715.

Bettstetter, M., Dechant, S., Ruemmele, P., Vogel, C., Kurz, K., Morak, M., Keller, G., Holinski-Feder, E., Hofstaedter, F., and Dietmaier, W. (2008). MethyQESD, a robust and fast method for quantitative methylation analyses in HNPCC diagnostics using formalin-fixed and paraffin-embedded tissue samples. Lab Invest *88*, 1367-1375.

Bleau, A. M., Hambardzumyan, D., Ozawa, T., Fomchenko, E. I., Huse, J. T., Brennan, C. W., and Holland, E. C. (2009). PTEN/PI3K/Akt pathway regulates the side population phenotype and ABCG2 activity in glioma tumor stem-like cells. Cell Stem Cell *4*, 226-235.

Bonavia, R., Inda, M. M., Cavenee, W. K., and Furnari, F. B. (2011). Heterogeneity maintenance in glioblastoma: a social network. Cancer Res *71*, 4055-4060.

Bonnet, D., and Dick, J. E. (1997). Human acute myeloid leukemia is organized as a hierarchy that originates from a primitive hematopoietic cell. Nat Med *3*, 730-737.

Brooks, P. J., and Theruvathu, J. A. (2005). DNA adducts from acetaldehyde: implications for alcohol-related carcinogenesis. Alcohol *35*, 187-193.

Brown, M., Schrot, R., Bauer, K., and Letendre, D. (2009). Incidence of first primary central nervous system tumors in California, 2001-2005. J Neurooncol *94*, 249-261.

Calabrese, C., Poppleton, H., Kocak, M., Hogg, T. L., Fuller, C., Hamner, B., Oh, E. Y., Gaber, M. W., Finklestein, D., Allen, M.*, et al.* (2007). A perivascular niche for brain tumor stem cells. Cancer Cell *11*, 69-82.

Campos, B., Centner, F. S., Bermejo, J. L., Ali, R., Dorsch, K., Wan, F., Felsberg, J., Ahmadi, R., Grabe, N., Reifenberger, G.*, et al.* (2011). Aberrant expression of retinoic acid signaling molecules influences patient survival in astrocytic gliomas. The American journal of pathology *178*, 1953-1964.

Campos, B., Wan, F., Farhadi, M., Ernst, A., Zeppernick, F., Tagscherer, K. E., Ahmadi, R., Lohr, J., Dictus, C., Gdynia, G.*, et al.* (2010). Differentiation therapy exerts antitumor effects on stem-like glioma cells. Clin Cancer Res *16*, 2715-2728.

Carico, C., Nuno, M., Mukherjee, D., Elramsisy, A., Dantis, J., Hu, J., Rudnick, J., Yu, J. S., Black, K. L., Bannykh, S. I., and Patil, C. G. (2012). Loss of PTEN Is Not Associated with Poor Survival in Newly Diagnosed Glioblastoma Patients of the Temozolomide Era. PLoS One *7*, e33684.

Cen, D., Gonzalez, R. I., Buckmeier, J. A., Kahlon, R. S., Tohidian, N. B., and Meyskens, F. L., Jr. (2002). Disulfiram induces apoptosis in human melanoma cells: a redox-related process. Mol Cancer Ther *1*, 197-204.

Chang, B., Liu, G., Xue, F., Rosen, D. G., Xiao, L., Wang, X., and Liu, J. (2009). ALDH1 expression correlates with favorable prognosis in ovarian cancers. Mod Pathol *22*, 817-823.

Chen, R., Nishimura, M. C., Bumbaca, S. M., Kharbanda, S., Forrest, W. F., Kasman, I. M., Greve, J. M., Soriano, R. H., Gilmour, L. L., Rivers, C. S.*, et al.* (2010). A hierarchy of self-renewing tumor-initiating cell types in glioblastoma. Cancer Cell *17*, 362-375.

Chute, J. P., Muramoto, G. G., Whitesides, J., Colvin, M., Safi, R., Chao, N. J., and McDonnell, D. P. (2006). Inhibition of aldehyde dehydrogenase and retinoid signaling induces the expansion of human hematopoietic stem cells. Proc Natl Acad Sci U S A *103*, 11707-11712.

Colvin, M., Russo, J. E., Hilton, J., Dulik, D. M., and Fenselau, C. (1988). Enzymatic mechanisms of resistance to alkylating agents in tumor cells and normal tissues. Adv Enzyme Regul *27*, 211-221.

Corti, S., Locatelli, F., Papadimitriou, D., Donadoni, C., Salani, S., Del Bo, R., Strazzer, S., Bresolin, N., and Comi, G. P. (2006). Identification of a primitive brain-derived neural stem cell population based on aldehyde dehydrogenase activity. Stem Cells *24*, 975-985.

Dahlstrand, J., Collins, V. P., and Lendahl, U. (1992). Expression of the class VI intermediate filament nestin in human central nervous system tumors. Cancer Res *52*, 5334-5341.

Dang, L., White, D. W., Gross, S., Bennett, B. D., Bittinger, M. A., Driggers, E. M., Fantin, V. R., Jang, H. G., Jin, S., Keenan, M. C.*, et al.* (2010). Cancer-associated IDH1 mutations produce 2-hydroxyglutarate. Nature *465*, 966.

Dean, M., Fojo, T., and Bates, S. (2005). Tumour stem cells and drug resistance. Nat Rev Cancer *5*, 275-284.

Deckbar, D., Birraux, J., Krempler, A., Tchouandong, L., Beucher, A., Walker, S., Stiff, T., Jeggo, P., and Lobrich, M. (2007). Chromosome breakage after G2 checkpoint release. J Cell Biol *176*, 749-755.

Deng, S., Yang, X., Lassus, H., Liang, S., Kaur, S., Ye, Q., Li, C., Wang, L. P., Roby, K. F., Orsulic, S.*, et al.* (2010). Distinct expression levels and patterns of stem cell marker, aldehyde dehydrogenase isoform 1 (ALDH1), in human epithelial cancers. PLoS One *5*, e10277.

Diehl, J. A., Cheng, M., Roussel, M. F., and Sherr, C. J. (1998). Glycogen synthase kinase-3beta regulates cyclin D1 proteolysis and subcellular localization. Genes Dev *12*, 3499-3511.

Dylla, S. J., Beviglia, L., Park, I. K., Chartier, C., Raval, J., Ngan, L., Pickell, K., Aguilar, J., Lazetic, S., Smith-Berdan, S.*, et al.* (2008). Colorectal cancer stem cells are enriched in xenogeneic tumors following chemotherapy. PLoS One *3*, e2428.

Eyler, C. E., and Rich, J. N. (2008). Survival of the fittest: cancer stem cells in therapeutic resistance and angiogenesis. Journal of clinical oncology : official journal of the American Society of Clinical Oncology *26*, 2839-2845.

Feng, Z., Hu, W., and Tang, M. S. (2004). Trans-4-hydroxy-2-nonenal inhibits nucleotide excision repair in human cells: a possible mechanism for lipid peroxidation-induced carcinogenesis. Proc Natl Acad Sci U S A *101*, 8598-8602.

Fotovati, A., Abu-Ali, S., Wang, P. S., Deleyrolle, L. P., Lee, C., Triscott, J., Chen, J. Y., Franciosi, S., Nakamura, Y., Sugita, Y.*, et al.* (2011). YB-1 bridges neural stem cells and brain tumor-initiating cells via its roles in differentiation and cell growth. Cancer Res *71*, 5569-5578.

Friedman, H. S., Johnson, S. P., Dong, Q., Schold, S. C., Rasheed, B. K., Bigner, S. H., Ali-Osman, F., Dolan, E., Colvin, O. M., Houghton, P.*, et al.* (1997). Methylator resistance mediated by mismatch repair deficiency in a glioblastoma multiforme xenograft. Cancer Res *57*, 2933-2936.

Friedman, H. S., Kerby, T., and Calvert, H. (2000). Temozolomide and treatment of malignant glioma. Clin Cancer Res *6*, 2585-2597.

Frosina, G. (2009). DNA repair and resistance of gliomas to chemotherapy and radiotherapy. Mol Cancer Res *7*, 989-999.

Fruehauf, J. P., and Meyskens, F. L., Jr. (2007). Reactive oxygen species: a breath of life or death? Clin Cancer Res *13*, 789-794.

Gago-Dominguez, M., Castelao, J. E., Pike, M. C., Sevanian, A., and Haile, R. W. (2005). Role of lipid peroxidation in the epidemiology and prevention of breast cancer. Cancer epidemiology, biomarkers & prevention : a publication of the American Association for Cancer Research, cosponsored by the American Society of Preventive Oncology *14*, 2829-2839.

Gaspar, N., Marshall, L., Perryman, L., Bax, D. A., Little, S. E., Viana-Pereira, M., Sharp, S. Y., Vassal, G., Pearson, A. D., Reis, R. M.*, et al.* MGMT-independent temozolomide resistance in pediatric glioblastoma cells associated with a PI3-kinase-mediated HOX/stem cell gene signature. Cancer Res *70*, 9243-9252.

Gaspar, N., Marshall, L., Perryman, L., Bax, D. A., Little, S. E., Viana-Pereira, M., Sharp, S. Y., Vassal, G., Pearson, A. D., Reis, R. M.*, et al.* (2010). MGMT-independent temozolomide resistance in pediatric glioblastoma cells associated with a PI3-kinase-mediated HOX/stem cell gene signature. Cancer Res *70*, 9243-9252.

Gilbertson, R. J., and Rich, J. N. (2007). Making a tumour's bed: glioblastoma stem cells and the vascular niche. Nat Rev Cancer *7*, 733-736.

Ginestier, C., Hur, M. H., Charafe-Jauffret, E., Monville, F., Dutcher, J., Brown, M., Jacquemier, J., Viens, P., Kleer, C. G., Liu, S.*, et al.* (2007). ALDH1 is a marker of normal and malignant human mammary stem cells and a predictor of poor clinical outcome. Cell Stem Cell *1*, 555-567.

Gurney, J. G., Chen, M., Skluzacek, M. C., Kasum, C. M., Carmella, S. G., Villalta, P. W., and Hecht, S. S. (2002). Null association between frequency of cured meat consumption and methylvaline and ethylvaline hemoglobin adduct levels: the N-nitroso brain cancer hypothesis. Cancer Epidemiol Biomarkers Prev *11*, 421-422.

Heddleston, J. M., Li, Z., McLendon, R. E., Hjelmeland, A. B., and Rich, J. N. (2009). The hypoxic microenvironment maintains glioblastoma stem cells and promotes reprogramming towards a cancer stem cell phenotype. Cell Cycle *8*, 3274-3284.

Hegi, M. E., Diserens, A. C., Gorlia, T., Hamou, M. F., de Tribolet, N., Weller, M., Kros, J. M., Hainfellner, J. A., Mason, W., Mariani, L.*, et al.* (2005). MGMT gene silencing and benefit from temozolomide in glioblastoma. N Engl J Med *352*, 997-1003.

Hegi, M. E., Liu, L., Herman, J. G., Stupp, R., Wick, W., Weller, M., Mehta, M. P., and Gilbert, M. R. (2008). Correlation of O6-methylguanine methyltransferase (MGMT) promoter methylation with clinical outcomes in glioblastoma and clinical strategies to modulate MGMT activity. J Clin Oncol *26*, 4189-4199.

Hermisson, M., Klumpp, A., Wick, W., Wischhusen, J., Nagel, G., Roos, W., Kaina, B., and Weller, M. (2006). O6-methylguanine DNA methyltransferase and p53 status predict temozolomide sensitivity in human malignant glioma cells. J Neurochem *96*, 766-776.

Hilton, J. (1984). Role of aldehyde dehydrogenase in cyclophosphamide-resistant L1210 leukemia. Cancer Res *44*, 5156-5160.

Hirose, Y., Berger, M. S., and Pieper, R. O. (2001). p53 effects both the duration of G2/M arrest and the fate of temozolomide-treated human glioblastoma cells. Cancer Res *61*, 1957-1963.

Hirose, Y., Katayama, M., Mirzoeva, O. K., Berger, M. S., and Pieper, R. O. (2005). Akt activation suppresses Chk2-mediated, methylating agent-induced G2 arrest and protects from temozolomide-induced mitotic catastrophe and cellular senescence. Cancer Res *65*, 4861-4869.

Huang, E. H., Hynes, M. J., Zhang, T., Ginestier, C., Dontu, G., Appelman, H., Fields, J. Z., Wicha, M. S., and Boman, B. M. (2009). Aldehyde dehydrogenase 1 is a marker for normal and malignant human colonic stem cells (SC) and tracks SC overpopulation during colon tumorigenesis. Cancer Res *69*, 3382-3389.

Inskip, P. D., Tarone, R. E., Hatch, E. E., Wilcosky, T. C., Shapiro, W. R., Selker, R. G., Fine, H. A., Black, P. M., Loeffler, J. S., and Linet, M. S. (2001). Cellular-telephone use and brain tumors. N Engl J Med *344*, 79-86.

Ishii, N., Maier, D., Merlo, A., Tada, M., Sawamura, Y., Diserens, A. C., and Van Meir, E. G. (1999). Frequent co-alterations of TP53, p16/CDKN2A, p14ARF, PTEN tumor suppressor genes in human glioma cell lines. Brain Pathol *9*, 469-479.

Jiang, F., Qiu, Q., Khanna, A., Todd, N. W., Deepak, J., Xing, L., Wang, H., Liu, Z., Su, Y., Stass, S. A., and Katz, R. L. (2009). Aldehyde dehydrogenase 1 is a tumor stem cell-associated marker in lung cancer. Mol Cancer Res *7*, 330-338.

Jorissen, R. N., Walker, F., Pouliot, N., Garrett, T. P., Ward, C. W., and Burgess, A. W. (2003). Epidermal growth factor receptor: mechanisms of activation and signalling. Exp Cell Res *284*, 31-53.

Kahlert, C., Bergmann, F., Beck, J., Welsch, T., Mogler, C., Herpel, E., Dutta, S., Niemietz, T., Koch, M., and Weitz, J. (2011). Low expression of aldehyde dehydrogenase 1A1 (ALDH1A1) is a prognostic marker for poor survival in pancreatic cancer. BMC Cancer *11*, 275.

Karran, P., and Bignami, M. (1994). DNA damage tolerance, mismatch repair and genome instability. Bioessays *16*, 833-839.

Karran, P., Macpherson, P., Ceccotti, S., Dogliotti, E., Griffin, S., and Bignami, M. (1993). O6-methylguanine residues elicit DNA repair synthesis by human cell extracts. J Biol Chem *268*, 15878-15886.

Kastan, M. B., Schlaffer, E., Russo, J. E., Colvin, O. M., Civin, C. I., and Hilton, J. (1990). Direct demonstration of elevated aldehyde dehydrogenase in human hematopoietic progenitor cells. Blood *75*, 1947-1950.

Korkaya, H., Paulson, A., Charafe-Jauffret, E., Ginestier, C., Brown, M., Dutcher, J., Clouthier, S. G., and Wicha, M. S. (2009). Regulation of mammary stem/progenitor cells by PTEN/Akt/beta-catenin signaling. PLoS Biol *7*, e1000121.

Kraus, A., Neff, F., Behn, M., Schuermann, M., Muenkel, K., and Schlegel, J. (1999). Expression of alternatively spliced mdm2 transcripts correlates with stabilized wild-type p53 protein in human glioblastoma cells. Int J Cancer *80*, 930-934.

Lahkola, A., Auvinen, A., Raitanen, J., Schoemaker, M. J., Christensen, H. C., Feychting, M., Johansen, C., Klaeboe, L., Lonn, S., Swerdlow, A. J.*, et al.* (2007). Mobile phone use and risk of glioma in 5 North European countries. Int J Cancer *120*, 1769-1775.

Lai, A., Tran, A., Nghiemphu, P. L., Pope, W. B., Solis, O. E., Selch, M., Filka, E., Yong, W. H., Mischel, P. S., Liau, L. M.*, et al.* (2011). Phase II study of bevacizumab plus temozolomide during and after radiation therapy for patients with newly diagnosed glioblastoma multiforme. J Clin Oncol *29*, 142-148.

Landen, C. N., Jr., Goodman, B., Katre, A. A., Steg, A. D., Nick, A. M., Stone, R. L., Miller, L. D., Mejia, P. V., Jennings, N. B., Gershenson, D. M.*, et al.* (2010). Targeting aldehyde dehydrogenase cancer stem cells in ovarian cancer. Mol Cancer Ther *9*, 3186-3199.

Lassen, N., Bateman, J. B., Estey, T., Kuszak, J. R., Nees, D. W., Piatigorsky, J., Duester, G., Day, B. J., Huang, J., Hines, L. M., and Vasiliou, V. (2007). Multiple and additive functions of ALDH3A1 and ALDH1A1: cataract phenotype and ocular oxidative damage in Aldh3a1(-/-)/Aldh1a1(-/-) knock-out mice. J Biol Chem *282*, 25668-25676.

Li, T., Su, Y., Mei, Y., Leng, Q., Leng, B., Liu, Z., Stass, S. A., and Jiang, F. (2010). ALDH1A1 is a marker for malignant prostate stem cells and predictor of prostate cancer patients' outcome. Lab Invest *90*, 234-244.

Li, Y. J., Sanson, M., Hoang-Xuan, K., Delattre, J. Y., Poisson, M., Thomas, G., and Hamelin, R. (1995). Incidence of germ-line p53 mutations in patients with gliomas. Int J Cancer *64*, 383-387.

Li, Z., Bao, S., Wu, Q., Wang, H., Eyler, C., Sathornsumetee, S., Shi, Q., Cao, Y., Lathia, J., McLendon, R. E.*, et al.* (2009). Hypoxia-inducible factors regulate tumorigenic capacity of glioma stem cells. Cancer Cell *15*, 501-513.

Livneh, E., Prywes, R., Kashles, O., Reiss, N., Sasson, I., Mory, Y., Ullrich, A., and Schlessinger, J. (1986). Reconstitution of human epidermal growth factor receptors and its deletion mutants in cultured hamster cells. J Biol Chem *261*, 12490-12497.

Louis, D. N., Ohgaki, H., Wiestler, O. D., Cavenee, W. K., Burger, P. C., Jouvet, A., Scheithauer, B. W., and Kleihues, P. (2007). The 2007 WHO classification of tumours of the central nervous system. Acta Neuropathol *114*, 97-109.

Magni, M., Shammah, S., Schiro, R., Mellado, W., Dalla-Favera, R., and Gianni, A. M. (1996). Induction of cyclophosphamide-resistance by aldehyde-dehydrogenase gene transfer. Blood *87*, 1097-1103.

Marcato, P., Dean, C. A., Pan, D., Araslanova, R., Gillis, M., Joshi, M., Helyer, L., Pan, L., Leidal, A., Gujar, S.*, et al.* (2011). Aldehyde dehydrogenase activity of breast cancer stem cells is primarily due to isoform ALDH1A3 and its expression is predictive of metastasis. Stem Cells *29*, 32-45.

Marchitti, S. A., Brocker, C., Stagos, D., and Vasiliou, V. (2008). Non-P450 aldehyde oxidizing enzymes: the aldehyde dehydrogenase superfamily. Expert Opin Drug Metab Toxicol *4*, 697-720.

Maynard, S., Schurman, S. H., Harboe, C., de Souza-Pinto, N. C., and Bohr, V. A. (2009). Base excision repair of oxidative DNA damage and association with cancer and aging. Carcinogenesis *30*, 2-10.

Meador, J. A., Zhao, M., Su, Y., Narayan, G., Geard, C. R., and Balajee, A. S. (2008). Histone H2AX is a critical factor for cellular protection against DNA alkylating agents. Oncogene *27*, 5662-5671.

Mihaliak, A. M., Gilbert, C. A., Li, L., Daou, M. C., Moser, R. P., Reeves, A., Cochran, B. H., and Ross, A. H. (2010). Clinically relevant doses of chemotherapy agents reversibly block formation of glioblastoma neurospheres. Cancer Lett *296*, 168-177.

Mihatsch, J., Toulany, M., Bareiss, P. M., Grimm, S., Lengerke, C., Kehlbach, R., and Rodemann, H. P. (2011). Selection of radioresistant tumor cells and presence of ALDH1 activity in vitro. Radiother Oncol *99*, 300-306.

Muramoto, G. G., Russell, J. L., Safi, R., Salter, A. B., Himburg, H. A., Daher, P., Meadows, S. K., Doan, P., Storms, R. W., Chao, N. J.*, et al.* (2010). Inhibition of aldehyde dehydrogenase expands hematopoietic stem cells with radioprotective capacity. Stem Cells *28*, 523-534.

Nagane, M., Coufal, F., Lin, H., Bogler, O., Cavenee, W. K., and Huang, H. J. (1996). A common mutant epidermal growth factor receptor confers enhanced tumorigenicity on human glioblastoma cells by increasing proliferation and reducing apoptosis. Cancer Res *56*, 5079-5086.

Neglia, J. P., Robison, L. L., Stovall, M., Liu, Y., Packer, R. J., Hammond, S., Yasui, Y., Kasper, C. E., Mertens, A. C., Donaldson, S. S.*, et al.* (2006). New primary neoplasms of the central nervous system in survivors of childhood cancer: a report from the Childhood Cancer Survivor Study. J Natl Cancer Inst *98*, 1528-1537.

Nishikawa, R., Sugiyama, T., Narita, Y., Furnari, F., Cavenee, W. K., and Matsutani, M. (2004). Immunohistochemical analysis of the mutant epidermal growth factor, deltaEGFR, in glioblastoma. Brain Tumor Pathol *21*, 53-56.

Nobusawa, S., Watanabe, T., Kleihues, P., and Ohgaki, H. (2009). IDH1 mutations as molecular signature and predictive factor of secondary glioblastomas. Clin Cancer Res *15*, 6002-6007.

Nutt, C. L., Betensky, R. A., Brower, M. A., Batchelor, T. T., Louis, D. N., and Stemmer-Rachamimov, A. O. (2005). YKL-40 is a differential diagnostic marker for histologic subtypes of high-grade gliomas. Clin Cancer Res *11*, 2258-2264.

Ohgaki, H., Dessen, P., Jourde, B., Horstmann, S., Nishikawa, T., Di Patre, P. L., Burkhard, C., Schuler, D., Probst-Hensch, N. M., Maiorka, P. C*., et al.* (2004). Genetic pathways to glioblastoma: a population-based study. Cancer Res *64*, 6892-6899.

Ohgaki, H., and Kleihues, P. (2005). Population-based studies on incidence, survival rates, and genetic alterations in astrocytic and oligodendroglial gliomas. J Neuropathol Exp Neurol *64*, 479-489.

Ohgaki, H., and Kleihues, P. (2011). Genetic profile of astrocytic and oligodendroglial gliomas. Brain Tumor Pathol *28*, 177-183.

Oliva, C. R., Moellering, D. R., Gillespie, G. Y., and Griguer, C. E. (2011). Acquisition of chemoresistance in gliomas is associated with increased mitochondrial coupling and decreased ROS production. PLoS One *6*, e24665.

Ostermann, S., Csajka, C., Buclin, T., Leyvraz, S., Lejeune, F., Decosterd, L. A., and Stupp, R. (2004). Plasma and cerebrospinal fluid population pharmacokinetics of temozolomide in malignant glioma patients. Clin Cancer Res *10*, 3728-3736.

Pappa, A., Brown, D., Koutalos, Y., DeGregori, J., White, C., and Vasiliou, V. (2005). Human aldehyde dehydrogenase 3A1 inhibits proliferation and promotes survival of human corneal epithelial cells. J Biol Chem *280*, 27998-28006.

Pelloski, C. E., Ballman, K. V., Furth, A. F., Zhang, L., Lin, E., Sulman, E. P., Bhat, K., McDonald, J. M., Yung, W. K., Colman, H*., et al.* (2007). Epidermal growth factor receptor variant III status defines clinically distinct subtypes of glioblastoma. J Clin Oncol *25*, 2288-2294.

Pettazzoni, P., Pizzimenti, S., Toaldo, C., Sotomayor, P., Tagliavacca, L., Liu, S., Wang, D., Minelli, R., Ellis, L., Atadja, P*., et al.* (2011). Induction of cell cycle arrest and DNA damage by the HDAC inhibitor panobinostat (LBH589) and the lipid peroxidation end product 4-hydroxynonenal in prostate cancer cells. Free Radic Biol Med *50*, 313-322.

Phillips, H. S., Kharbanda, S., Chen, R., Forrest, W. F., Soriano, R. H., Wu, T. D., Misra, A., Nigro, J. M., Colman, H., Soroceanu, L*., et al.* (2006). Molecular subclasses of high-grade glioma predict prognosis, delineate a pattern of disease progression, and resemble stages in neurogenesis. Cancer Cell *9*, 157-173.

Ponten, J., and Macintyre, E. H. (1968). Long term culture of normal and neoplastic human glia. Acta Pathol Microbiol Scand *74*, 465-486.

Preusser, M., de Ribaupierre, S., Wohrer, A., Erridge, S. C., Hegi, M., Weller, M., and Stupp, R. (2011). Current concepts and management of glioblastoma. Ann Neurol *70*, 9-21.

Quinones-Hinojosa, A., Sanai, N., Soriano-Navarro, M., Gonzalez-Perez, O., Mirzadeh, Z., Gil-Perotin, S., Romero-Rodriguez, R., Berger, M. S., Garcia-Verdugo, J. M., and Alvarez-Buylla, A. (2006). Cellular composition and cytoarchitecture of the adult human subventricular zone: a niche of neural stem cells. J Comp Neurol *494*, 415-434.

Rasheed, Z. A., Yang, J., Wang, Q., Kowalski, J., Freed, I., Murter, C., Hong, S. M., Koorstra, J. B., Rajeshkumar, N. V., He, X.*, et al.* (2010). Prognostic significance of tumorigenic cells with mesenchymal features in pancreatic adenocarcinoma. J Natl Cancer Inst *102*, 340-351.

Rasper, M., Schafer, A., Piontek, G., Teufel, J., Brockhoff, G., Ringel, F., Heindl, S., Zimmer, C., and Schlegel, J. (2010). Aldehyde dehydrogenase 1 positive glioblastoma cells show brain tumor stem cell capacity. Neuro Oncol *12*, 1024-1033.

Ratnam, K., and Low, J. A. (2007). Current development of clinical inhibitors of poly(ADP-ribose) polymerase in oncology. Clin Cancer Res *13*, 1383-1388.

Redon, C. E., Nakamura, A. J., Zhang, Y. W., Ji, J. J., Bonner, W. M., Kinders, R. J., Parchment, R. E., Doroshow, J. H., and Pommier, Y. (2010). Histone gammaH2AX and poly(ADP-ribose) as clinical pharmacodynamic biomarkers. Clin Cancer Res *16*, 4532-4542.

Reya, T., Morrison, S. J., Clarke, M. F., and Weissman, I. L. (2001). Stem cells, cancer, and cancer stem cells. Nature *414*, 105-111.

Reynolds, B. A., and Weiss, S. (1992). Generation of neurons and astrocytes from isolated cells of the adult mammalian central nervous system. Science *255*, 1707-1710.

Ricci-Vitiani, L., Lombardi, D. G., Pilozzi, E., Biffoni, M., Todaro, M., Peschle, C., and De Maria, R. (2007). Identification and expansion of human colon-cancer-initiating cells. Nature *445*, 111-115.

Ruder, A. M., Waters, M. A., Butler, M. A., Carreon, T., Calvert, G. M., Davis-King, K. E., Schulte, P. A., Sanderson, W. T., Ward, E. M., Connally, L. B.*, et al.* (2004). Gliomas and farm pesticide exposure in men: the upper midwest health study. Arch Environ Health *59*, 650-657.

Sampson, J. H., Heimberger, A. B., Archer, G. E., Aldape, K. D., Friedman, A. H., Friedman, H. S., Gilbert, M. R., Herndon, J. E., 2nd, McLendon, R. E., Mitchell, D. A.*, et al.* (2010). Immunologic escape after prolonged progression-free survival with epidermal growth factor receptor variant III peptide vaccination in patients with newly diagnosed glioblastoma. J Clin Oncol *28*, 4722-4729.

Sarkaria, J. N., Kitange, G. J., James, C. D., Plummer, R., Calvert, H., Weller, M., and Wick, W. (2008). Mechanisms of chemoresistance to alkylating agents in malignant glioma. Clin Cancer Res *14*, 2900-2908.

Schmidt, M. C., Antweiler, S., Urban, N., Mueller, W., Kuklik, A., Meyer-Puttlitz, B., Wiestler, O. D., Louis, D. N., Fimmers, R., and von Deimling, A. (2002). Impact of genotype and morphology on the prognosis of glioblastoma. J Neuropathol Exp Neurol *61*, 321-328.

Schnier, J. B., Kaur, G., Kaiser, A., Stinson, S. F., Sausville, E. A., Gardner, J., Nishi, K., Bradbury, E. M., and Senderowicz, A. M. (1999). Identification of cytosolic aldehyde dehydrogenase 1 from non-small cell lung carcinomas as a flavopiridol-binding protein. FEBS Lett *454*, 100-104.

Schwartzbaum, J. A., Fisher, J. L., Aldape, K. D., and Wrensch, M. (2006). Epidemiology and molecular pathology of glioma. Nat Clin Pract Neurol *2*, 494-503; quiz 491 p following 516.

Seidel, S., Garvalov, B. K., Wirta, V., von Stechow, L., Schanzer, A., Meletis, K., Wolter, M., Sommerlad, D., Henze, A. T., Nister, M.*, et al.* (2010). A hypoxic niche regulates glioblastoma stem cells through hypoxia inducible factor 2 alpha. Brain *133*, 983-995.

Simpson, L., and Parsons, R. (2001). PTEN: life as a tumor suppressor. Exp Cell Res *264*, 29-41.

Singh, S. K., Clarke, I. D., Terasaki, M., Bonn, V. E., Hawkins, C., Squire, J., and Dirks, P. B. (2003). Identification of a cancer stem cell in human brain tumors. Cancer Res *63*, 5821-5828.

Singh, S. K., Hawkins, C., Clarke, I. D., Squire, J. A., Bayani, J., Hide, T., Henkelman, R. M., Cusimano, M. D., and Dirks, P. B. (2004). Identification of human brain tumour initiating cells. Nature *432*, 396-401.

Sladek, N. E. (2003). Human aldehyde dehydrogenases: potential pathological, pharmacological, and toxicological impact. J Biochem Mol Toxicol *17*, 7-23.

Sladek, N. E., Kollander, R., Sreerama, L., and Kiang, D. T. (2002). Cellular levels of aldehyde dehydrogenases (ALDH1A1 and ALDH3A1) as predictors of therapeutic responses to cyclophosphamide-based chemotherapy of breast cancer: a retrospective study. Rational individualization of oxazaphosphorine-based cancer chemotherapeutic regimens. Cancer Chemother Pharmacol *49*, 309-321.

Smith, J. S., Tachibana, I., Passe, S. M., Huntley, B. K., Borell, T. J., Iturria, N., O'Fallon, J. R., Schaefer, P. L., Scheithauer, B. W., James, C. D.*, et al.* (2001). PTEN mutation, EGFR amplification, and outcome in patients with anaplastic astrocytoma and glioblastoma multiforme. J Natl Cancer Inst *93*, 1246-1256.

Soeda, A., Park, M., Lee, D., Mintz, A., Androutsellis-Theotokis, A., McKay, R. D., Engh, J., Iwama, T., Kunisada, T., Kassam, A. B.*, et al.* (2009). Hypoxia promotes expansion of the CD133-positive glioma stem cells through activation of HIF-1alpha. Oncogene *28*, 3949-3959.

Stein, G. H. (1979). T98G: an anchorage-independent human tumor cell line that exhibits stationary phase G1 arrest in vitro. Journal of cellular physiology *99*, 43-54.

Stummer, W., Pichlmeier, U., Meinel, T., Wiestler, O. D., Zanella, F., and Reulen, H. J. (2006). Fluorescence-guided surgery with 5-aminolevulinic acid for resection of malignant glioma: a randomised controlled multicentre phase III trial. Lancet Oncol *7*, 392-401.

Stupp, R., Hegi, M. E., Neyns, B., Goldbrunner, R., Schlegel, U., Clement, P. M., Grabenbauer, G. G., Ochsenbein, A. F., Simon, M., Dietrich, P. Y*., et al.* (2010). Phase I/IIa study of cilengitide and temozolomide with concomitant radiotherapy followed by cilengitide and temozolomide maintenance therapy in patients with newly diagnosed glioblastoma. J Clin Oncol *28*, 2712-2718.

Stupp, R., Mason, W. P., van den Bent, M. J., Weller, M., Fisher, B., Taphoorn, M. J., Belanger, K., Brandes, A. A., Marosi, C., Bogdahn, U*., et al.* (2005). Radiotherapy plus concomitant and adjuvant temozolomide for glioblastoma. N Engl J Med *352*, 987-996.

Sullivan, J. P., Spinola, M., Dodge, M., Raso, M. G., Behrens, C., Gao, B., Schuster, K., Shao, C., Larsen, J. E., Sullivan, L. A*., et al.* (2010). Aldehyde dehydrogenase activity selects for lung adenocarcinoma stem cells dependent on notch signaling. Cancer Res *70*, 9937-9948.

Syljuasen, R. G., Jensen, S., Bartek, J., and Lukas, J. (2006). Adaptation to the ionizing radiation-induced G2 checkpoint occurs in human cells and depends on checkpoint kinase 1 and Polo-like kinase 1 kinases. Cancer Res *66*, 10253-10257.

Taghizadeh, K., McFaline, J. L., Pang, B., Sullivan, M., Dong, M., Plummer, E., and Dedon, P. C. (2008). Quantification of DNA damage products resulting from deamination, oxidation and reaction with products of lipid peroxidation by liquid chromatography isotope dilution tandem mass spectrometry. Nat Protoc *3*, 1287-1298.

Tang, J. B., Svilar, D., Trivedi, R. N., Wang, X. H., Goellner, E. M., Moore, B., Hamilton, R. L., Banze, L. A., Brown, A. R., and Sobol, R. W. (2011). N-methylpurine DNA glycosylase and DNA polymerase beta modulate BER inhibitor potentiation of glioma cells to temozolomide. Neuro Oncol *13*, 471-486.

Terada, K., Tamiya, T., Daido, S., Kambara, H., Tanaka, H., Ono, Y., Matsumoto, K., Ito, S., Ouchida, M., Ohmoto, T., and Shimizu, K. (2002). Prognostic value of loss of heterozygosity around three candidate tumor suppressor genes on chromosome 10q in astrocytomas. J Neurooncol *58*, 107-114.

Therneau TM, G. P., Fleming TR. (1990). Martingale-based residuals and survival models. Biometrika *77*, 147–160.

Tohyama, T., Lee, V. M., Rorke, L. B., Marvin, M., McKay, R. D., and Trojanowski, J. Q. (1992). Nestin expression in embryonic human neuroepithelium and in human neuroepithelial tumor cells. Lab Invest *66*, 303-313.

Torroglosa, A., Murillo-Carretero, M., Romero-Grimaldi, C., Matarredona, E. R., Campos-Caro, A., and Estrada, C. (2007). Nitric oxide decreases subventricular zone stem cell proliferation by inhibition of epidermal growth factor receptor and phosphoinositide-3-kinase/Akt pathway. Stem Cells *25*, 88-97.

Uchida, N., Buck, D. W., He, D., Reitsma, M. J., Masek, M., Phan, T. V., Tsukamoto, A. S., Gage, F. H., and Weissman, I. L. (2000). Direct isolation of human central nervous system stem cells. Proc Natl Acad Sci U S A *97*, 14720-14725.

Ullrich, A., Coussens, L., Hayflick, J. S., Dull, T. J., Gray, A., Tam, A. W., Lee, J., Yarden, Y., Libermann, T. A., Schlessinger, J., and et al. (1984). Human epidermal growth factor receptor cDNA sequence and aberrant expression of the amplified gene in A431 epidermoid carcinoma cells. Nature *309*, 418-425.

Vander Heiden, M. G., Cantley, L. C., and Thompson, C. B. (2009). Understanding the Warburg effect: the metabolic requirements of cell proliferation. Science *324*, 1029-1033.

Vazquez, F., Ramaswamy, S., Nakamura, N., and Sellers, W. R. (2000). Phosphorylation of the PTEN tail regulates protein stability and function. Mol Cell Biol *20*, 5010-5018.

Verhaak, R. G., Hoadley, K. A., Purdom, E., Wang, V., Qi, Y., Wilkerson, M. D., Miller, C. R., Ding, L., Golub, T., Mesirov, J. P.*, et al.* (2010). Integrated genomic analysis identifies clinically relevant subtypes of glioblastoma characterized by abnormalities in PDGFRA, IDH1, EGFR, and NF1. Cancer Cell *17*, 98-110.

Vogelstein, B., Fearon, E. R., Hamilton, S. R., Kern, S. E., Preisinger, A. C., Leppert, M., Nakamura, Y., White, R., Smits, A. M., and Bos, J. L. (1988). Genetic alterations during colorectal-tumor development. N Engl J Med *319*, 525-532.

Wang, W., McLeod, H. L., and Cassidy, J. (2003). Disulfiram-mediated inhibition of NF-kappaB activity enhances cytotoxicity of 5-fluorouracil in human colorectal cancer cell lines. International journal of cancer Journal international du cancer *104*, 504-511.

Weller, M. (2011). Novel diagnostic and therapeutic approaches to malignant glioma. Swiss Med Wkly *141*, w13210.

Witusik-Perkowska, M., Rieske, P., Hulas-Bigoszewska, K., Zakrzewska, M., Stawski, R., Kulczycka-Wojdala, D., Bienkowski, M., Stoczynska-Fidelus, E., Gresner, S. M., Piaskowski, S.*, et al.* (2011). Glioblastoma-derived spheroid cultures as an experimental model for analysis of EGFR anomalies. J Neurooncol *102*, 395-407.

Wohrer, A., Waldhor, T., Heinzl, H., Hackl, M., Feichtinger, J., Gruber-Mosenbacher, U., Kiefer, A., Maier, H., Motz, R., Reiner-Concin, A.*, et al.* (2009). The Austrian Brain Tumour Registry: a cooperative way to establish a population-based brain tumour registry. J Neurooncol *95*, 401-411.

www.cbtrus.org (2012). CBTRUS Statistical Report: Primary Brain and Central Nervous System Tumors Diagnosed in the United States in 2004-2008. In.

Yan, H., Bigner, D. D., Velculescu, V., and Parsons, D. W. (2009a). Mutant metabolic enzymes are at the origin of gliomas. Cancer Res *69*, 9157-9159.

Yan, H., Parsons, D. W., Jin, G., McLendon, R., Rasheed, B. A., Yuan, W., Kos, I., Batinic-Haberle, I., Jones, S., Riggins, G. J.*, et al.* (2009b). IDH1 and IDH2 mutations in gliomas. N Engl J Med *360*, 765-773.

Yin, A. H., Miraglia, S., Zanjani, E. D., Almeida-Porada, G., Ogawa, M., Leary, A. G., Olweus, J., Kearney, J., and Buck, D. W. (1997). AC133, a novel marker for human hematopoietic stem and progenitor cells. Blood *90*, 5002-5012.

Zanet, J., Freije, A., Ruiz, M., Coulon, V., Sanz, J. R., Chiesa, J., and Gandarillas, A. (2010). A mitosis block links active cell cycle with human epidermal differentiation and results in endoreplication. PLoS One *5*, e15701.

Zeng, Y., Yang, Z., Xu, J. G., Yang, M. S., Zeng, Z. X., and You, C. (2009). Differentially expressed genes from the glioblastoma cell line SHG-44 treated with all-trans retinoic acid in vitro. J Clin Neurosci *16*, 285-294.

Zhang, W. B., Wang, Z., Shu, F., Jin, Y. H., Liu, H. Y., Wang, Q. J., and Yang, Y. (2010). Activation of AMP-activated protein kinase by temozolomide contributes to apoptosis in glioblastoma cells via p53 activation and mTORC1 inhibition. J Biol Chem *285*, 40461-40471.

Zhao, D., McCaffery, P., Ivins, K. J., Neve, R. L., Hogan, P., Chin, W. W., and Drager, U. C. (1996). Molecular identification of a major retinoic-acid-synthesizing enzyme, a retinaldehyde-specific dehydrogenase. Eur J Biochem *240*, 15-22.

Zhao, S., Lin, Y., Xu, W., Jiang, W., Zha, Z., Wang, P., Yu, W., Li, Z., Gong, L., Peng, Y.*, et al.* (2009). Glioma-derived mutations in IDH1 dominantly inhibit IDH1 catalytic activity and induce HIF-1alpha. Science *324*, 261-265.

Zucchetti, M., Catapano, C. V., Filippeschi, S., Erba, E., and D'Incalci, M. (1989). Temozolomide induced differentiation of K562 leukemia cells is not mediated by gene hypomethylation. Biochem Pharmacol *38*, 2069-2075.

H. Abbreviations

aa	Amino acid
Akti	Akt 1/2 kinase inhibitor
ALDH1	Aldehyde dehydrogenase 1
ALDH1A1	Aldehyde dehydrogenase 1 A1
Amp	Ampicillin
AP site	Abasic site
APE	AP endonuclease
BSA	Bovine serum albumin
CSC	Cancer stem cell
DAF2/DA	Diaminofluoresceindiacetate solution
DEAB	4-Diethylaminobenzaldehyde
DFX	Deferoxamine
DHE	Dihydroethdium
DMSO	Dimethyl sulfoxide
DTT	Dithiothreitol
EGF	Epidermal growth factor
EGFR	Epidermal growth factor receptor
FABP5	Fatty acid binding protein 5
FGF	Fibroblast Growth Factor
G418	Geneticin
GalC	Galactocerebroside
GFAP	Glial fibrillary acidic protein
GSK-3	Glycogen synthase kinase-3
Gy	Gray
h	Hour
HE	Hämatoxylin-Eosin
HIF1A	Hypoxia inducible factor 1
HNE	4-Hydroxynonenal
IDH1/2	Isocitrate dehydrogenase 1 and 2
Kan	Kanamycin
LB	Lysogeny broth
LOH	Loss of heterozygosity
MGMT	O-6-methylguanine-DNA methyltransferase

MTIC	MTIC (3-methyl-(triazen-1-yl) imidazole-4-carboxamide).
mTOR	Mammalian target of rapamycin
MTT	(3-(4,5-Dimethylthiazol-2-yl)-2,5-diphenyltetrazolium bromide)
NAC	N-Acetyl-L-cysteine
NER	Nucleotide excision repair
NF1	Neurofibromatosis type I
NGF	Nerve growth factor
NO	Nitric oxide
Olig2	Oligodendrocyte transcription factor 2
PAR	Poly(ADP-ribosylation)
PARP1	Poly(ADP-ribose) polymerase 1
PBS	Phosphate buffered saline
pCDNA3	pCDNA^{TM}3.1(-)
PI	Propidiumiodid
PI3K	Phosphoinositide 3-kinase
PIP3	phosphatidylinositol (3,4,5)-trisphosphate
PMSF	Phenylmethylsulfonyl fluoride
PTB	Phospho-tyrosine binding
PTEN	Phosphatase and tensin homolog
RAR	Retinoic acid receptor
ROS	Reactive oxygen species
RXR	Retinoid X receptor
s	Second
SDS-PAGE	Sodium dodecyl sulfatepolyacrylamidegel electrophoresis
Ser	Serine
SH2	Src-homology 2
SOX	Sry-related HMG box
Thr	Threonine
TMZ	Temozolomide
Tuj1	Beta-III-tubulin
Tyr	Tyrosine
VEGF	Vascular endothelial growth factor
Wt	Wild-type
XRCC1	X-ray cross-complementing gene 1
YKL-40	Chitinase-3-like protein 1 (CHI3L1)

I. Supplementary data

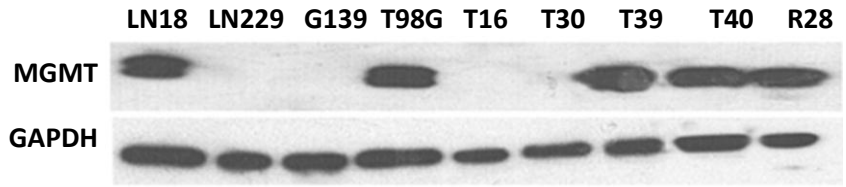

Supplementary figure S 1: Western blot analysis of MGMT repair protein expression.

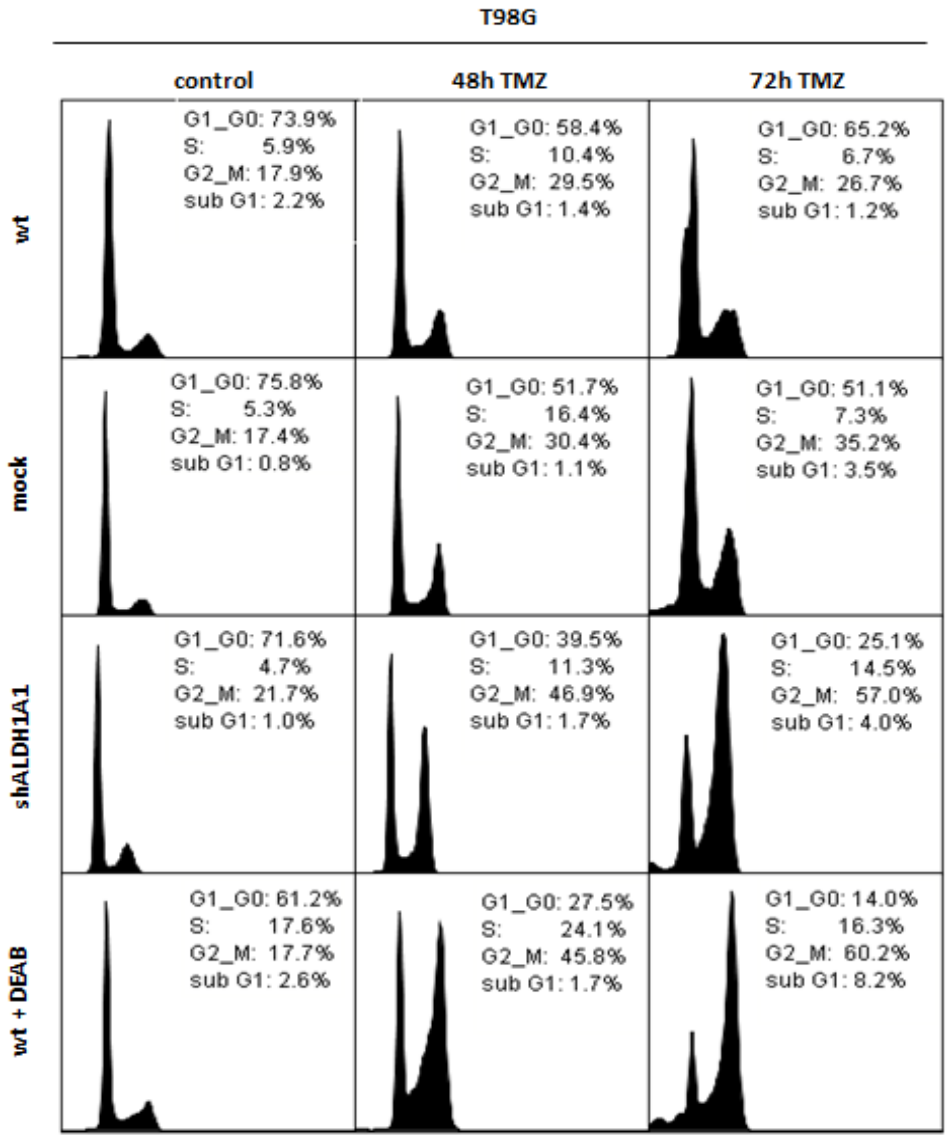

Supplementary figure S 2: Representative flow cytometry histograms of T98G cells after treatment with 500µM TMZ, 300µM DEAB or a combination of both for 48 and 72 hours; Y-axes: DNA content, X-axes: FL3-H;

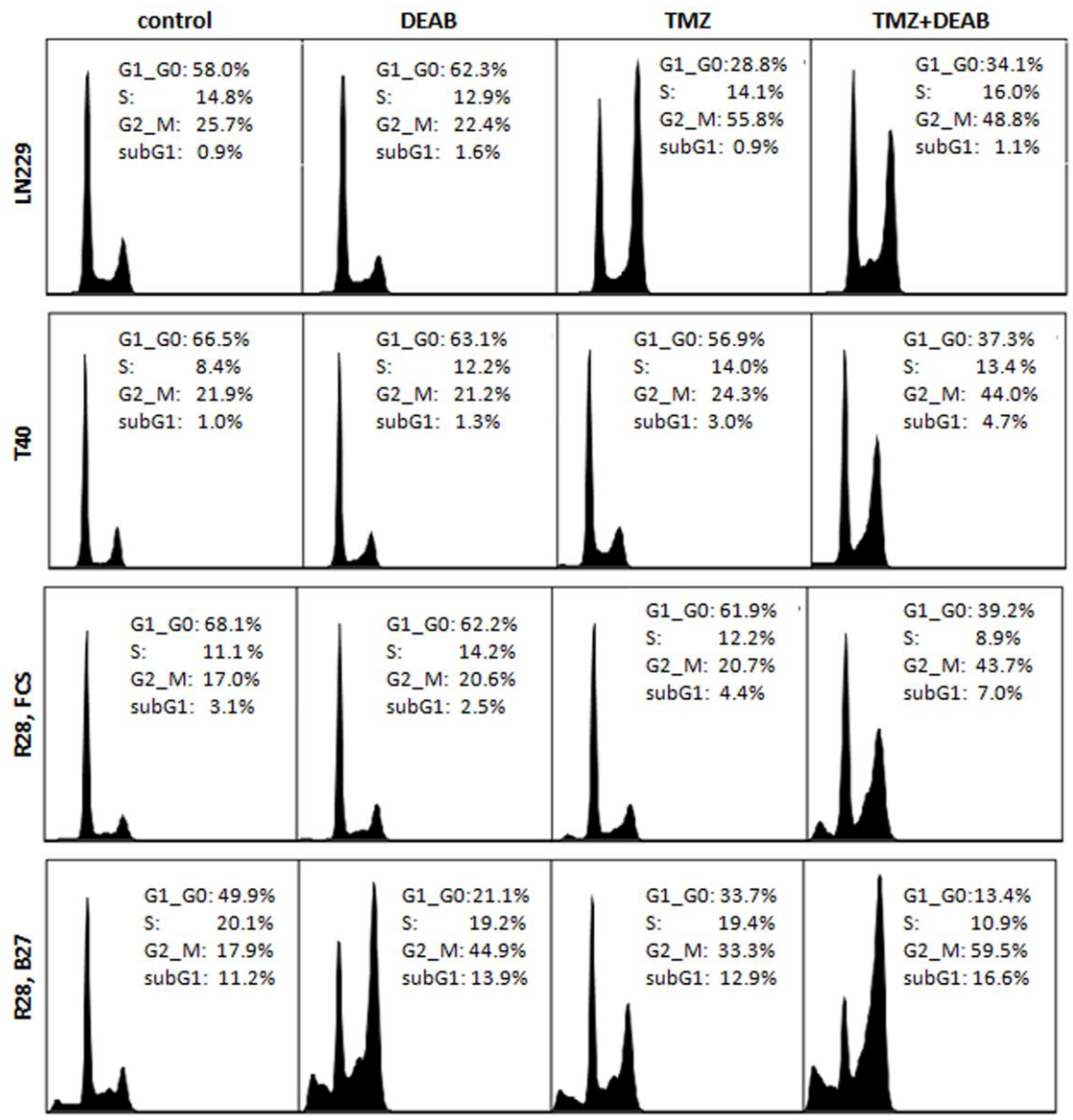

Supplementary figure S 3: Representative flow cytometry histograms of LN229, T40 and R28 cells after treatment with 200µM TMZ, 300µM DEAB or a combination of both for 48 hours; R28 cells were additionally treated in neurobasal medium + B27 (R28, B27) with 200µM TMZ and 100µM DEAB; Y-axes: DNA content, X-axes: FL3-H;

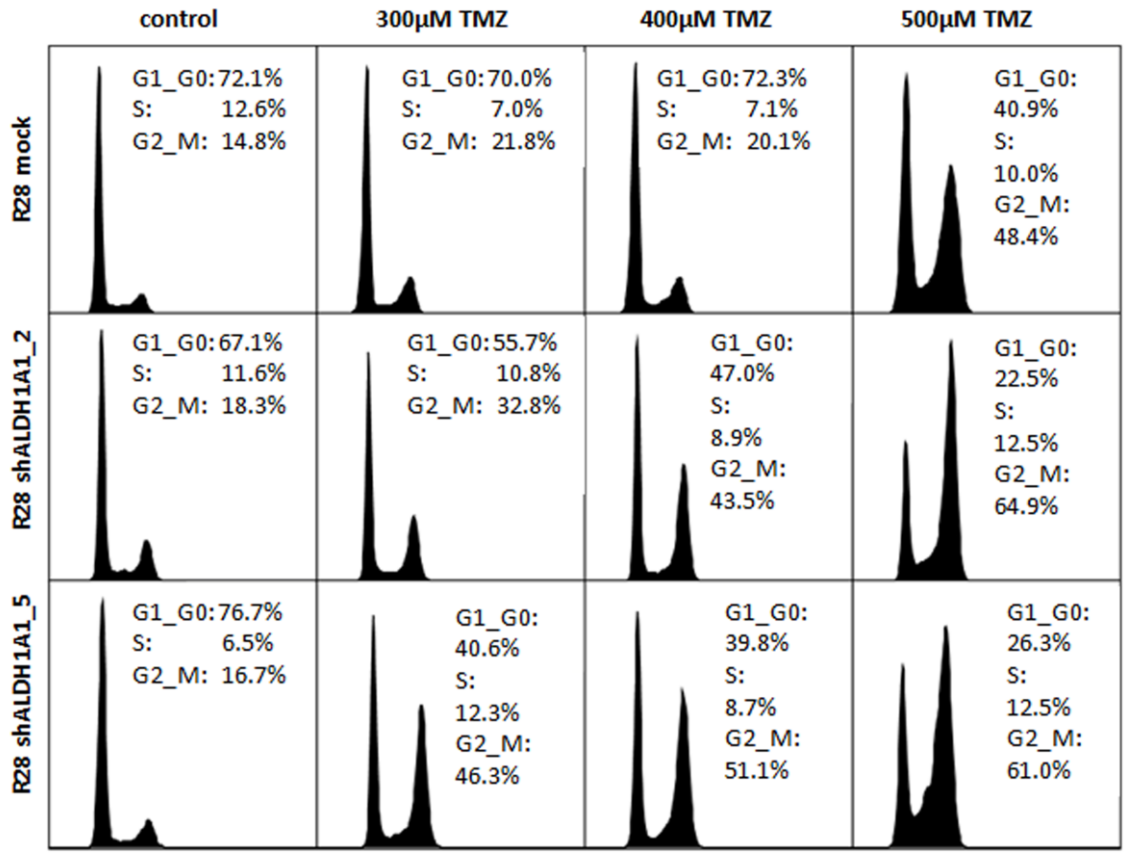

Supplementary figure S 4: Representative flow cytometry histograms of R28 mock and shALDH1A1 cells after treatment with 300µM TMZ, 400µM TMZ or 500µM TMZ for 48 hours in DMEM + FBS; two different shRNA plasmids were applied (Clone ID: shALDH1_2 corresponds to TRCN0000026417, shALDH1_5 corresponds to TRCN0000026502); Y-axes: DNA content, X-axes: FL3-H;

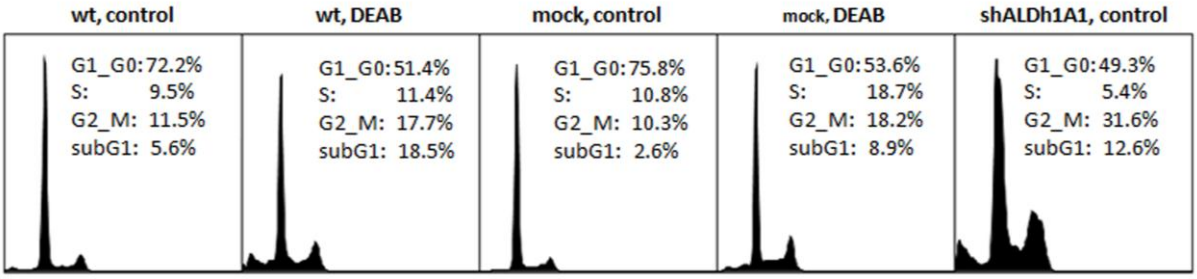

Supplementary figure S 5: Cell cycle analysis of LN18 wt, mock and shALDH1A1 cells treated under stem cell-preserving conditions. LN18 shALDH1A1 cells showed accumulation in G2/M and apoptosis when cultivated in neurobasal medium;

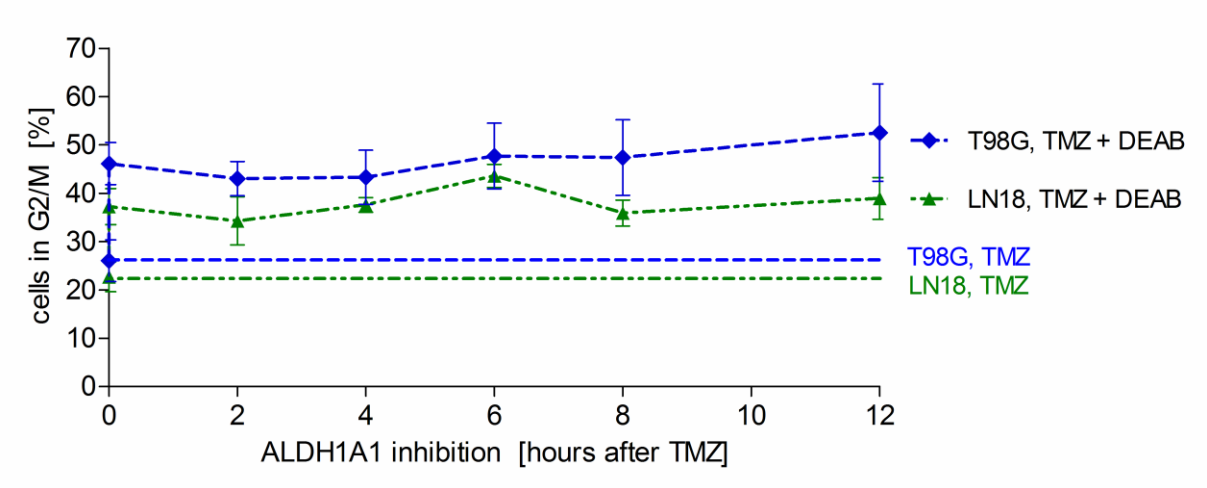

Supplementary figure S 6: Percentage of LN18 and T98G cells in G2/M following treatment with mere TMZ (dashed line) or with TMZ and DEAB (DEAB was either given concomitant or 2-12 hours after TMZ);

J. List of publications

Aldehyde dehydrogenase 1 A1 – a new mediator of resistance to temozolomide in glioblastoma
A. Schäfer, J. Teufel, F. Ringel, M. Bettstetter , I. Hoepner, M. Rasper, J. Gempt, J. Koeritzer, F. Schmidt-Graf, B. Meyer, C.P. Beier, J. Schlegel;
Neuro-Oncology, December 2012

RE: ALDH1A1 is a marker of astrocytic differentiation during brain development and correlates with better survival in glioblastoma patients
A. Schäfer, J. Schlegel;
Letter to the editor, Brain Pathology, July 2012

Disconnecting the yin and yang relation of epidermal growth factor receptor (EGFR) mediated delivery: a fully synthetic, EGFR-targeted gene transfer system avoiding receptor activation
A. Schäfer, A. Pahnke, D. Schaffert, W.M. van Weerden, C.M. de Ridder, W. Rödl, A. Vetter, C. Spitzweg, R. Kraaij, E. Wagner, M. Ogris;
Human Gene Therapy, August 2011

Hirntumorstammzellen und Therapieresistenz in malignen Gliomen
J. Schlegel, A. Schäfer, C. Zimmer;
Der Onkologe, January 2011

Aldehyde dehydrogenase 1 positive glioblastoma cells show brain tumor stem cell capacity
M. Rasper#, A. Schäfer#, G. Piontek, J. Teufel, G. Brockhoff, F. Ringel, S. Heindl, C. Zimmer, J. Schlegel; # authors contributed equally
Neuro-Oncology, October 2010

K. Lebenslauf

PERSÖNLICHE DATEN

Name:	Andrea Schäfer
Geboren am:	01.12.1982 in Heidelberg

AUSBILDUNG

10/2002 – 08/2008 **Technische Universität (TU) Berlin**
(Berlin, Deutschland)
Studium Biotechnologie mit Vertiefungsrichtung medizinische Biotechnologie
Abschluss: Diplom-Ingenieur (Universität)
Note: 1.2 („mit Auszeichnung“)

08/2005 – 02/2006 **Royal Institute of Technology (KTH)**
(Stockholm, Schweden)
Auslandssemester

08/1993 – 06/2002 **St. Raphael Gymnasium**
(Heidelberg, Deutschland)
Allgemeine Hochschulreife
Note: 1.5

WISSENSCHAFTLICHE ARBEITEN

Seit 10/2008 **Technische Universität München (TUM)**
(München, Deutschland)
Promotion im Institut für allgemeine Pathologie und pathologische Anatomie, Fachgebiet Neuropathologie;
Thema: *„Aldehyde dehydrogenase 1 A1 is expressed by cancer stem cells and mediates chemoresistance in human glioblastoma*“

10/2007 – 08/2008 **Ludwig-Maximilians-Universität (LMU)**
(München, Deutschland)
Diplomarbeit im Department für pharmazeutische Biotechnologie;
Thema: *„Internalisation studies with EGF receptor peptide ligands for gene delivery into tumor cells“*
Note: 1.0

09/2005 – 01/2006 **Royal Institute of Technology (KTH)**
(Stockholm, Schweden)
Studienarbeit in der Abteilung für molekulare Biotechnologie;
Thema: *„Phage display selection to discover Zwt dimer binders in a new ABD random peptide library”*
Note: 1.0